MASTER COPY KEEP THIS COPY FOR REPRODUCTION PURPOSES

REPORT DOCUMENTATION PAGE

Form Approved
OMB No. 0704-0188

1. AGENCY USE ONLY (Leave blank)	2. REPORT DATE	3. REPORT TYPE AND DATES COVERED
	December 8, 1994	Final Technical Report

4. TITLE AND SUBTITLE
Growth and Evaluation of Nonlinear Optical Crystals for Laser Applications: Lithium Borate, Barium Borate and Silver Gallium Selenide

5. FUNDING NUMBERS
Grant N00014-90-J-4092
APPA No. A07397

6. AUTHOR(S)
Robert S. Feigelson
Roger K. Route

7. PERFORMING ORGANIZATION NAME(S) AND ADDRESS(ES)
Center for Materials Research
Stanford University
Stanford, CA 94305-4045

8. PERFORMING ORGANIZATION REPORT NUMBER

9. SPONSORING/MONITORING AGENCY NAME(S) AND ADDRESS(ES)
Department of the Navy
Office of the Chief of Naval Research
800 North Quincy Street, Code 1512A=SAM
Arlington, VA 22217-5000

10. SPONSORING/MONITORING AGENCY REPORT NUMBER

11. SUPPLEMENTARY NOTES
The view, opinions and/or findings contained in this report are those of the author(s) and should not be construed as an official Department of the Navy position, policy, or decision, unless so designated by other documentation.

12a. DISTRIBUTION/AVAILABILITY STATEMENT
Approved for public release; distribution unlimited.

12b. DISTRIBUTION CODE

13. ABSTRACT (Maximum 200 words)

This report summarizes a four year program on the development of high efficiency nonlinear optical materials. Major achievements were the development of effective top-seeded solution growth techniques for beta-barium borate (BBO) and lithium triborate (LBO). BBO crystals were also grown for the first time in the US by the direct melt growth technique, a metastable method that leads to significantly higher growth rates than the commercial solution-growth technique. High quality crystals were made available for optical property determinations and nonlinear optical device development at government and commercial laboratories.

Additional accomplishments involved development of an optimum heat-treatment technology for eliminating optical scattering centers from as-grown crystals of silver gallium selenide. Cooperative programs were carried out with NRL to quantify the effects of intrinsic and extrinsic defects on residual absorption. It was discovered that silver gallium selenide and silver gallium sulfide crystals grown from silver-rich solutions are free of anomolous absorption in the 2 micron waveband which is currently the major problem limiting generation of high intensity, tunable 3-5 micron radiation by OPO methods using these materials.

A new nonlinear optical material, $(La,Gd)Sc_3(BO_3)_4$ has been identified for future study.

14. SUBJECT TERMS
Nonlinear optical materials, barium borate, lithium borate, silver gallium selenide, BBO, LBO, $AgGaSe_2$

15. NUMBER OF PAGES

16. PRICE CODE

17. SECURITY CLASSIFICATION OF REPORT	18. SECURITY CLASSIFICATION OF THIS PAGE	19. SECURITY CLASSIFICATION OF ABSTRACT	20. LIMITATION OF ABSTRACT
UNCLASSIFIED	UNCLASSIFIED	UNCLASSIFIED	UL

The Board of Trustees of the
Leland Stanford Junior University
Center for Materials Research
Stanford, California 94305-4045
Santa Clara, 12th Congressional District

Final Technical Report
on

GROWTH AND EVALUATION OF NONLINEAR OPTICAL CRYSTALS FOR LASER APPLICATIONS: LITHIUM BORATE, BARIUM BORATE AND SILVER GALLIUM SELENIDE

for the period
August 1, 1990 through June 30, 1994

Grant N00014-90-J-4092

Submitted to
Office of Naval Research
800 North Quincy Street
Arlington, VA 22217-5000

CMR-94-4
Stanford SPO #8334

Principal Investigator:

Robert S. Feigelson
Professor, Research
Center for Materials Research
Stanford, California 94305-4045
(415)723-4007

December 1994

ABSTRACT

This report summarizes a four year program on the development of high efficiency nonlinear optical materials. Major achievements were the development of effective crystal growth techniques for beta-barium borate (BBO) and lithium triborate (LBO). A top-seeded solution growth technique used for growing both materials is described, along with an assessment of their respective growth rate limiting mechanisms. BBO crystals were also grown for the first time in the US by the direct melt growth technique, a metastable method that leads to significantly higher growth rates than the commercial solution-growth technique. High quality crystals were successfully produced and made available for optical property determinations and nonlinear optical device development at Stanford and at government and commercial laboratories.

Additional major accomplishments involved development of an optimum heat-treatment technology for eliminating optical scattering centers from as-grown crystals of silver gallium selenide. A microchemical analysis and a mass balance model that explained the dynamics of the heat-treatment process led to the identification of an new annealing medium that resulted in an improvement in the heat-treatment process. Cooperative programs were carried out with NRL to quantify the effects of intrinsic and extrinsic defects on residual absorption. Most importantly, it was discovered that silver gallium selenide and silver gallium sulfide crystals grown from silver-rich solutions are free of anomolous absorption in the 2 micron waveband which is currently the major problem limiting generation of high intensity, tunable 3-5 micron radiation by OPO methods using these materials.

A new nonlinear optical material, $(La,Gd)Sc_3(BO_3)_4$ has been identified by making cationic substitutions in known NLO materials to create derivative materials.

TABLE OF CONTENTS

FORWARD

This is the final technical report on N00014-90-J-4092, "Growth and Evaluation of Nonlinear Optical Crystals for Laser Applications: Lithium Borate, Barium Borate and Silver Gallium Selenide" which began at Stanford University on August 1, 1990 and was completed on June 30, 1994. The overall objective of the program was further development of these important, high efficiency nonlinear optical materials. Initial emphasis was placed on solution growth of the low temperature phase of barium borate, β-BaB_2O_4, which is a highly nonlinear material important for harmonic generation and mixing applications in the visible and UV, and on lithium tri-borate (LiB_3O_5), a relatively newer nonlinear material with a somewhat different set of applications, also in the visible and UV. Research studies on BBO were carried out during the entire period. Research studies on LBO, though quite successful, ended in 1993 due to patent issues that made commercial application of this material in the U.S. questionable.

A successfully-completed Ph. D. dissertation focused on understanding diffusion phenomena in the important infrared nonlinear optical material silver gallium selenide ($AgGaSe_2$), work which derived from earlier ARO programs, DAAG29-84-K-0071 and DAAL03-88-K 0113. The driving force for this study was the need to minimize residual optical scatter in melt-grown and heat-treated crystals and to reduce the residual optical absorption of melt-grown material in the 2 micron waveband which currently limits OPO generation of tunable radiation in the 3-5 micron region.

The program has been highly successful. When it began, there was little direct experience or activity in this country on the crystal growth and characterization of either barium borate of lithium borate. Research on the preparation of these materials under this program resulted in the first US-grown samples for optical studies. During this program's timeframe, a viable crystal growth technology was developed for each, and successfully transfered to industry. The first BBO crystals grown in the US by the metastable melt growth process (75 times faster than solution growth methods) were produced. Research on silver gallium selenide resulted in a significant improvement in our understanding of the thermodynamics of this material and in the heat-treatment process that eliminates as-grown optical scattering centers. The discovery late in the program that both silver gallium sulfide and silver gallium selenide crystals grown from silver-rich solutions are free of anomolous absorption in the 2 micron waveband, suggests that this material may yet have important applications in high power 3-5 micron generation.

The search for new NLO materials continued throughout, focusing primarily on borate compounds which contain structural elements known to possess superior NLO properties. A promising new material, $La_{0.5}Gd_{0.5}Sc(BO_3)_4$, has been identified and it is being studied with continuing support from ARPA/ONR through the Center for Nonlinear Optical Materials at Stanford.

I. INTRODUCTION

A. OBJECTIVES

The overall objective of the program was the development of the high efficiency nonlinear optical materials, β-barium borate (BBO), lithium borate (LBO) and silver gallium selenide. Initial emphasis was placed on solution growth techniques for the low temperature phase of barium borate, β-BaB_2O_4 (BBO), a highly nonlinear material important for harmonic generation and mixing applications in the visible and UV. When the program began, there was little direct experience with this material beyond several joint studies that had been made on a few crystals from Fujian in the PRC. A major program goal became the development of a reproducible crystal growth technique that would yield useable size crystals and be transferable to the commercial sector. Additional objectives related to improving optical quality : early crystals all contained inclusions in varying densities that were caused by solvent entrapment on the growing interface. The approach taken was the use of high thermal gradient, top-seeded solution growth (TSSG) furnaces that would enhance growth interface stability, facilitate forced/natural convection (stirring) at the growth interface, and permit the highest possible growth rates. The identification of an optimum solvent was also recognized to be important and a number of solvent systems were investigated. Pulling methods were also investigated in order to grow longer BBO and LBO boules: normal TSSG boules though large in diameter, tended to be quite thin, severely limiting the yield of cm size crystals. Midway through the program, we initiated experiments on the direct melt growth of BBO, a metastable high growth rate method discovered by researchers at NEC in Japan.

Lithium tri-borate (LiB_3O_5) is a relatively newer nonlinear material with a somewhat different set of applications in the visible and UV. We also began the growth of this material using the TSSG approach. Even less was known about the growth properties of LBO when we began beyond the phase equilibrium in the Li_2O-B_2O_3 system which had been worked out twenty years earlier. Our approach was to use similar high gradient solution growth furnaces to evaluate possible solvent systems and to determine the range of parameters over which the desired phase could be grown. The need for flux modification to reduce solution viscosities became clear, and accurate measurements of growth solution viscosities were undertaken. Surface decomposition problems during growth had been alluded to in the literature, and this issue was studied in detail.

Our studies on silver gallium selenide, greatly expanding work initiated under ARO Grant DAAL03-88-K-0113, focused on improving the post-growth heat-treatment of this

material through an increased understanding of the chemistry and kinetics of the heat-treatment process. Experiments were carried out using as-grown crystals, varying the heat-treatment conditions and the annealing medium which is used to control the final composition of the crystal by a solid state diffusion mechanism. Surface microchemical analysis was relied on to develop a chemical mass transport model for the heat-treatment process upon which predictions for process improvement could be made.

In all cases, we sought to obtain additional optical characterization from commercial and government researchers by making Stanford-grown crystals available on a loan basis.

The fact that BBO and LBO are difficult to grow in large dimensions with high optical quality, and the fact that BBO is known to undergo surface and bulk degradation under high power UV illumination, argues for continued development of newer NLO materials with superior growth characteristics and UV properties. Strategies used in the search for new NLO materials involved cationic and anionic substitution, isostructural analogs, and overlooked phases. Candidate materials were synthesized in powder and single crystal form for detailed optical characterization.

II. RESEARCH RESULTS

A. BARIUM BORATE

1. Objectives

Program objectives relating to barium borate were two-fold: 1) optimizing the growth of large, high optical quality crystals by the top-seeded solution growth (TSSG) method at reasonable growth rates; and 2) developing an alternative direct melt growth method to overcome the slow growth rates intrinsic to the TSSG method.

2. Background

Barium borate, a relatively new and important material for nonlinear optical applications in the visible and ultraviolet regions[1-7], has a number of physical properties which make it particularly attractive, including large effective SHG coefficients (d_{eff} = 6 x d_{eff} for KDP at 1.06 μm), a wide transparent waveband (190 nm to 3500 nm), low dispersion, a large birefringence, high damage thresholds (13.5 ± 2 GW/cm^2 for 1 ns pulses at 1.06 μm and 7.0±1 GW/cm^2 for 250 ps pulses at 532 nm), and high optical homogeneity ($\Delta n \approx 10^{-6}$/cm). It has good mechanical properties, polishes well and, although it appears to be weakly water soluble, does not appear to be hygroscopic under reasonably dry laboratory conditions.

Barium borate is known to exist in two phases, a high temperature α-phase and the low temperature β-phase [8] that is useful for nonlinear applications. The trigonal structure of the low temperature β-phase, R3m, consists of $(B_3O_6)^{3-}$ units which form nearly planar rings that are the key to its optical properties. Barium borate exists as an intermediate compound in the BaO-B_2O_3 pseudobinary system and melts congruently at 1096° C, [9] but because of the structural reordering that occurs during the phase transition (at 925° C), it is generally grown from solution below 925° C. Problems encountered in growth of all materials from high temperature borate-containing oxide solutions relate to growth interface instability and the occurrence of solvent inclusions, particularly in the core regions of the crystals. This is a serious problem in the growth of BBO.

3. Phase Equilibria and Solvent Studies

Na_2O was the first solvent studied that was found to be useable for top-seeded growth of this material. The Na_2O system [10] offers an adequate cooling range and it was quickly found to yield crystals of high quality, Fig. 1. Solution viscosities in the Na_2O system are larger than one would like, however, and this led us to carry out

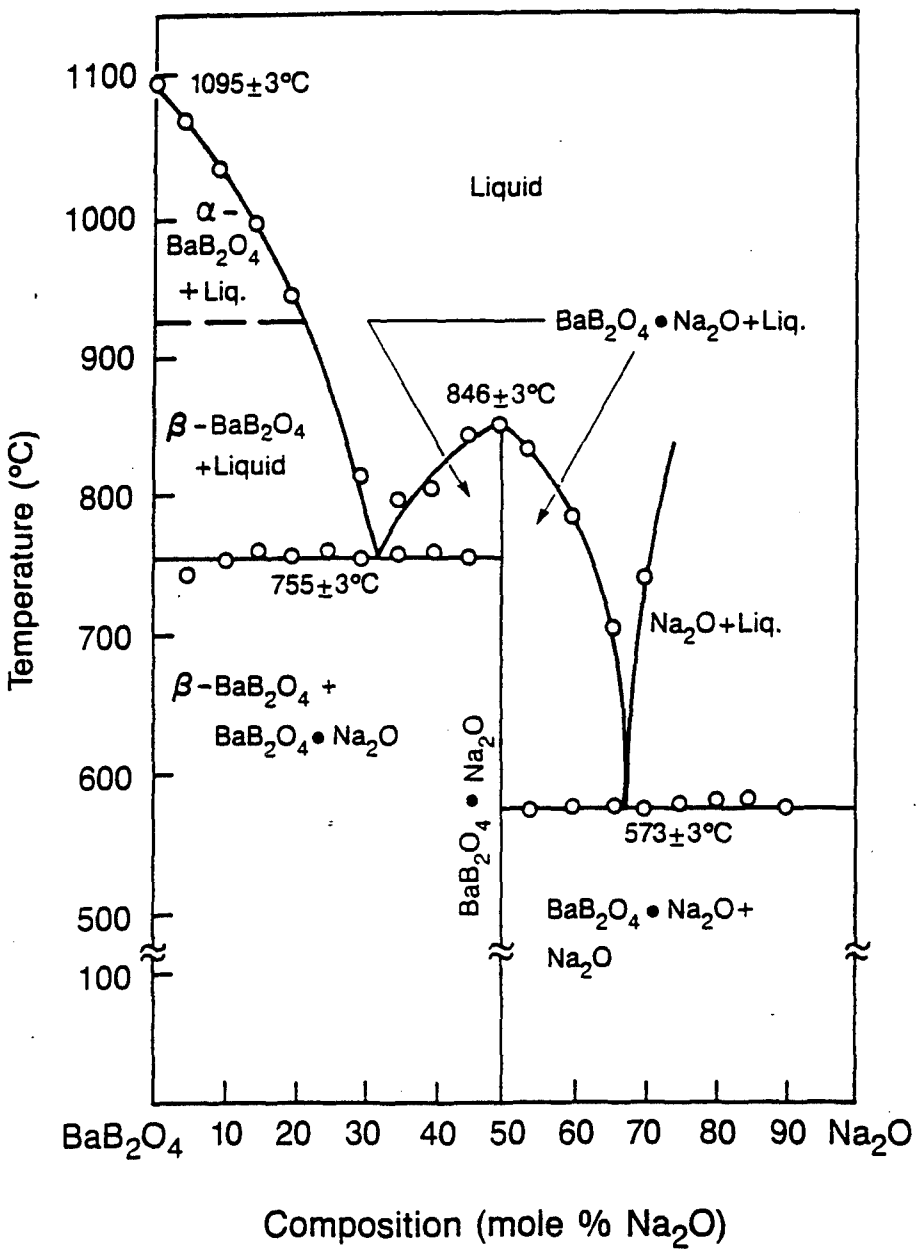

Figure 1. Phase equilibria in the BaB_2O_4 - Na_2O system after Huang and Liang. [10]

experiments with minor additions of BaF_2 to the BaB_2O_4-Na_2O system as a viscosity modifier. No substantial improvements in crystal quality were found. Additional studies were carried out in the BaO-Na_2O-B_2O_3 system after the work of Nikolov and Peshev. [11] Their findings of improved crystal morphology from solvents with composition 75%Na_2O-25%B_2O_3 compared to pure Na_2O solvents could not be verified in our TSSG experiments. Their later claim of reduced solvent viscosity at temperatures in the 850 °C range [12] where constitutional supercooling instability inevitably occurs with pure Na_2O solvents may be worth further investigation, but this was not carried out due to time constraints.

More extensive studies were carried out in the BaB_2O_4-Na_2O-NaF system after initial work by Oseledchik et al. [13]. Figure 2 shows the three flux compostions studied, Na_2O:NaF, Na_2O:2NaF and pure NaF. Accurate phase equilibria in these systems are not known and the flux compositions required to give liquidus temperatures near 925 °C were determined experimentally. NaF-containing solutions appeared to have lower viscosities than pure Na_2O-fluxed solutions, though actual measurements were not made. Of these three solvent compositions, pure NaF was found to give the best results in terms of the lowest solvent inclusion densities and the best boule surface morphologies. It was also easier to pull relatively long crystals prior to interface breakdown compared to growth from Na_2O solutions, Fig. 3.

The biggest problem encountered with NaF flux was chemical decomposition of the melt. Under atmospheric ambients freshly prepared growth solutions consistently gave crystals almost free of solvent inclusions. Second runs resulted in crystals with six-fold patterns of heavy solvent inclusions, similar to those found in BBO crystals grown from mixed NaF-Na_2O solutions. This suggested melt decomposition, with possible decomposition mechanisms:

$$1.)\ 2NaF + H_20 \rightarrow 2HF\uparrow + Na_2O, \text{ or}$$

$$2.)\ 2NaF + O_2 \rightarrow F_2\uparrow + Na_2O.$$

Neither could be verified by analyzing system components after growth.

Growth under dry nitrogen was investigated as a means to control the proposed decomposition processes. However, solvent loss rates increased from ~0.3%/day to over 1.5%/day, which was considered too large for growth runs which typically required a month to complete. If the problem of melt volatility / decomposition can be resolved, NaF appears to give better results than Na_2O. Na_2O growth solutions do not decompose, however, and volatilization rates are manageable (~1.0%/day). Therefore, we concentrated on the use of pure BaB_2O_4-Na_2O melts with approximate starting compositions of 18-20

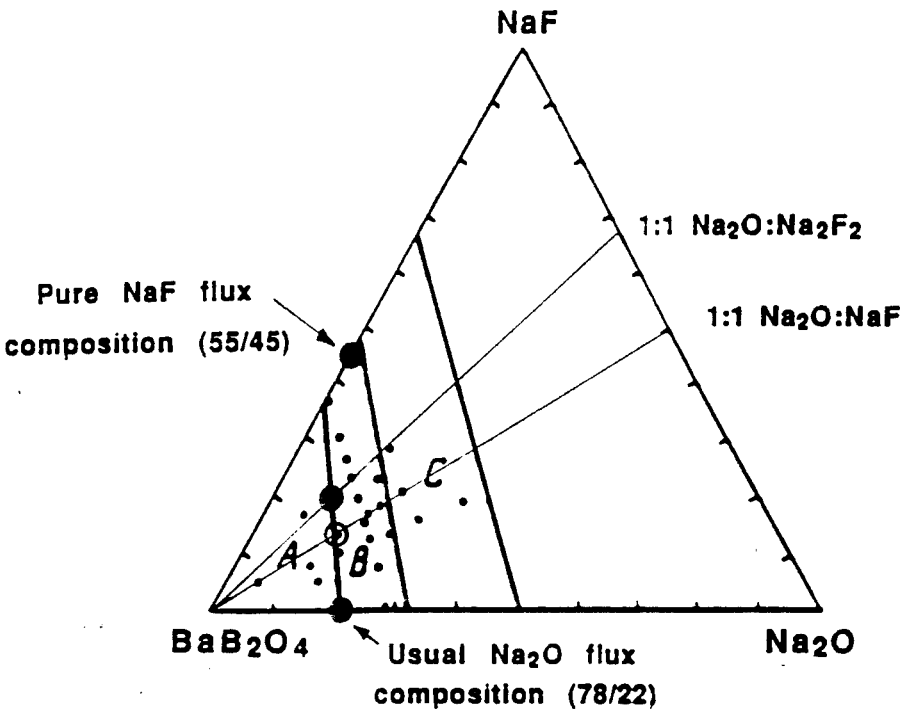

Figure 2. Compositions studied in the ternary BaB_2O_4-Na_2O-NaF system after Osedledchik et al. [13]

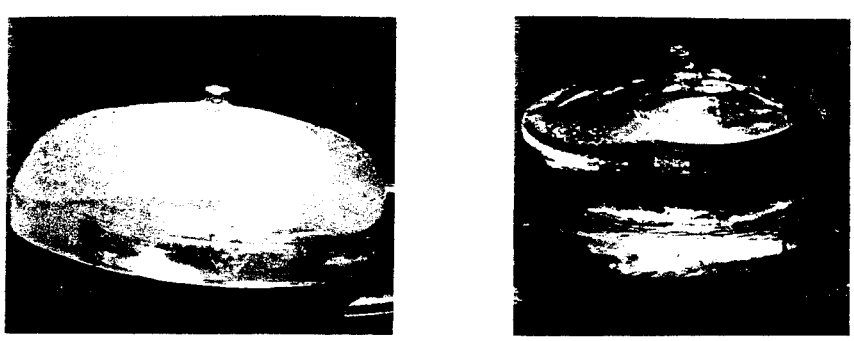

(a) (b)

Figure 3. BaB_2O_4 crystals pulled from a.) Na_2O solutions and b.) NaF solutions.

mole % Na_2O which resulted in liquidus temperatures near 925° C, and on methods to enhance stirring at the growth interface as a means to control solvent inclusions.

4. Top-Seeded Solution Growth Experiments

The melt synthesis and top-seeded solution growth (TSSG) methods described in detail in a previous publication [14] were used for the bulk of our studies. Best results were obtained from SiC-heated box furnaces having steep radial and axial temperature gradients. Because the solubility of BaB_2O_4 increases with temperature in the Na_2O solvent system, growth of β-BaB_2O_4 from solution was carried out using a slow cooling technique. Crystal growth experiments utilized c-axis seeds, 10 cm dia short-form platinum crucibles holding 1.2-1.4 Kg melts, slow rotation rates in the range of 1-5 rpm, and cooling rates on the order of 1-4 °C/day.

Initially, c-axis crystals had been grown without pulling and these assumed the shallow lens shape typical of the BaB_2O_4 crystals grown in the PRC. Thicker crystals were grown by pulling slowly during growth. Typically, we used a cooling rate of 2-3° C/day and a pulling rate of 0.5-1.0 mm/day with reasonably good results. Growth was continued until the onset of interface breakdown (cellular growth instability) which occurred because of increasing melt viscosities at lower system temperatures, Fig. 4. On average, we were able to cool the melts 70-85° C and pull approximately 20 mm before the growth interface became totally unstable, which is one major limitation to growth by this method. The second is the crytals' natural tendency to undercut under conditions of constant cooling and pulling rates. Considerable effort was devoted to developing a phenomenological model for this behavior, with the ultimate goal of growing uniform diameter crystals as long as possible. Isothermal solubility data did not agree with growth system yields: for a given amount of cooling under high gradient conditions, crystals were found to weigh only about half that predicted by equilibrium thermodynamic data, Fig. 5. Working with impirical growth system yields, Y ≈ 1.75 g(BBO) / Kg(melt) °C determined by analyzing a number of growth runs, crystal diameter, d, was related to cooling ($\Delta T / \Delta t$) and pulling ($\Delta Z / \Delta t$) rates using the following equation which compensates for melt level drop caused by pulling:

$$\frac{\Delta Z}{\Delta T} = \frac{4Y}{\pi D^2 \rho_L}\left(\frac{D^2 \rho_L}{d^2 \rho_c} - 1\right)$$

where D = crucible diameter, and ρ_L = liquid density (~3.8g /cm^3) and ρ_c = crystal density (~3.7 g/cm^3) at the growth temperature. Normalized values, shown in Fig. 6, allowed us to adjust pulling and cooling rates depending on the observed crystal diameter.

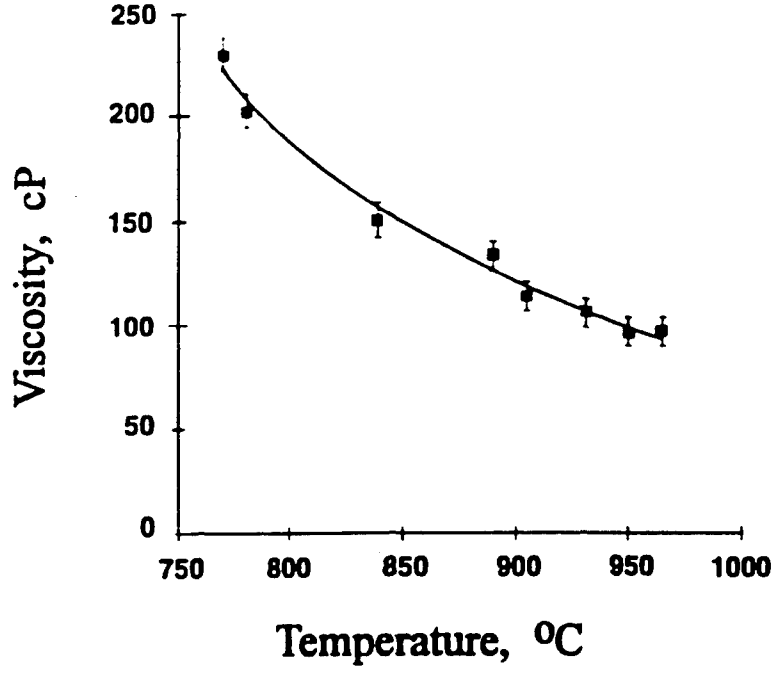

Figure 4. Melt viscosity along the liquidus line in the BaB_2O_4 - Na_2O system after Perlov and Roth. [21]

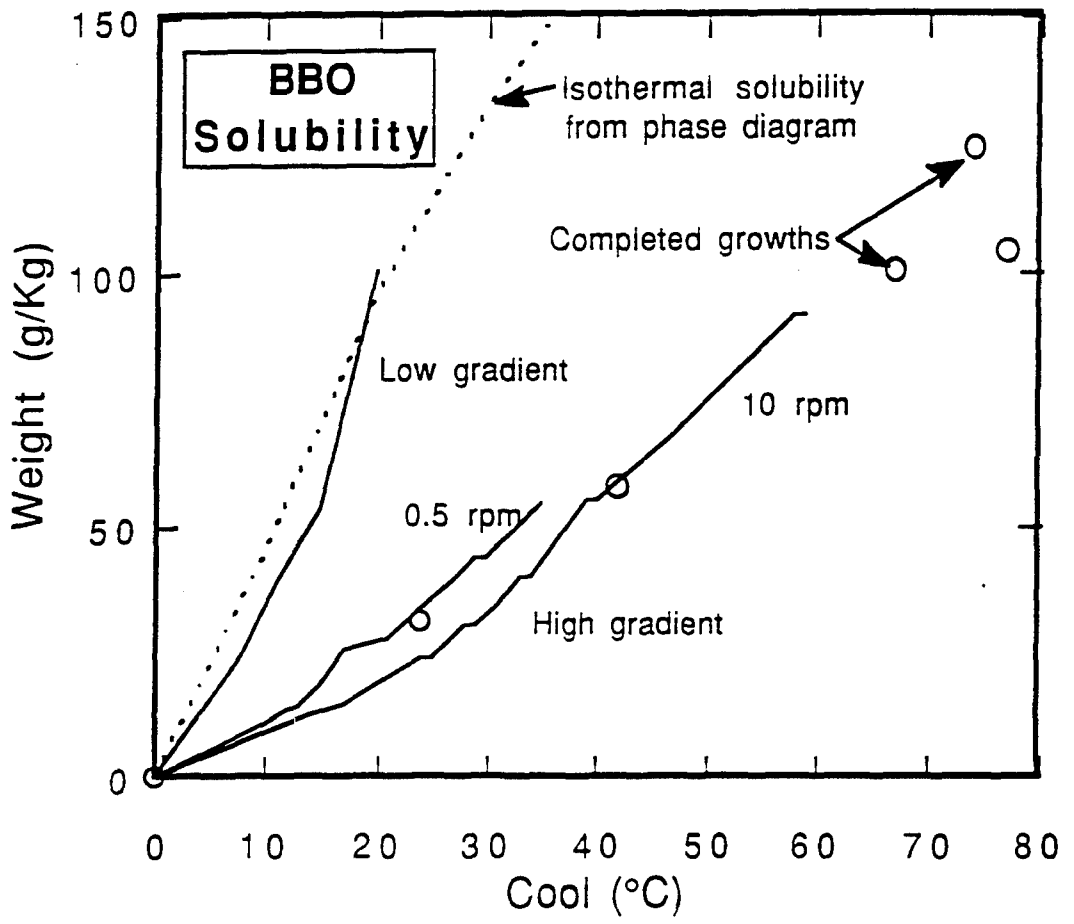

Figure 5. Melt solubility studies in the BaB_2O_4 - Na_2O system in low and high thermal gradient furnaces showing that the actual solubilities in high gradient systems differ significantly from the equilibrium (isothermal) thermodynamic case, rejecting less solute (BBO) from the growth solution than expected.

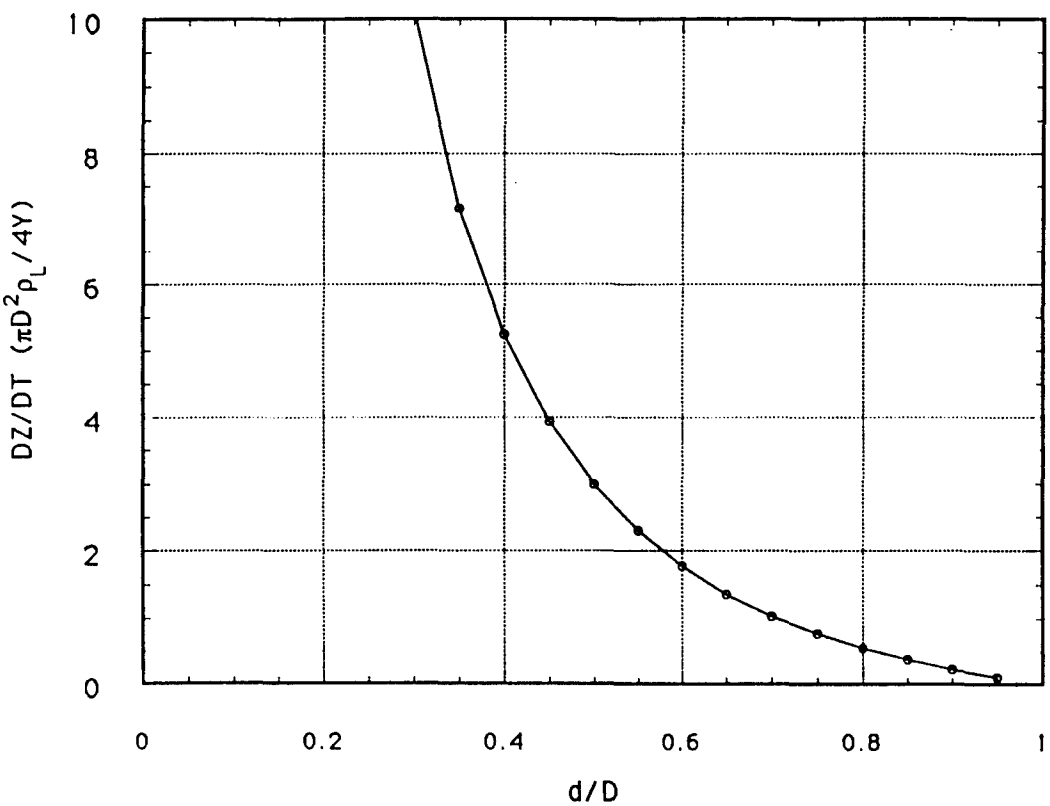

Figure 6. Normalized relationship between crystal pulling and furnace cooling rates based on impirically determined yield. It takes into account melt level drop due to the combined effects of pulling and volumetric changes upon solidification.

An additional complication occurs when crystals are pulled during growth because their radial growth rate depends on the meniscus height. Meniscus height, h, in turn depends on the wetting angle, ϕ, where the melt contacts the crystal [15], Fig. 7:

$$h=\sqrt{\beta(1-\cos\phi)+\left(\frac{\beta\sin\phi}{4r}\right)^2}-\frac{\beta\sin\phi}{4r}.$$

Here, the Laplace constant, β, is given by $\beta = 2\sigma_{LG}/\Delta\rho g$, with σ_{LG} the liquid/gas interfacial free energy, $\Delta\rho$ the difference between the liquid and gas densities, and g the acceleration due to gravity. This equation relates the wetting angle to the meniscus height. The equilibrium interfacial wetting angle, ϕ_{0L}, for a crystal growing at a constant diameter (in an isothermal system) is given by

$$\cos\phi_{0L}\approx\left(\frac{\sigma_{SG}^2+\sigma_{LG}^2-\sigma_{SL}^2}{2\sigma_{SG}\sigma_{LG}}\right),$$

where σ_{LG} is the surface tension and σ_{GS} and σ_{SL} are the average values of the surface free energy of the solid and the solid-liquid interfacial free energy, respectively. [16] Ultimately, however, the position of the freezing isotherm determines meniscus height, and the actual wetting angle, ϕ, may differ from the equilibrium value. When this occurs, there is a radial growth rate component given by

$$\frac{dr}{dt} = \frac{dZ}{dt}\tan(\phi-\phi_{0L}).$$ [17-19]

Small signal, perturbation analysis has been carried out by Surek [17] and Fejer [19] for floating zone geometries ignoring thermal effects, to determine the time dependent response of zone shape to small perturbations. Oscillatory, underdamped behavior is predicted under a broad range of conditions. A complete solution that takes into effect the thermal fields due to conduction, radiation, and convection (mass transport in the melt due to buoyancy and Marangoni effects) is exceedingly complex and has not yet been done. Oscillatory behavior should be expected to occur in this case, as well. It is intuitively obvious that if a crystal is pulled upward more quickly than the rate at which the growth solution adds material to its growth interface, the height of the meniscus must increase, the wetting angle must decrease, the radial growth rate must ultimately become negative, and the diameter of the crystal must decrease until equilibrium is restored. We have observed

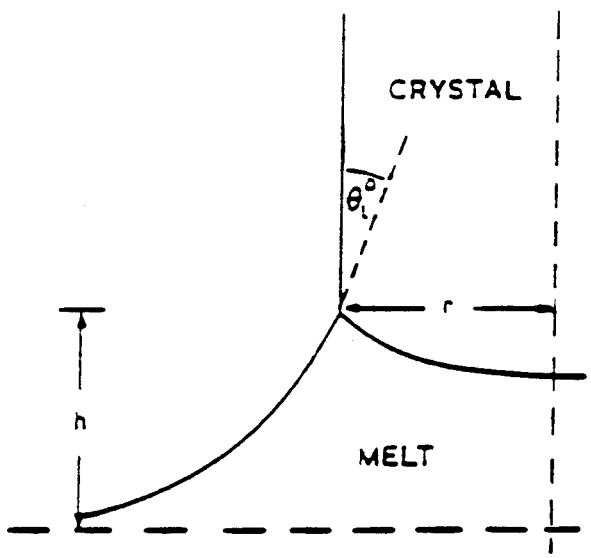

Figure 7. Schematic representation of the meniscus height above the melt in Czochralski and top-seeded solution growth.

that if constant cooling and pulling rates are used and the freezing isotherm is near the melt surface, considerable overshoot always occurs as the crystal is widening to its equilibrium diameter, with the diameter becoming much larger than the pulling/cooling rate can sustain. This is followed by an undercutting process that reduces crystal diameter, as illustrated in Fig. 8. If left unchecked, it may even lead to the crystal pulling out the melt. This underdamped behavior is similar to the diameter instability observed in Czochralski growth from the melt,with the presence of a solvent adding to the system's tendency to instability. [18] Our best results in terms of diameter control were obtained by making cooling/pulling rate adjustments according to the normalized data in Fig. 6 once the crystal reached a suitable diameter. The weakness in this approach lay in the fact that growth system yields were not really constant during growth runs, but varied somewhat due to the crystal's influence on the thermal distribution above the melt surface, and to melt level drop. We were, never-the-less, successful and grew crystals up to 25 mm in height with reasonably constant diameters.

Attempts to achieve diameter control by in-situ weighing using a puller equipped with a high resolution HBM load cell were unsuccessful because it was not possible to decouple the true weight of the crystal from its apparent weight which included the weight of the liquid column. Differential methods can only be used if the height of the growth interface above the melt surface remains constant, and if the crystal's diameter remains constant. Unfortunately, neither can be well-controlled in the TSSG process.

Yields of high quality optical material also depended on the density of inclusions in the core region, and this was controlled by factors relating to melt viscosity and convective stirring at the melt interface. For this reason, alternative growth methods were continually investigated for their potential to increase growth interface stability.

5. Melt Recharging Experiments

Two factors contribute to growth interface instability according to the theory of constitutional supercooling, the relationship between growth rate and temperature gradient ahead of the growth interface, and the effective solute diffusion coefficient in the melt. This seen in the classical equation for the stable growth condition,

$$\frac{R}{G} \leq \frac{kD}{mC_0(1-k)},$$

where R = growth rate, G = temperature gradient in the liquid ahead of the growth interface, k = slope of the liqiudus, C_0 = concentration of the solvent phase in the growth

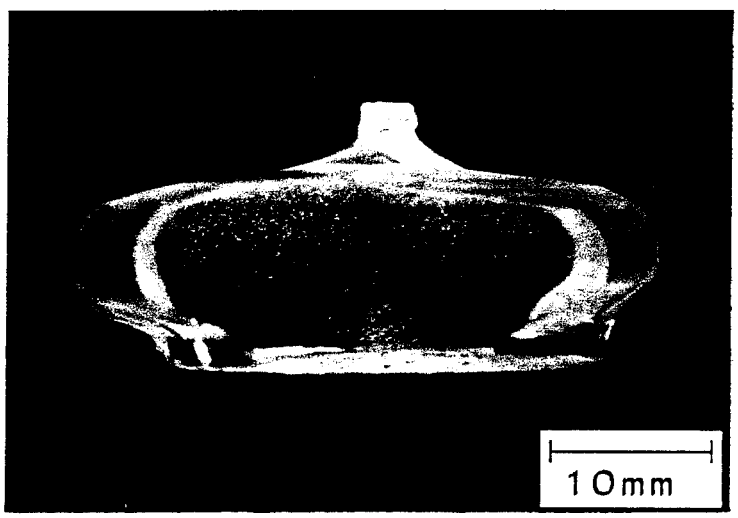

Figure 8. BBO crystals pulled at a constant rate exhibit diameter instability during the widening out process because the meniscus does not rise to its equilibrium height before the crystal diameter has exceeded the equilibrium diameter permitted by thermodynamic solubility and the system cooling rate.

solution, and D = effective solute diffusion coefficient. Since D varies inversely with solution viscosity according to the Einstein-Stokes equation, melts with reduced viscosities were sought. The alternate solvent systems discussed previously were one approach studied. The second was growth under steady-state conditions using melt recharging in order to maintain the melt temperature at the highest temperature possible where its viscosity is known to be the lowest, Fig. 4. The system was configured using a 10 cm OD double crucible configuration after Kitamura et al.[20], shown in Fig. 9, and experiments were aimed at reaching a steady state under isothermal conditions near 925 °C. Unfortunately, we were not able to determine an effective mass transfer function for the system described under apparent equilibrium conditions. (5g of solute added to the annular reservoir at higher temperature did not produce 5g of material added to the growing crystal at lower temperature.) The inability to finely control the growth process in this manner forced us to use slow cooling to initiate growth and produce a crystal several cm in dia. prior to switching to melt replenishment as the driving force. (A similar method was resorted to by Perlov and Roth in their recent melt replenishment studies on BBO.[21]) A histogram of a typical growth experiment is shown in Fig. 10, in which it was found that even with a steady cooling rate of 1 °C/day to provide an additional driving force for crystallization, one-to-one transfer of mass from the reservoir to the growing crystal was not achieved. The crystal after 16 days was not yet gaining mass as fast as mass was being added to the growth solution. (Mass values were estimated using the HBM load cell mounted on the pulling unit, with a constant meniscus height assumed.) It was concluded from these preliminary experiments that other factors such as the influence that the growing crystal exerts on the temperature distribution in the growth system are significant and must be accurately understood before the method can be used to advantage. Additionally, the density of solvent inclusions appeared to be similar to normal TSSG-grown boules and the crystal interface became unstable after 16.3 mm of growth, which was also similar to TSSG results.

The most massive crystals remained those grown by the standard TSSG method with large diameters, slow cooling rates, low pulling rates, and consequently low overall heights. Using this method, β-BaB_2O_4 crystals, free of secondary grains, were successfully grown in sizes exceeding 75 mm diameter and weighing as much as 185 g from melts in the 1.2 Kg range, Fig. 11. The tops of the crystals always contained shallow, well-developed facets reflecting the three-fold symmetry along the c-axis. Growth interfaces varied from concave to convex, depending on growth conditions. Most were smooth and contained three rounded facets.

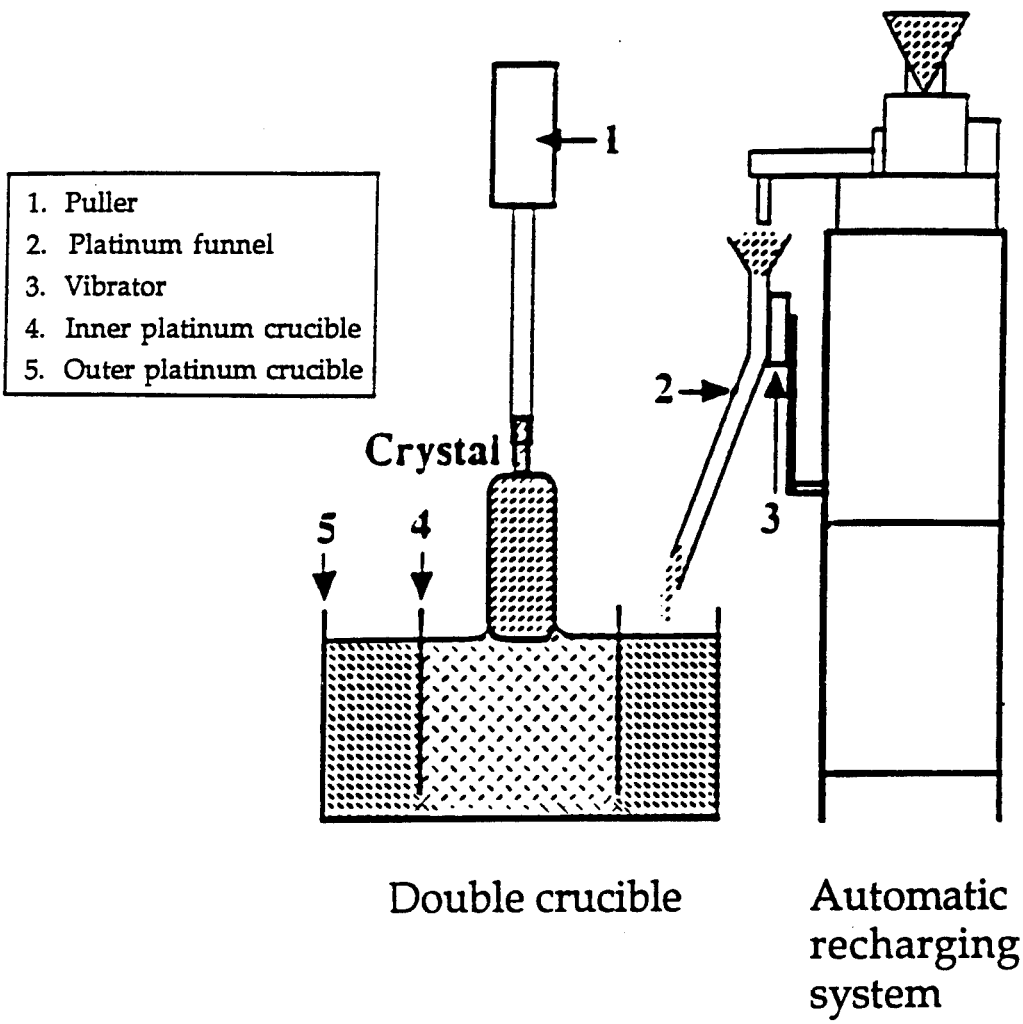

Figure 9. Melt recharging configuration after Kitamura [20] incorporating a concentric double platinum crucible with communication between the two sections, permitting a higher solute concentration to be maintained in the annular region that supplies material to the growth interface by a steady-state concentration gradient.

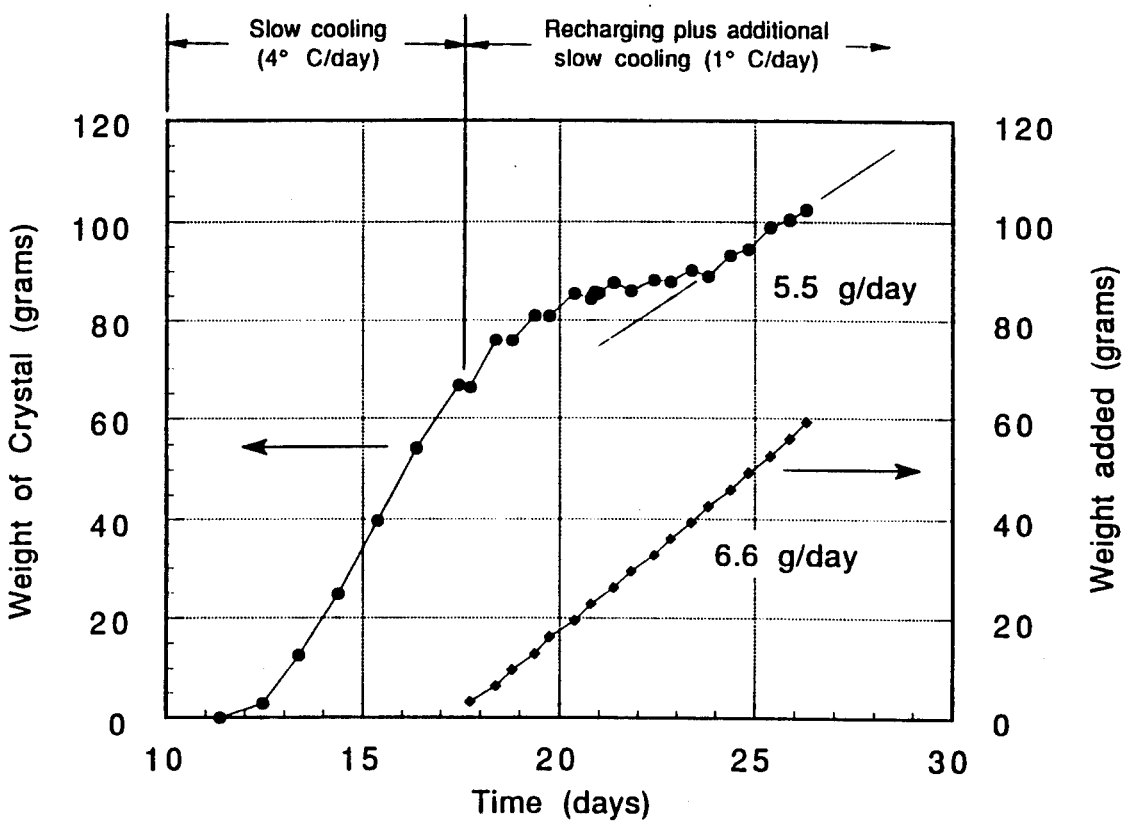

Figure 10. Histogram of a typical melt recharging experiment in which it was found that the BaB_2O_4-Na_2O system has a very sluggish approach to steady-state. After 16 days, the crystal was still not gaining mass as fast as it was being added to the melt.

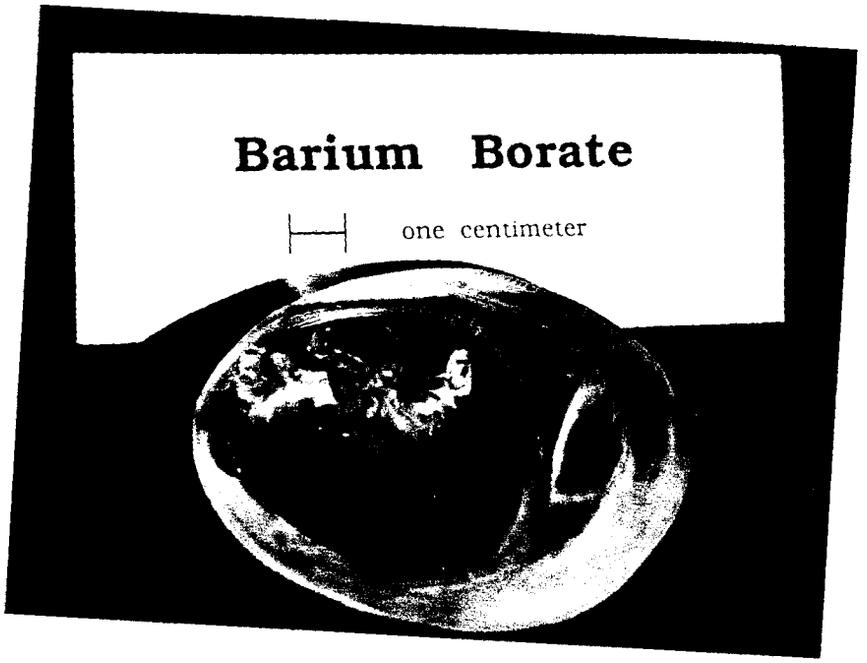

Figure 11. Typical (185 g) BBO crystal grown by the top-seeded solution growth method using slow cooling and slow pulling.

6. Controlling Solvent Inclusions in TSSG BBO Boules

Virtually all c-axis β-BaB_2O_4 crystals contained internal microscopic defects to some degree, with a higher density in the core region, as illustrated in Fig. 8. In a previous program, these defects were studied extensively by optical microscopy, electron microscopy, and electron microprobe analysis. Energy dispersive SEM analysis showed the microscopic defects to be inclusions with the major constituent consisting of sodium.[14] These studies were the first to conclusively demonstrate that the localized scattering defects in β-BaB_2O_4 are caused by small amounts of solvent trapped on the growth interface. (Laser tomographic studies by Mao et al. [22] have since revealed flux-decorated dislocation loops as well in TSSG BBO boules grown from Na_2O solvents.) In an unpublished set of experiments on the effects of seed rotation, better mixing and a greater sweeping of melt across the growth interface were found to reduce inclusions. While uniform rotation rates in the 1-5 rpm range were not particularly effective, computer-controlled periodic reversals in seed rotation did decouple forced convection (sweeping rate) from irregular buoyancy-driven thermal convection and gave us one means to independently control melt sweeping on the growth interface. Although the use of modulated seed rotation rates was complicated and probably not ideal from a commercial point of view, He-Ne laser scattering measurements indicated that major fractions of crystals grown by this method were virtually free of solvent inclusions.

The exact mechanism(s) leading to the formation of solvent inclusions and voids in bulk BBO crystals is(are) still not known with certainty. Although interface instability due to thermal fluctuations and reduced thermal gradients are considered to be the most likely, other possibilities such as insoluble particles in the melt, poisoning of the growth interface by impurities and evolution of dissolved gas at the growth interface cannot be eliminated. This led us to investigate possible chemical interactions between the melts and atmospheric constituents such as CO_2 and H_2O which might create insoluble particles in the melt. (Melts always look somewhat opaque at growth temperatures.) Test crystals were grown by the usual TSSG method in a controlled high purity nitrogen gas atmosphere. Solvent inclusion densities appeared to be reduced by a significant amount, although not totally eliminated from the core region. Under microscopic examination, large regions away from the core region were discovered to be totally free of He-Ne laser scatter, and thus the first solution -grown BBO material that we considered to be totally free of microscopic defects was achieved. The technology for growth under nitrogen, in comparison with modulated seed rotation rate, is fairly simple and it was used routinely during the balance of the program for the TSSG of BBO. A cross-sectional view of an early N_2-grown BBO crystal

is shown in Fig. 12. Significantly larger crystals with very high yields, some exceeding 240 g in mass, have been grown under CNOM.

7. Direct Melt Growth of BBO Crystals

Until 1990, when researchers at NEC [23] reported on a new growth technique which we now refer to as the direct melt growth method, it was thought that cm size β-phase crystals of of BBO had to be grown from solvents like Na_2O at temperatures within their thermodynamic existence range (below the α-β phase transition temperature at 925 °C.) They had extrapolated an earlier study of ours on the metastable growth of BBO fibers from solutions with very low solvent contents, [24] to the metastable growth of BBO fibers with no solvent content at all. [25] This was followed by the discovery that relatively small volume (< 50 cm^3), pure BBO melts which would normally crystallize at 1100 °C could be supercooled and crystallization initiated with a platinum cold finger to yield β-phase material at an apparent growth temperature near 1050 °C. The mechanism was attributed to the Ostwald step rule [26] which predicts step-wise crystallization in solutions such as borates which tolerate large amounts of supercooling. A free energy diagram illustrating this process is shown in Fig. 13. The first publications on the process were very confusing in their physical description of the process and in their emphasis on convoluted melt synthesis procedures to control melt compositions very precisely to the stoichiometric value. Nor, were the initial results particularly impressive in terms of the crystals shown. The significant feature of these works was that the crystals grew stably at 3 mm/hr which is 75 times faster than growth rates obtainable by TSSG.

We began investigating the direct melt growth of BBO which we refer to as "DMBBO" in 1991, because of the higher growth rates it offered. Our initial emphasis was on the question of melt chemistry. Since our established TSSG melt systhesis process relied on commonly available and easy to decompose barium carbonate, we needed to determine if it could be used for DMBBO. The three reactions investigated were:

1.) $BaCl_2 + 2H_2O + 2H_3BO_3 \rightarrow BaB_2O_4 \cdot 4H_2O + 2HCl \rightarrow$

$BaB_2O_4(\beta) + 4H_2O \uparrow$ (NEC) [23],

2.) $Ba(NO_3)_2 + B_2O_3 \rightarrow BaB_2O_4(\beta) + NO_2 \uparrow$ (Sumitomo) [27], and

3.) $BaCO_3 + B_2O_3 \rightarrow BaB_2O_4(\alpha \text{ or } \beta) + CO_2 \uparrow$ (Stanford).

The first reaction was found to produce copious amounts of vapor during the final step of melting and to have a low product yield. The (NEC) authors felt that this particular synthesis process was critical to the growth of β–phase BBO because it yielded polycrystalline β-phase starting material. The second (Sumitomo, solid-state) reaction had

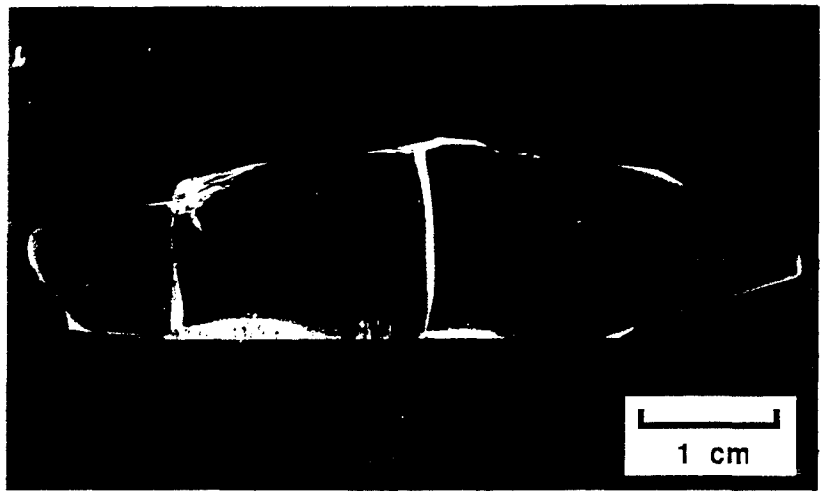

Figure 12. Cross-section under dark field illumination of a BBO crystal grown under nitrogen.

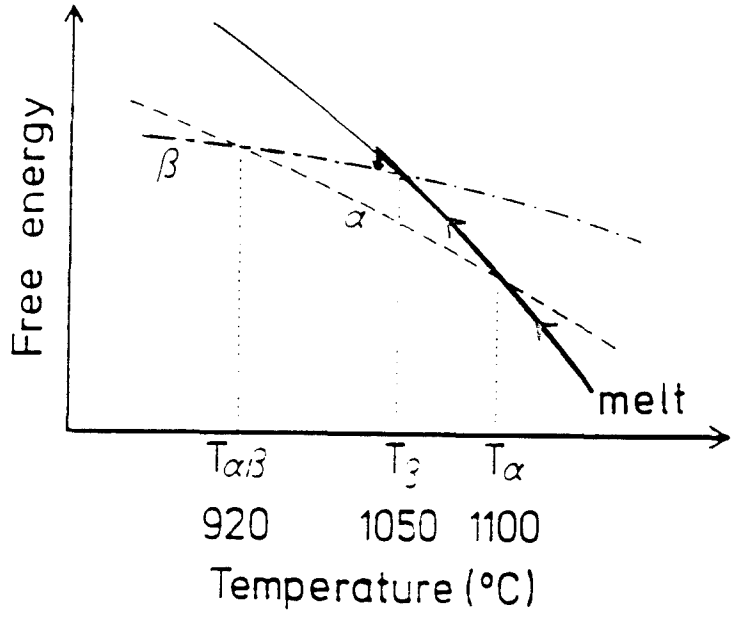

Figure 13. Free energy diagram illustrating Ostwald step-solidification of a supercooled melt to form a metastable β-phase solid even though the α-phase solid has lower free energy.

a higher product yield and also yielded polycrystalline β-phase starting material, but was found to give off corrosive NO_2 vapor which was damaging to the reaction furnace. After some experimentation, we found that carbonate based melts prepared by simple, direct fusion were adequate to produce β-phase crystals by the DMBBO process.

Spontaneously nucleated DMBBO - The furnace configuration used is shown in Fig. 14. We used 67 mm ϕ x 67 m high Czochralski platinum crucibles which were somewhat larger than the typical ~40 mm ϕ crucibles used by the previous authors. Melts were synthesized in the same manner used for TSSG. Spontaneously nucleated DMBBO growth was carried out in the following manner. A pure BBO charge was first taken to the point of just melting and then cooled by several degrees. This caused a small region of supercooled liquid to form on the melt surface in the center of the crucible where the surface temperature is lowest, Fig. 15. A thermocouple measurement of the surface temperature registered values in the range of 1050-1095 °C, depending on the melt height in the crucible and the amount of thermal insulation surrounding the upper part of the furnace. This value was always below BBO's thermodynamic melting point at 1100 °C, a discrepancy that is not currently understood. Spontaneous crystallization did not occur under these circumstances. (BBO melts can be supercooled 100 °C or more before spontaneous crystallization occurs). Generally, the lower the melt level in the crucible, the lower the melting point temperature found. The melts were supercooled anywhere from 5-15 °C, crystallization was initiated by inserting a platinum wire at the coldest point on the melt surface, and pulling was begun. The crystal immediately began to grow out to its equilibrium position which is defined by the melting isotherm, and from then on growth was controlled by slow pulling and slow cooling. We found that both α- and β-phase crystals could be grown this way, depending on the degree of supercooling used. By varying melt heights and the furnace insulation thickness above the crucible, we were able to quantify the thermal gradient conditions under which it was possible to reproducibly grow β-phase BBO from carbonate-based melts.

Typical growth parameters used were 3 mm/hr pulling rate, 10 rpm seed rotation rate, and supercoolings on the order of 6-12 °C. With high melt levels in the crucibles, moderate axial and radial temperature gradients above the melt surface were found, while with low melt levels, low axial and radial gradients were found, Fig. 16. Equilibrium diameters reached soon after nucleation occurred were counter-intuitive. Steeper radial temperature gradients, which would normally cause crystal diameters to remain smaller, resulted in larger equilibrium diameters. Lower radial temperature gradients which would normally permit crystal diameters to grow larger, resulted in smaller equilibrium diameters,

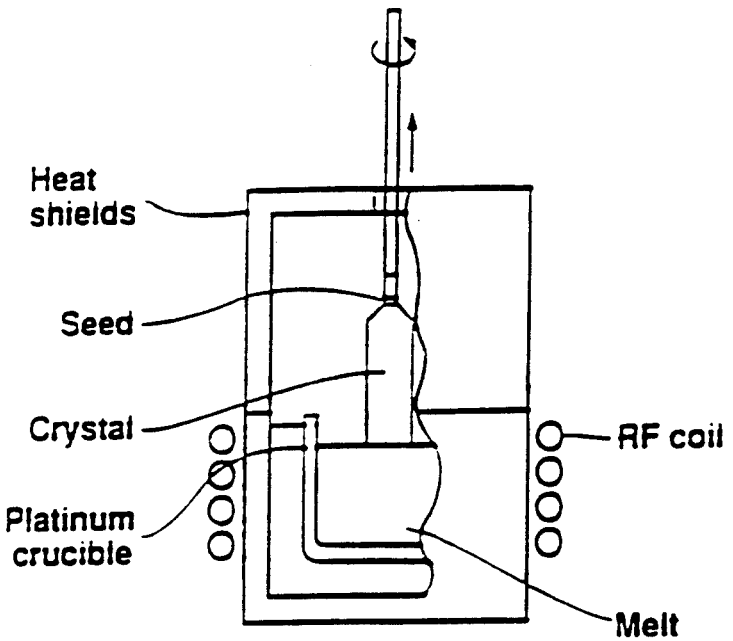

Figure 14. Furnace configuration used for the direct melt growth of spontaneously nucleated BBO crystals.

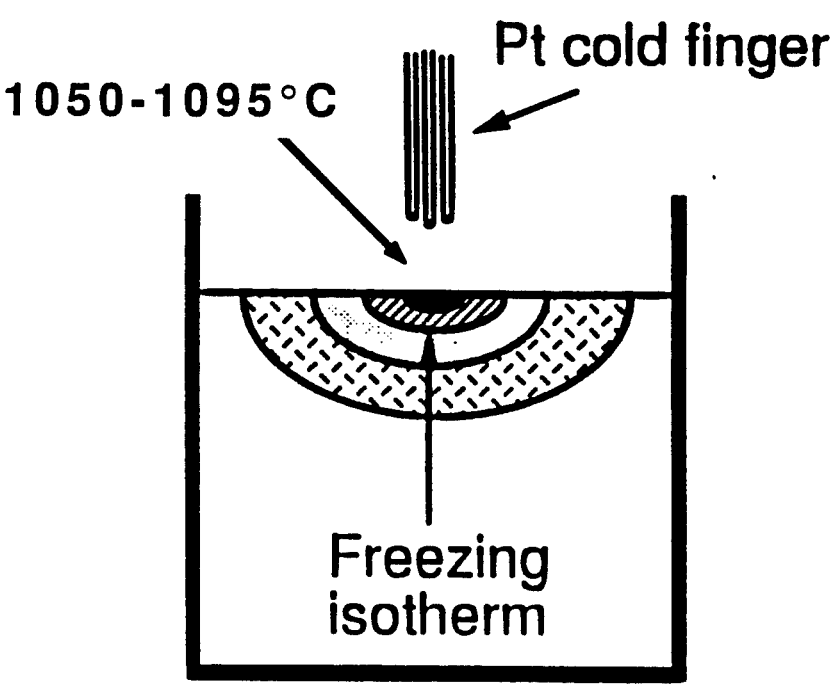

Figure 15. Thermal conditions at the initiation of spontaneously nucleated growth.

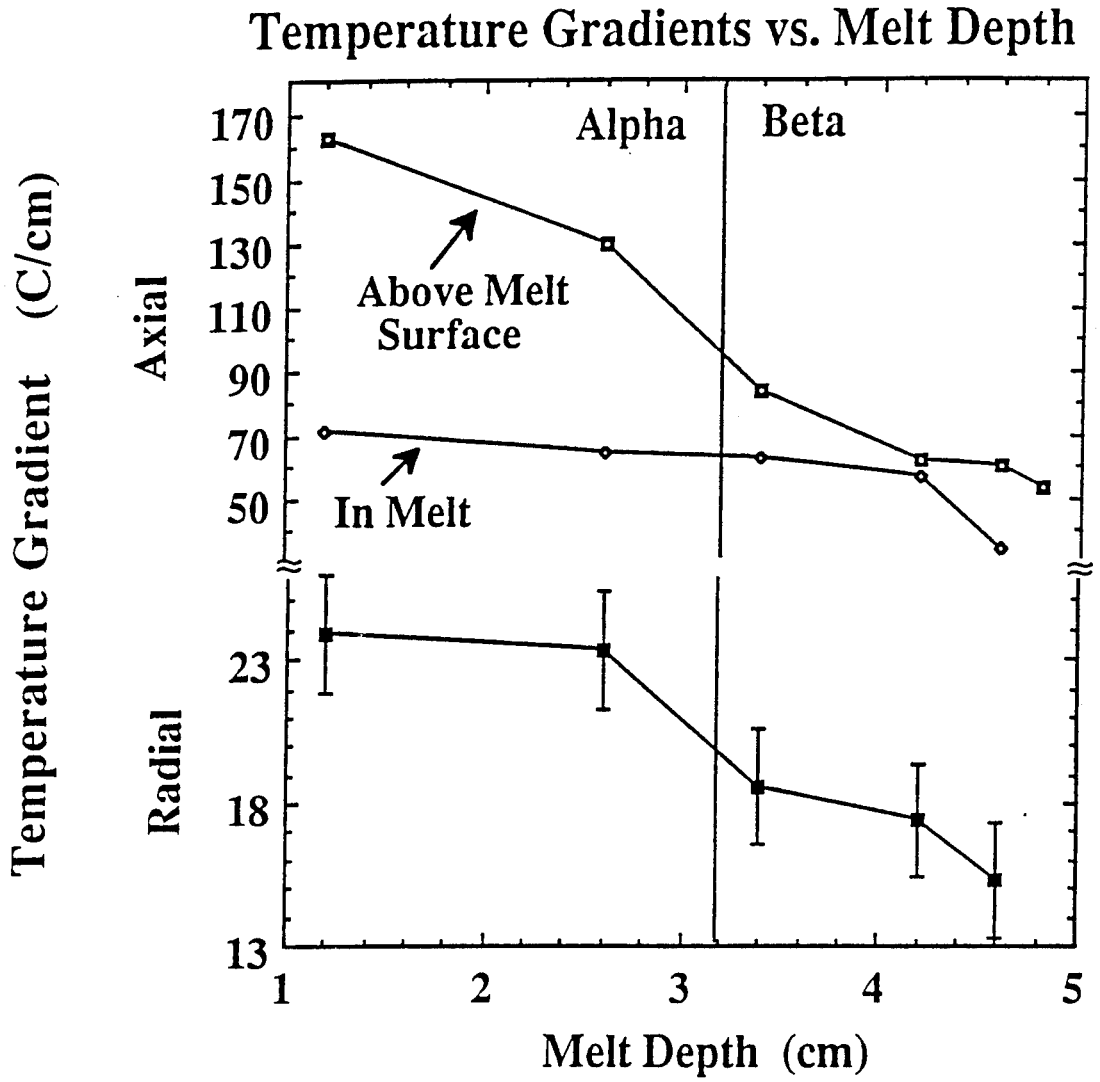

Figure 16. Radial and axial temperature gradients in and above the melts used for the spontaneously-nucleated direct melt growth of BBO.

as shown in Fig. 17. Figure 18 shows the relationship between supercooling and thermal gradient with that of the phase produced and initial equilibrium crystal diameter. Higher supercoolings resulted in β-phase material, while the well-defined boundary between the α- and the β-phase regimes moved toward lower supercoolings with lower melt levels and lower gradients. Neither effect is understood, but both could be caused by temperature-dependent structural changes in the melt that have recently been detected by micro-Raman spectroscopy.[28] For high melt levels in the crucibles, it was necessary to supercool >12 °C in order to produce β-phase material. Lower supercoolings resulted in α-phase crystals.

During growth, crystals spontaneously undercut until they ultimately lost contact with the melt surface unless the melts were simultaneously cooled at 1-5 °C/hr. With slow cooling, it was possible to prevent pull-out and control the necking-in process to effect the selection of a single grain. Then, with continued slow cooling, the crystals were widened back out for (single) crystal growth. This behavior is illustrated in Fig. 19a. Low melt levels and reduced equilibrium crystal diameters led to better control of the necking-in process, and in this way, the growth of spontaneously nucleated single crystal β-phase BBO was accomplished. The necking-in process was not always successful in selecting a single grain, and crystals containing more than one inevitably cracked during cooling due to differential expansion between grains. Fig. 20 shows a 105 g DMBBO boule that contained a minor secondary grain and fractured in the manner shown. This crystal was significantly more massive than any reported in the literature, and considerable amounts of high optical quality material up to 1 cm in length could be obtained. The biggest problem with relying on spontaneous nucleation and grain selection was that even single grain crystals whose growth direction deviated significantly from the c-axis were found to crack during cooling due to grown-in radial strain gradients and BBO's easy cleavege along the basal plane, as shown in Fig. 19b.

Seeded DMBBO - The fact that the yield and growth direction of spontaneously nucleated BBO crystals could not be controlled during growth from a platinum wire led us, during the last year, to investigate the use of c-axis β-phase seeds to initiate growth. The advantages of oriented growth are 1.) total avoidance of polycrystallinity, 2.) reduced strain caused by thermal asymmetry, and 3.) improved control over crystal diameter and length. The requirements are 1.) that the β- to α-phase transition be prevented from occurring in the seed as it is brought into contact with the melt surface, 2.) that surface imperfections on the surface of the seeds be minimized in order to reduce the likelihood of nucleating the α- to β– phase transition or the seed cracking during growth and post-growth cooling, and 3.) that the melt wet the seed at a sufficiently high temperature that an equilibrium liquid-solid interface is formed and epitaxial growth occurs. Experiments on (β-phase) seed stability vs

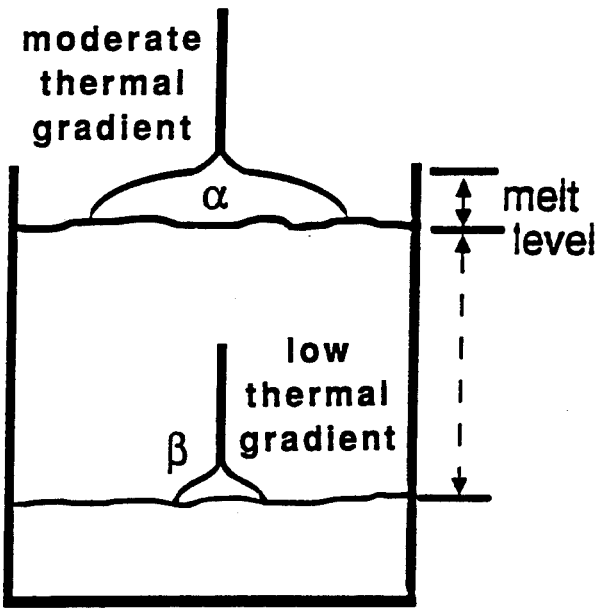

Figure 17. Illustration of melt level effects on equilibrium crystal diameter and radial temperature gradient.

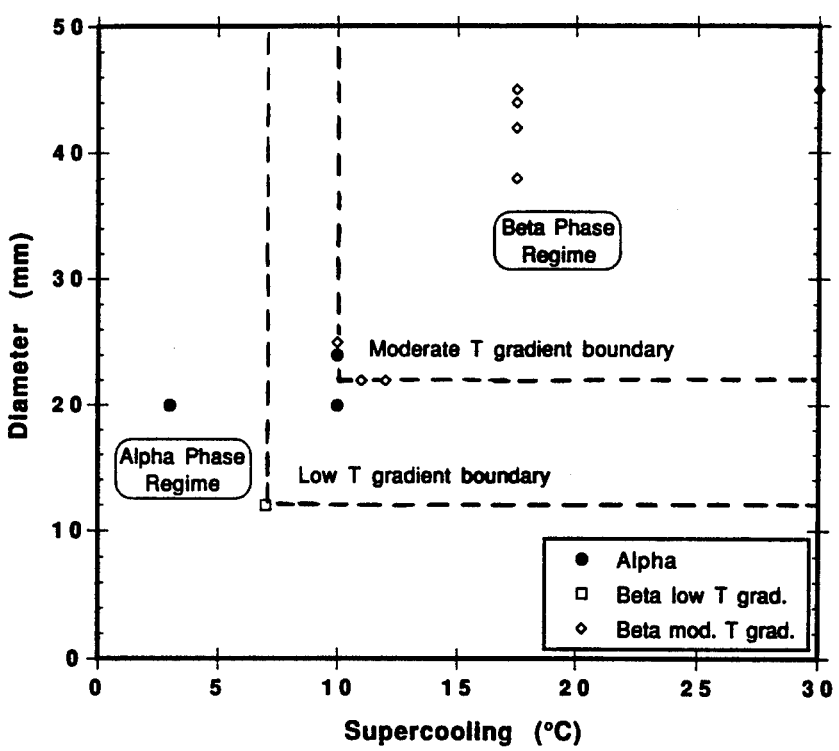

Figure 18. Relationship between supercooling and equilibrium crystal diameter for moderate radial temperature gradient (high melt level) conditions and for low thermal gradient (low melt level) conditions.

A.)

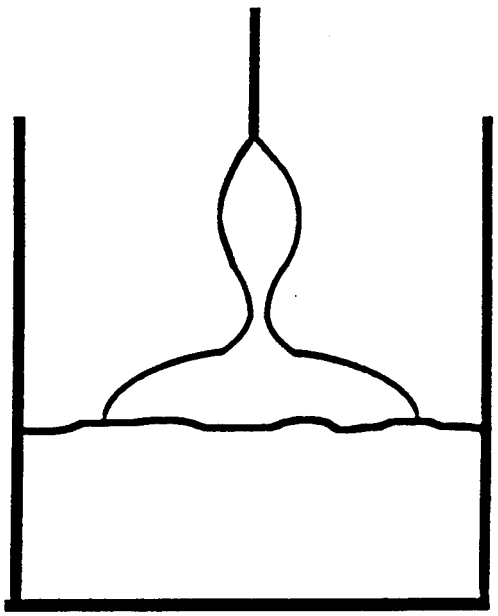

B.)

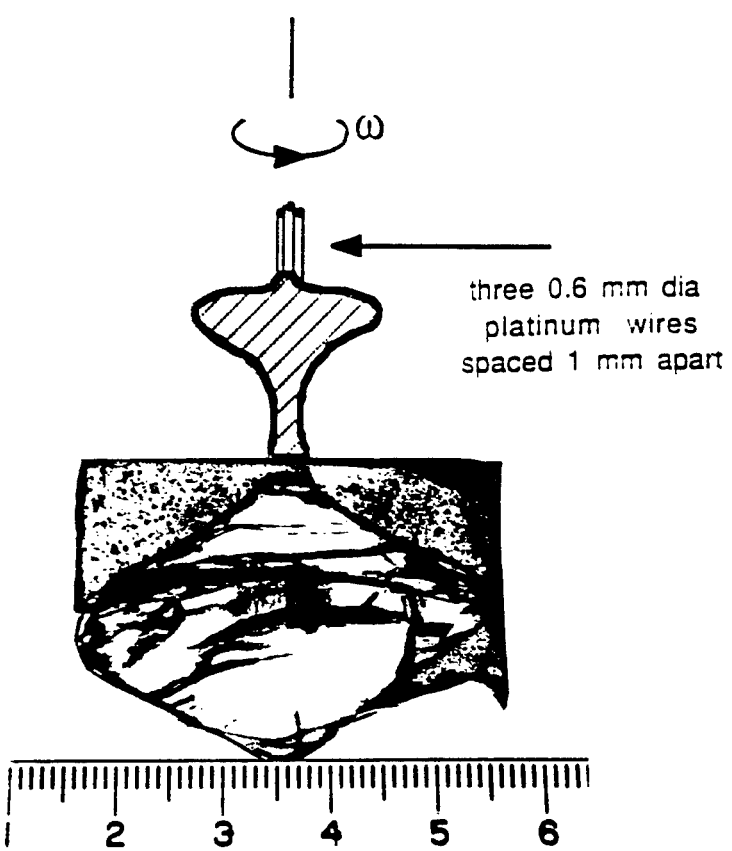

Figure 19. A.) Illustration of growth initiation and grain selection by necking-in under low melt level, low thermal gradient conditions, B.) Cross-section of off axis single crystal that cracked due to radial strain.

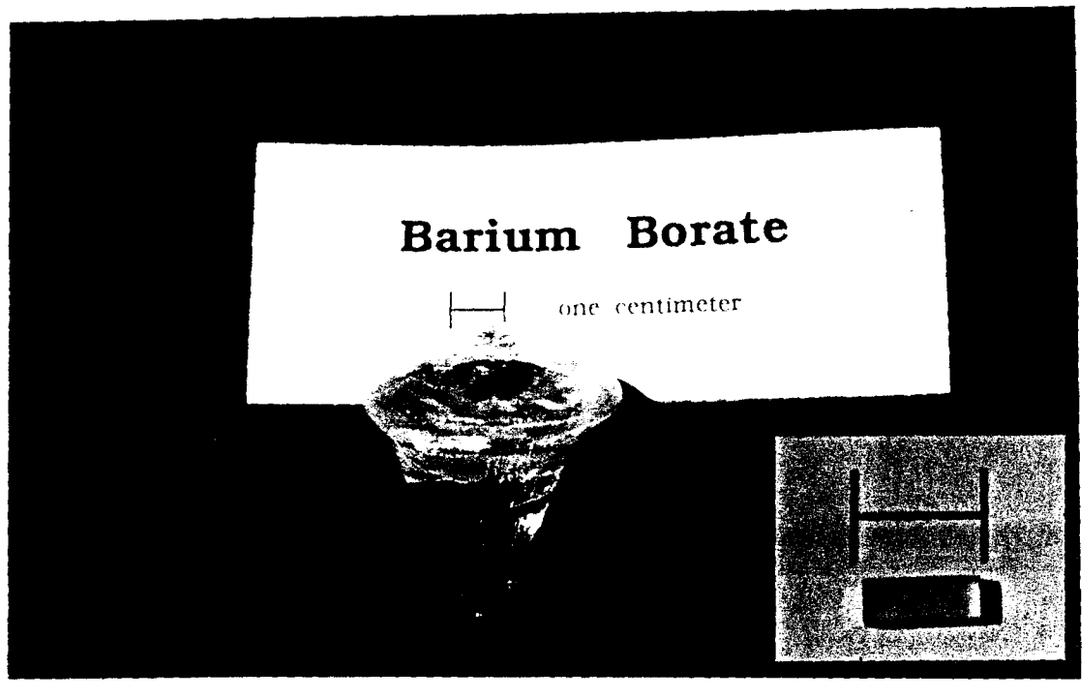

Figure 20. DMBBO crystal grown by the necking-in technique. Grain selection was unsuccessful in this case, and the resultant fractures along the basal planes were caused by differential thermal expansion stresses which result from inevitable radial temperature gradients present durning growth coupled with BBO's highly anisotropic physical properties.

temperature indicated that the seeds should be maintained below ~1050 °C to avoid the region where the α-β phase transition kinetics increase rapidly, Fig. 21. Fortunately, above the melt surfaces, temperature gradients on the order of 50-100 °C/mm were found, Fig. 22, and at only two mm above the surface, seed temperatures were already below 975 °C. In this temperature range, the phase transition kinetics are very sluggish and seeds could be maintained in the β-phase for periods exceeding one hour.

Experiments were carried out with 3.6 mm, square cross-section, c-axis seeds fabricated from TSSG boules. Seed surfaces had been finished by fine grinding with 600 grit paper, and they were used as-is with only the corners chamfered, as well as after polishing by abrasive and chemical methods. (Virtually all seeds used for both these studies and the TSSG studies contained macroscopic solvent inclusions.) An air cooled seed with the configuration shown in Fig. 23 was used to maintain the seed as cool as possible during initiation of growth. Initially, we tried air flow rate as a control variable to influence radial gradients and initial equilibrium crystal diamter. With the cooled seed rod, however, we were unable to achieve seed wetting, and it was abandoned in favor of an uncooled alumina seed rod.

None of the experiments carried out were successful in achieving β-phase, c-axis seeded crystals. In most cases, transverse cracks developed at the time the seeds contacted the melt surfaces. Deeper immersion to melt off the cracked material only generated further cracking. This was thought to be a problem as it would reduce thermal conductive cooling of the seed and increase the likelyhood of phase conversion. (Other researchers have now verified that seed cracking inevitably results in the growth of α-phase material.[28]) In addition, because we were in a "learning phase," most growth experiments were carried out with insufficient superhheating to achieve adequate seed melt-back at the initiation of growth. This resulted in a polycrystalline region which led to the growth of α-phase crystals, exactly like the spontaneously nucleated case with small amounts of undercooling. Seeds always developed a series of transverse cracks during cooling, also illustrated in Fig. 23, which led to seed disintegration. Analysis of seed remnants revealed only XRD β-phase lines, though the surfaces appeared to be covered by a thin "skin" of unknown composition/structure. Our best result, a near c-axis, α-phase single crystal is shown in Fig. 24.

(By actively pursuing the groundwork described here, the growth of c-axis seeded DMBBO crystals has since been solved under follow-on funding through the Center for Nonlinear Optical Materials (CNOM) at Stanford with principal support from ONR - N00014-92-J-1903, and the techniques are described under that program's auspices.) The history of the DMBBO is summarized in Table 1.

Table I. History of the Direct Melt Growth of BBO

1988	Stanford (Tang et al) [24]	Very little solvent needed to grow β-phase under relatively steep temperature gradients (LHPG process).
1990	NEC (Kuwano et al) [30]	First report of DMBBO at CLEO. Synthesis of β-phase starting materials from chlorides. Controlled emperature gradient important. Growth rates 50 x TSSG (3-5 mm/hr).
1990	TIT and NEC (Itoh et al) [23]	Growth at 1040/1050° C under metastable conditions. Nucleation on Pt wire.
1991	NEC and TIT (Kouta et al) [31]	Melts age, and superheating gives α-phase. β powder stable to 1090° C. $\Delta T/\Delta z$ = 180° C/mm
1991	Sumitomo (Kôzuki et al) [27]	Sintered nitrate melts also works. Growth at ≤1048° C. $\Delta T/\Delta z$ = 10° C/mm.
1993	NEC (Kouta et al) [32]	α- or β-phase starting material gives β-phase, implying melt structure not important.
1993	Stanford	Carbonate melts synthesized by direct fusion. $\Delta T/\Delta z$ = 40° C/mm. >100 g boules, strained if polycrystalline.
1993	IEMT (Lukasiewicz et al) [29]	MRS Boston, oral presentation. High quality boules using c-axis seeds. Moderate temperature gradients of 14° C/cm.
1994	SONY (private communication)	C-axis seeding sufficiently reproducible for production of all solid-state UV source. Crystals 20 mm ϕ x 8 cm long. Reduced UV degradation in seeded DMBBO crystals (?).
1994	NEC (private communication)	C-axis seeding reproducible for small size crystals. Crystals 15 mm ϕ x 4-5 cm long.

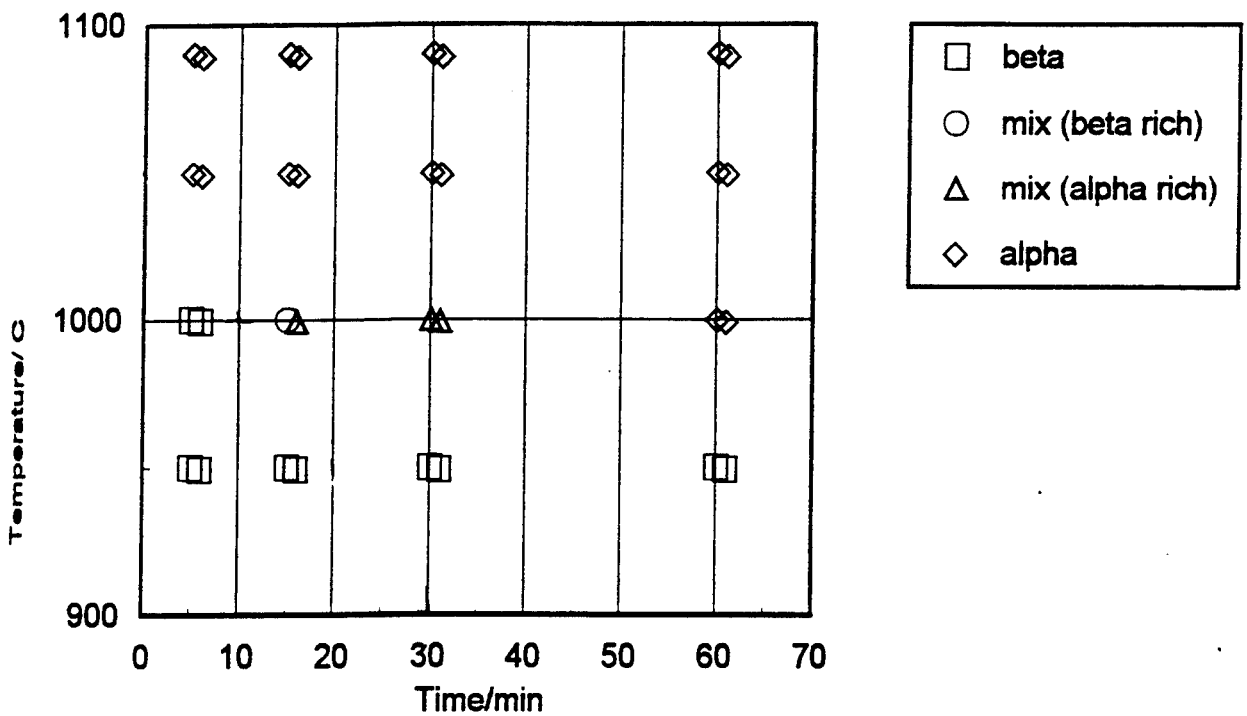

Figure 21. Time dependence of the β to α phase transformation occurring in bulk BBO. β-BBO crystals begin to undergo phase converstion at 1050 °C after only a few minutes.

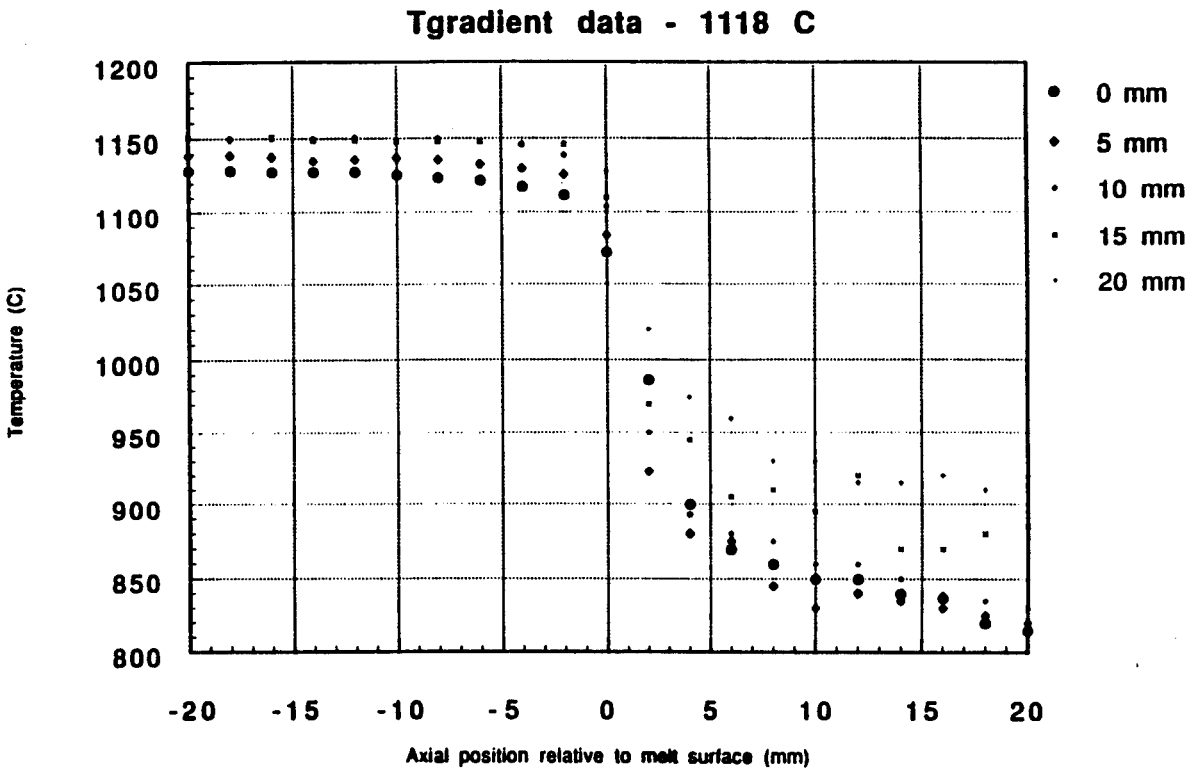

Figure 22. Axial and radial temperature distribution relative to the melt surface in the DMBBO growth furnace.

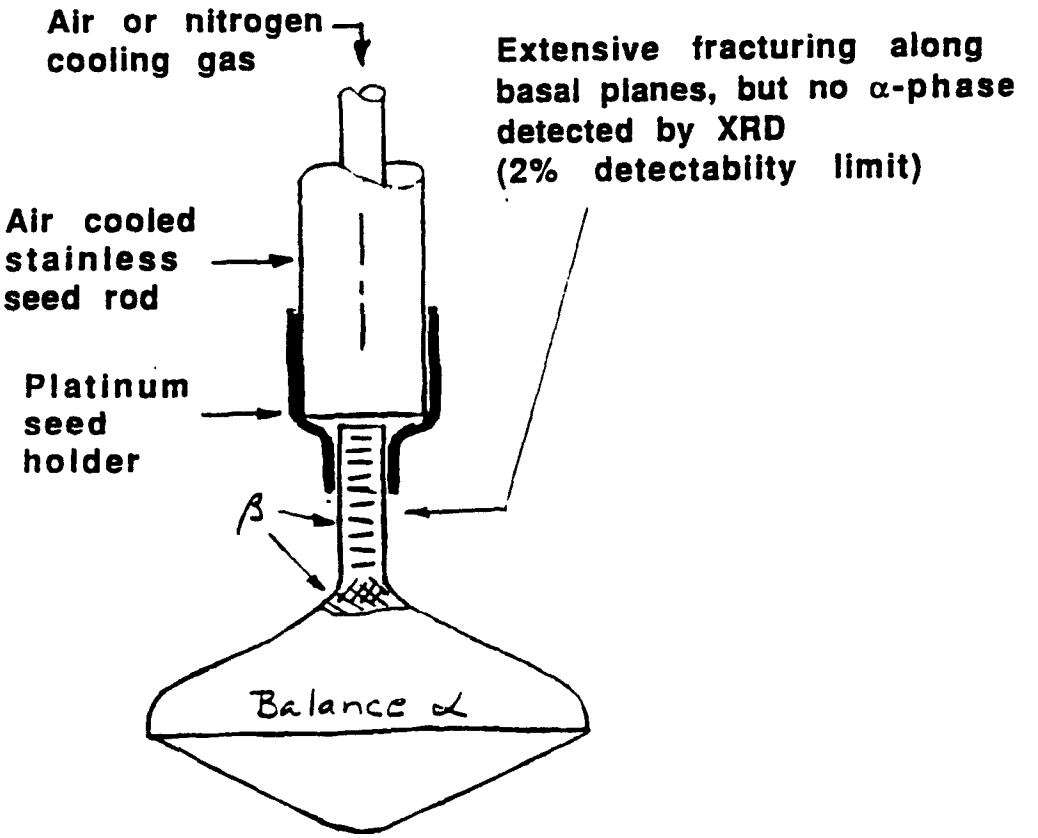

Figure 23. Illustration of our results using an air-cooled seed rod to prevent phase conversion of the seed during its introduction into the melt at the initiation of growth. In all cases, a cold dip occurred, the resulting crystal was α-phase, and the seed disintegrated during cooling even though it had not apparently not undergone a phase transition.

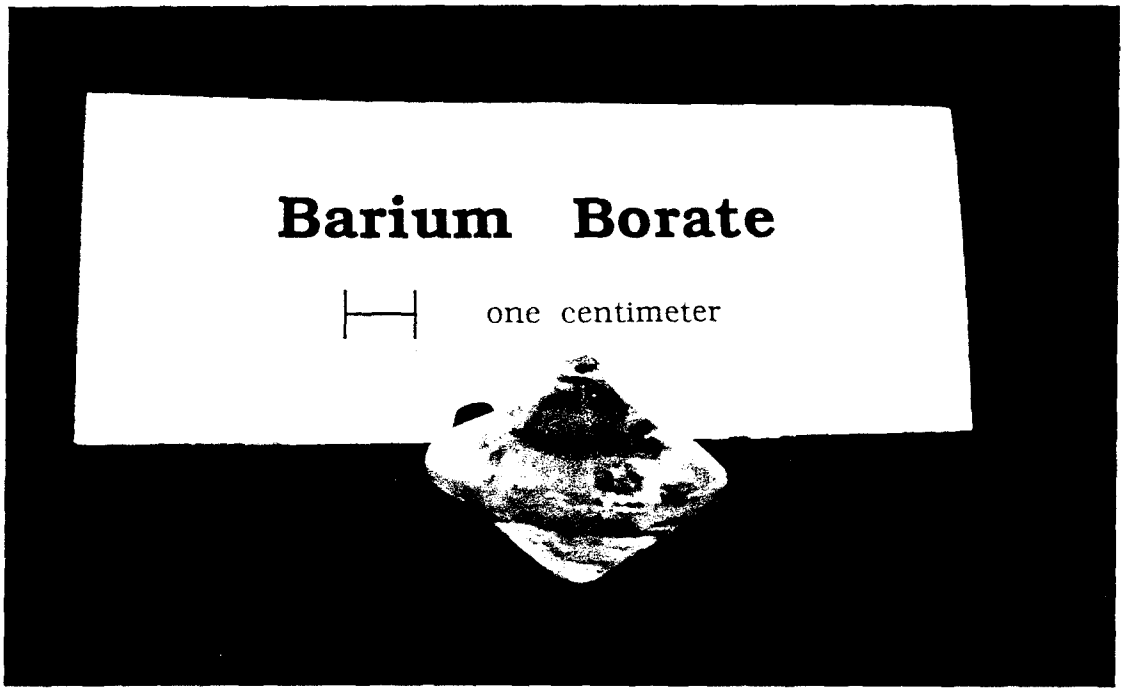

Figure 24. Single crystal, α-phase BBO boule that was grown on a c-axis seed from a cold dip.

8. UV Absorption Mechanisms in BBO Crystals

The most significant problem with BBO crystals after variable concentrations of scattering centers (microscopic solvent inclusions) is UV absorption and UV damage. Far less has been documented in these two areas beyond anecdotal feedback from commercial users. Crystals typically "degrade" over time under intense illumination at wavelengths shorter than 400 nm. [33,34] Both permanent surface and partially reversible bulk effects have been seen, but the actual "damage" mechanisms are not known. During the course of this program, we collaborated with Cleveland Crystals, Inc. and Aculight Corp. on measuring UV absorption and UV fluorescence in DMBBO and TSSG-BBO material. UV damage studies were not carried out because of the difficulty in standardization. Nonlinear (two-photon?) absorption illustrated in Fig. 25 was found in all crystals studied, including both TSSG and DMBBO crystals. Typical absorption coefficients under 266 nm, high intensity illumination were in the range of 0.20-0.45 cm^{-1}, and these values were similar to absorption coefficients found in crystals from other commercial sources, some of which are also shown. Weak visible fluorescence under 266 nm illumination was also observed in all crystals.

To elucidate possible causes such as point defects due to impurities in the starting materials, we carried out melt purity studies on stoichiometric BBO melts synthesized from 4Ns and 5Ns $BaCO_3$ and $Ba(NO_3)_2$. (Barium compounds are the most likely source of impurities in the growth process, followed by contamination from the furnace itself which we did not think likely because our furnace was constructed of high purity refractory components.) Arc emission spectrographic analysis, mass spectrographic, and inductively-coupled plasma emission spectrographic analysis were carried out using different vendors. Except for anomolous levels of europium detected by ICP, no significant or consistent contaminant was detected in newly synthesized melts or in grown crystals. Although differences in UV fluorescence were seen between α- and β-phase DMBBO crystals grown from the same high purity melts, blue and pink, respectively, no other correlations were found. A more thorough analysis is clearly needed as the UV performance of BBO under moderate to high power conditions is the key to commercial utilization of this material.

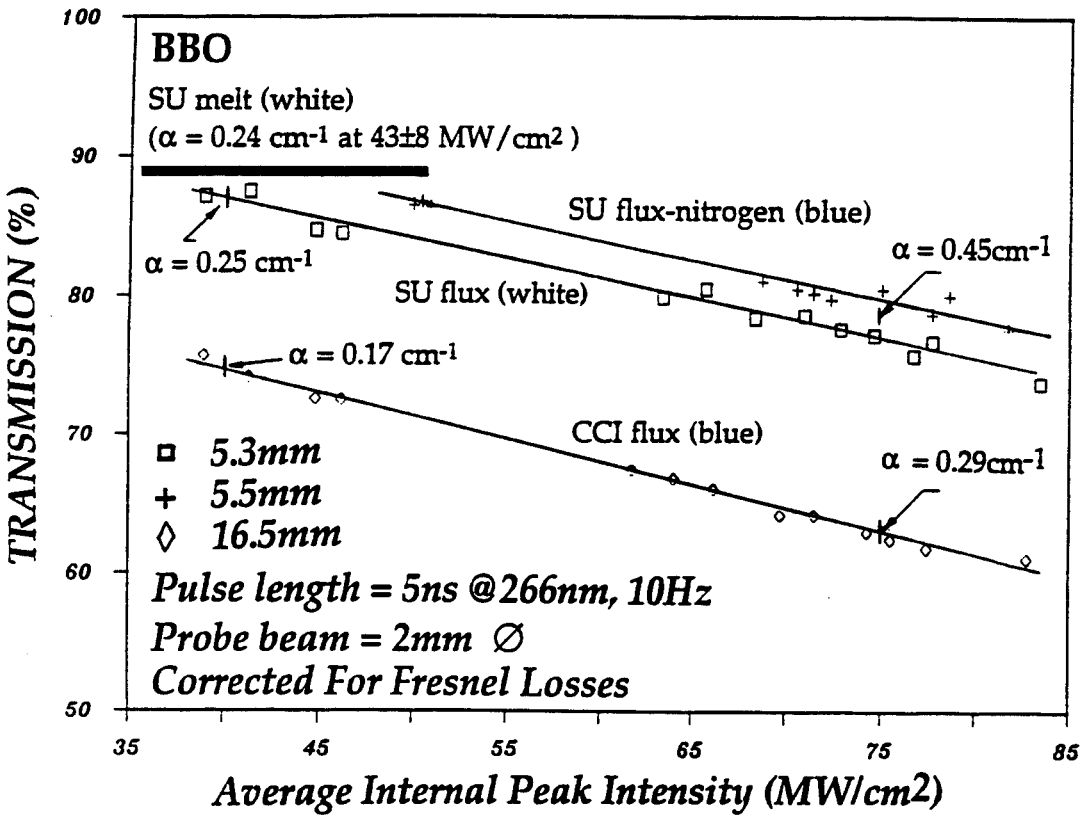

Figure 25 Nonlinear (multi-photon?) optical absorption measurements at 266 nm made at Cleveland Crystals, Inc. on BBO boules grown in different laboratories using different growth methods. Similar behavior is seen in virtually all BBO boules, but it is not yet known if, or how, it relates to optical degradation.

9. Summary of Results

1. Large c-axis single crystals of β-BaB_2O_4 were grown from 80 at % BaB_2O_4 - 20 at % Na_2O solutions using the top-seeded solution growth method.
2. An efficient top-seeded solution growth process was developed and the technology transfered to both Cleveland Crystals, Inc. and INRAD during the course of the program.
3. Optical defects were found to be controllable by effective sweeping of the melt across the growth interface combined with a nitrogen atmosphere in the furnace, and the first laser-scatter-free BBO material to be grown in the US was produced in this way.
4. Sodium fluoride was found to be a superior flux compared to sodium oxide if its higher volatility under nitrogen can be controlled.
5. The first (and also the largest reported) spontaneously nucleated, direct melt-grown BBO crystals to be grown in the US were accomplished.
6. Confusing issues about the DMBBO process were resolved, and quantifiable conditions under which the low temperature β-phase can be reproducibly grown using commercially compatible methods were determined.
7. Nonlinear UV absorption in virtually all commercially available BBO, as well as Stanford-grown BBO, was characterized, and the need for continued research on UV absorption and "damage" mechanisms was recognized.

10. References: Part A

1. C.-T. Chen, B. Wu, G. You, and Y. Huang, "High-efficiency and wide-band second-harmonic generation properties of new crystal β-BaB_2O_4," Dig. Tech. Papers XIII IQEC, Paper MCC5 (1984).

2. C. Chen, B. Wu, A. Jiang, and G. You, "A new type ultraviolet SHG crystal β-BaB_2O_4," Sci Sinica (Ser B) **28**, 235 (1985).

3. J.-K. Zhu, B. Zhang, and S.-H. Liu, "A study of second harmonic generation coefficients and ultraviolet absorption edge of barium borate crystal," SPIE Conf. on basic properties of Optical Materials, Gaithersburg, Md, May 7-9, 1985.

4. K. Kato, "Second-harmonic generation to 2048 A in β-BaB_2O_4," IEEE J. Quantum. Electron. **22**, 1013 (1986).

5. K. Miyazaki, H. Sakie, and T. Sato, "Efficient deep-ultraviolet generation by frequency doubling in β-BaB_2O_4 crystals," Opt. Lett. 11, 797 (1986).

6. G. Zhang, C. Jin, F. Lin, C. Chen and B. Wu, "Second harmonic generation of a copper vapor laser by using a beta-barium borate (BaB_2O_4) crystal," Guangxue Xuebao 4, 513 (1984).

7. C. Chen, Y. X. Fan, R. C. Eckardt, and R. L. Byer, "Recent developments in β-BaB_2O_4," SPIE Conf. on Lasers, San Diego, Calif., July 1986, Proc. SPIE 684(4) (to be published).

8. J. Liebertz and S. Stahr, "Zur tieftemperaturphase von BaB_2O_4," Z. Kirstall. 165, 91 (1983).

9. E. M. Levin and H. F. McMurdie, "The system BaO-B_2O_3," J. Res. Natl. Bur. Stand. 42, 131 (1949).

10. Q.-Z. Huang and J.-K. Liang, "The crystal growth of barium borate low temperature phase and the study of phase diagrams of related systems," Acta Physica Sinica 30(4), 559 (1981).

11. V. Nikolov and P. Pehshev, "On the growth of β-BaB_2O_4 (BBO) single crystals from high temperature solutions: I.Study of the BaO-Na_2O-B_2O_3 system," J. Solid State Chem. 96, 48 (1992).

12. V. Nikolov and P. Pehshev, "On the growth of β-BaB_2O_4 (BBO) single crystals from high temperature solutions: II. Physiochemical properties of BBO solutions and estimates of the conditions for stable growth" J. Solid State Chem. 97, 36 (1992).

13. Y. S. Oseledchik, V. Osadchuk, A Prosvirnin and A Selevich, "Growth of high-quality barium metaborate crystals from Na_2O-NaF solution," J. Crystal Growth 131, (1993).

14. R. S. Feigelson, R. J. Raymakers and R. K. Route, "Solution growth of barium metaborate crystals by top seeding," J. Crystal Growth 97, 352-355 (1989).

15. S. V. Tsvinskii, Inzh. Fiz. Zhur. 5, 59 (1962).

16. W. Bardsley, G. W. Green, C. H. Holliday and D. T. J. Hurle, J. Crystal Growth 16, 277 (1972).

17. T. Surek and S. R. Coriell, "Shape stability in float zoning of silicon crystals," J. Crystal Growth 37, 253 (1977).

18. D. T. J. Hurle, "Surface aspects of crystal growth from the melt," Adv. in Colloid Interface Sci. 15, 101 (1981).

19. M. M. Fejer, "Single Crystal Fibers: Growth Dynamics and Nonlinear Optical Interactions," Ph. D. dissertation, Stanford University (1986).

20. K. Kitamura, J. K. Yamamoto, N. Iyi and S. Kimura, "Stoichiometric $LiNbO_3$ single crystal growth by double crucible Czochralski method using automatic powder supply system," J. Crystal Growth 116, 327 (1992).

21. D. Perlov and M. Roth, "Isothermal growth of β-barium metaborate single crystals by continuous feeding in the top-seeded solution growth configuration," J. Crystal Growth 137, 123 (1994).

22. H. Mao, Q. Tan, B. Wu and C. Chen, "Characteristics of dislocations in beta-barium metaborate bulk crystals investigbated via light scattering tomography," Appl. Phys. Lett. 58, 1149 (1991).

23. K. Itoh, F. Marumo and Y. Kuwano, "β-barium borate single crystals grown by a direct Czochralski method," J. Crystal Growth 106, 728 (1990).

24. D. Y. Tang, R. K. Route, and R. S. Feigelson, "The Growth of Barium Metaborate (BaB_2O_4) Single Crystal Fibers by the Laser-Heated Pedestal Growth Method," J. Crystal Growth 91, 81 (1988).

25. N. Onishi, Ceramics (Japan) 24, 319 (1989).

26. W. Ostwald, Z. Physik. Chem. 22, 289 (1897).

27. Y. Kozuki and M. Itoh, "Metsastable crystal growth of the low temperature phase of barium metaborate from the melt," J. Crystal Growth 114, 683 (1991).

28. Y. K. Voronko, A. V. Gorbachev, V. V. Osiko, A. A. Sobol, R. S. Feigelson and R. K. Route, " Correlation of the structure of melts and crystals of alkali and alkali earth borates: the crystallization behavior of barium metaborate," J. Physics and Chemistry of Solids 54, 1579 (1993).

29. Private communication with T. Lukasiewicz [Inst. Electronic Mats. Tech., Warsaw, Poland] at the 1993 MRS Symposium (Boston).

30. Y. Kuwano and H. Kouta, "β-BaB_2O_4 crystals grown by a new method," CLEO collected abstracts CTH129 (1990).

32. H, Kouta, S. Imoto and Y. Kuwano, "β-BaB_2O_4 single crysals growth by Czochralski method using β-BaB_2O_4 and β-BaB_2O_4 single crystals as starting material," J. Crystal Growth 128, 938 (1993).

33. Private communication with R. Blackman [Crystal Technology, Inc.]

34. Private communication with R. Zare [Chemistry Dept., Stanford University]

B. LITHIUM BORATE

1. Objectives

Program objectives relating to lithium borate (LBO) were twofold: 1.) developing a reproducible growth technonogy for LBO that could be applied in a commercial setting, and 2.) cooperating with device researchers at Stanford and elsewhere in determining the device potential for LBO crystals.

2. Background

Lithium triborate (LiB_3O_5), commonly known as LBO, is a relatively new nonlinear optical material that combines wide transparency extending into the UV, moderately large nonlinear optical coefficients, high laser damage threshold and good chemical/mechanical properties. The advantageous nonlinear optical properties and potential applications of this material were first reported by Chen et al in 1989 [1] as an extension of his work on BBO. High conversion efficiencies have been demonstrated in noncritical second harmonic conversion of 1.064 μm radiation in high peak power, Q-switched operation, [2] and in high average power, cw operation. [3] In 1990, crystals became available in limited sizes, on the order of one centimeter maximum, on the commercial market. However, when this program began, there were no sources available in this country and researchers in nonlinear optics had to rely on a few crystals from the PRC and university-based crystal growth efforts such as ours.

LBO was first reported by Mazetti and Carli in 1926 [4], and later by Rollet and Bouaziz [5] in 1955. In 1978, Konig and Hoppe [6] determined the crystal structure of the 1-3-5 phase which is orthorhombic, belonging to space group $Pbn2_1$. The structural elements that make up LBO are $(B_3O_7)^{5-}$ rings in which one of the three borons is tetrahedrally coordinated. The rings, which form endless spiral chains along the c-axis, are responsible for the large out-of-plane z-component in the second order polarizability that makes non-critical phasematched interactions possible.

Lithium borate has good mechanical properties: it is slightly harder than BBO (6 vs. 4.5 on the Moh scale, respectively), it polishes well, and in contrast to BBO, its surfaces do not degrade with time due to reactivity with water vapor in the ambient atmosphere.

3. Phase Equilibria

In 1958, Sastry and Hummel [7, 8] published the first accurate determination of the phase equilibria in the Li_2O-B_2O_3 pseudobinary system, Fig. 1. They were the first to grow small needles of the 1-3-5 phase, which they solidified from excess B_2O_3 solution,

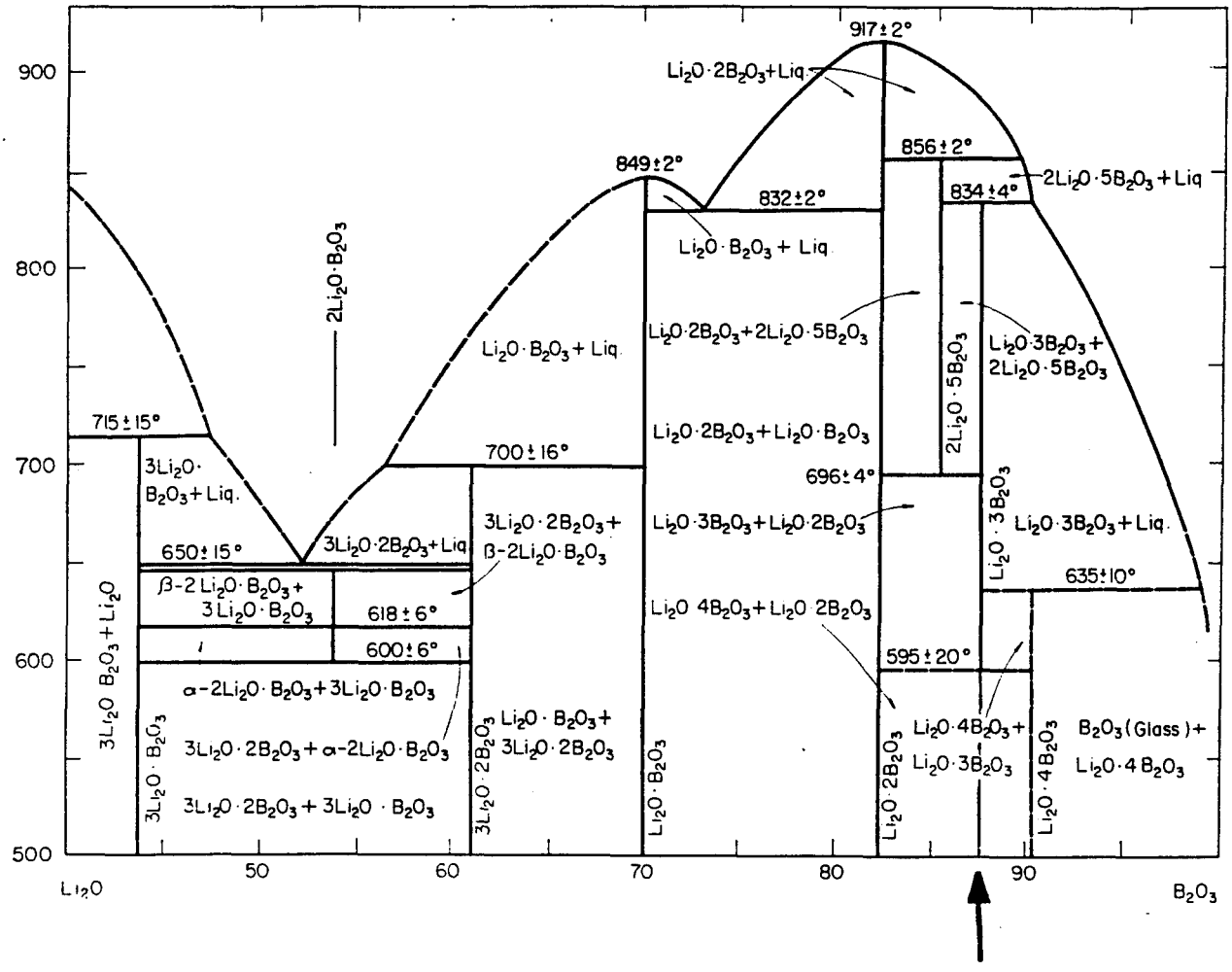

Figure 1. Phase equilibria in the Li_2O-B_2O_3 system safter Sastry and Hummel. [7,8]

and which they used for optical property determinations. They found the 1-3-5 (LiB_3O_5) phase to decompose peritectically at 834 ± 4° C. The low temperature decomposition postulated to occur around 595° C has not been verified in subsequent studies by other researchers, and the 1-3-5 composition is now felt to be a stable phase down to room temperature. In 1988/9, Jiang et al. [9] reported the growth of larger LBO crystals from viscosity-modified B_2O_3 fluxes, the composition of which they did not report. In 1989, Chen et al. reported growth from MoO_3 solutions. [10] However, MoO_3 was reported to produce crystals with flux inclusions by others who explored this route. [11] Also in 1989, Zhao et al. reported the growth from solutions modified by LiF and other unidentified additives. [12]

4. Crystal Growth Experiments

According to the phase equilibria of Sastry and Hummel op cit., LBO can be grown from excess B_2O_3 solutions by using slow cooling. Initially, we undertook the growth of LBO from B_2O_3-rich melts using 125-250 g charges synthesized from Li_2CO_3 and B_2O_3 in high gradient TSSG furnaces like those used for the growth of BBO. Axial and radial temperature gradients were in the range of 20° C/cm and 25° C/cm, respectively. Melts compositions were chosen to place the liquidus around 800° C, which corresponded to compositions in the 90% B_2O_3 range. X-ray powder diffraction analysis of the first crystals grown from these solutions indicated that the phase produced was not the desired 1-3-5 phase. B_2O_3-rich solutions in the Li_2O-B_2O_3 system were found to tolerate considerable undercooling, and without the correct 1-3-5 phase as a substrate, $Li_4B_{10}O_{17}$, a neighboring phase slightly richer in Li and slightly higher in its (also peritectic) decomposition temperature, was found to crystallize metastably instead. The desired 1-3-5 phase was successfully grown only after a polycrystalline 1-3-5 sample was first synthesized by recrystallizing a glass of the desired composition and using it as a polycrystalline seed.

Growth solutions with liquidus temperatures in the 800° C range were found to be quite viscous. Rotating cylinder melt rheological studies in our laboratory found melt viscosities as high as 80 poise near the point of saturation (800° C), in general agreement with Shartsis et al. [13] Viscosities were measured at several different shear rates, but the values obtained were within ±5%, suggesting that the melts were Newtonian. The melt viscosities were found to display typical Arrhenius type behavior, with an activation energy of 43 Kcal/mole, as shown in Fig. 2. Room temperature simulation experiments using glycerine/water mixtures of equal viscosity, revealed that mixing due to seed rotation was minimal, Fig. 3. This finding suggested that a very thick diffusion boundary layer could

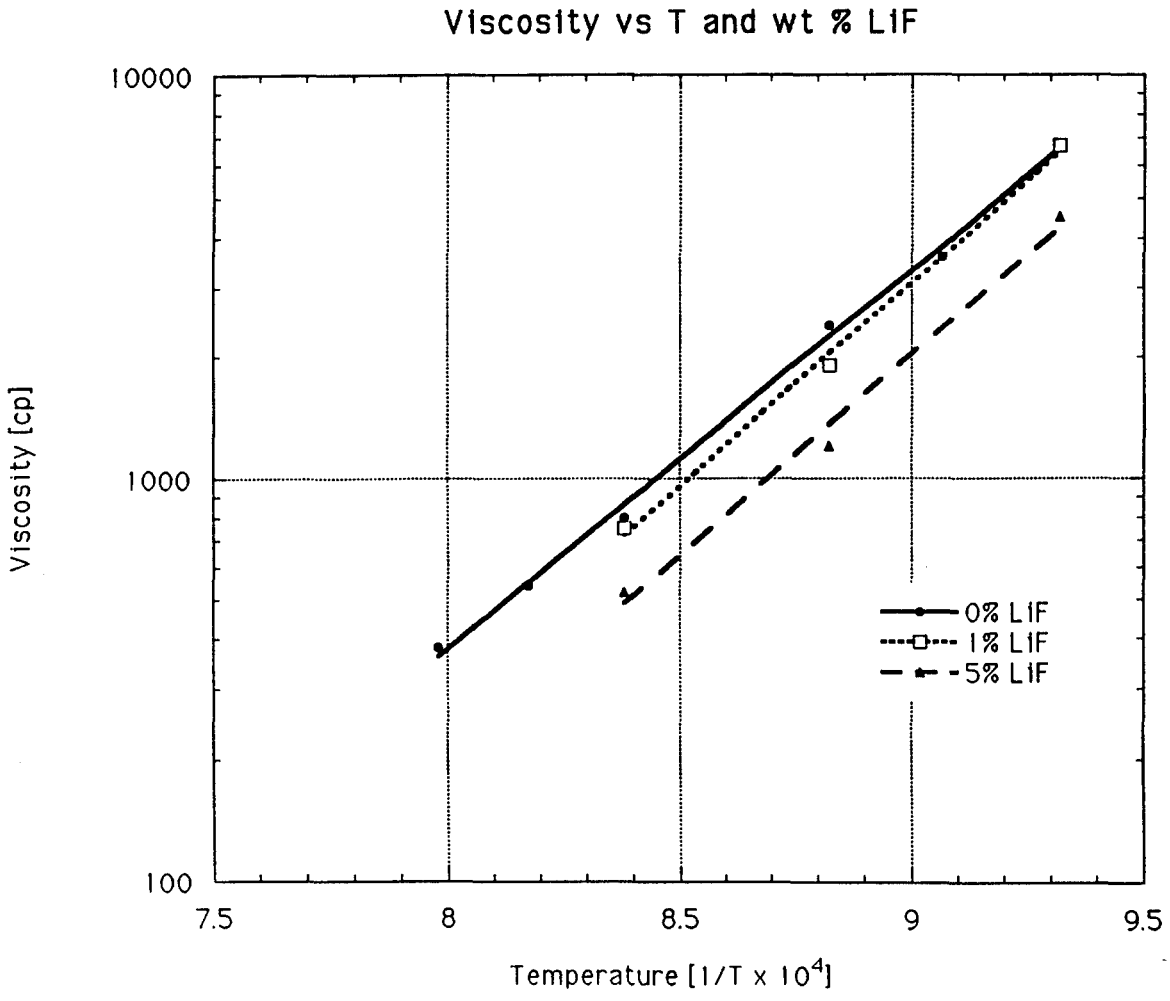

Figure 2. Viscosity of 90 wt% Li_20 - 20 wt% B_2O_3 growth solutions with small amounts of LiF added as a viscosity modifier.

Figure 3. Flow patterns in a water - glycerol solution of 1 Stokes kinematic viscosity shows minimal mixing as a result of forcing convective fluid motion by "crystal rotation" at 45 rpm.

be expected during growth, and that very low growth rates corresponding to the early literature reports [1,12] could be expected.

Anticipating that high growth solution viscosities would present a problem, a series of viscosity experiments on the behavior of solutions with up to 5 wt % LiF added as a viscosity modifier were carried out. The results are also shown in Fig. 2, where it can be seen that approximately 50 % reductions in viscosity were achieved with 5 wt% LiF addition. When the thermal stability of LiF-modified solutions was investigated, however it was discovered that over a two week period, melt viscosities had increased by approximately 15 %, suggesting that the LiF was decomposing or evaporating from the growth solutions, Fig. 4. Nor, were clear benefits over pure B_2O_3 melts obvious, even though the solution viscosities of LiF-modified melts had been reduced by a significant amount. The LiF-modified solutions exhibited a strong tendency to develop numerous elongated prismatic needles, and the stability of the crystal growth interfaces was poor.

We also studied test solutions with up to 25 at % Na_2O (partially replacing Li_2O) as a viscosity modifier. Somewhat better crystal morphology was achieved using these solution compositions. However, in neither case was a clear advantage over the use of pure B_2O_3 apparent, and the bulk of the growth studies were carried out using pure B_2O_3 as a solvent.

Seed introduction and the initiation of growth in the case of LBO was found to be much more difficult than the case of BBO in which the melt can be brought to saturation very precisely. Its very sluggish dissolution and growth kinetics combined with a strong tendency to supercool make it extremely tedious to bring an LBO melt to the point of saturation prior to seed introduction. A hot dip technique in which the saturation temperature needed to be determined to within only a few degrees was used instead. In this method, the melts were superheated above the estimated saturation temperature by 10-15° C, the seed was dipped and held for approximately 10 minutes at temperature, and finally the furnace was cooled rapidly to approximately 2° C below the estimated saturation temperature. The slight amount of dissolution that occurred at elevated temperature reduced the likelihood of secondary nucleation due to spurious crystallites on the seed surface, and it reduced the occurrence of spontaneously-nucleated crystallites on the melt surface.

Almost all the growth experiments were carried out with some degree of seed pulling in order to achieve boules of greater length than would have occurred without seed pulling. The TSSG method without pulling has a general tendency to produce shallow lens-shaped boules less than 20 mm thick , and this limited maximum crystal dimensions to even shorter lengths because of the need to cut them along specific phase matching directions.

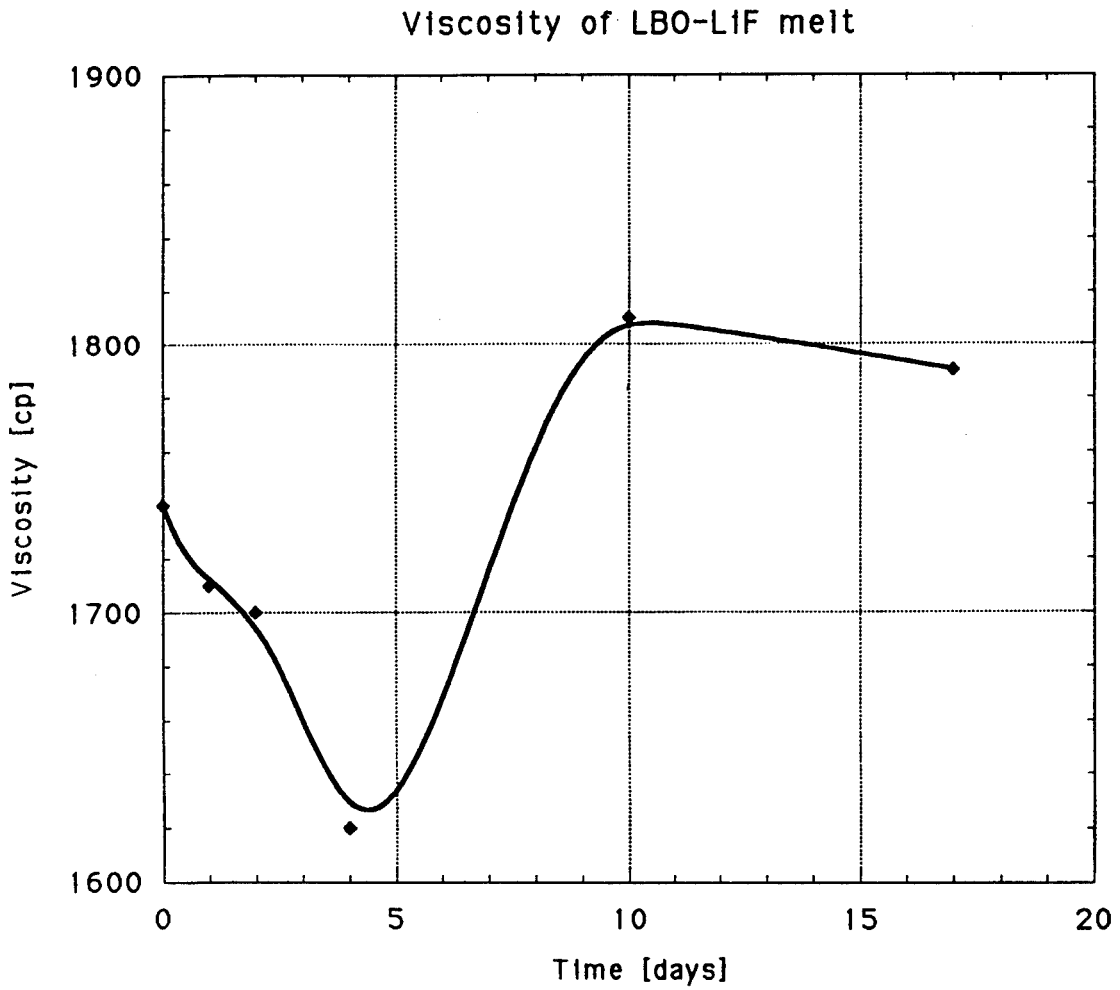

Figure 4. Time resolved viscosity data for an 8 wt% Li_2O - 90 wt% B_2O_3 - 2 wt% LiF growth solution showing that melt homogenization with a resultant reduction in viscosity occurred over a 5 day interval, but within 10 days, the viscosity of the solution had returned to its original value, presumably because of LiF evaporation.

Once the problem of seeding and initiation of growth was solved, the growth of single crystal boules of LiB_3O_5 from Li_2O-B_2O_3 solutions using the TSSG method was found to be relatively straightforward. Growth rates had to be maintained at minimal levels in order to avoid the occurrence of cellular breakdown on the growth interfaces, however, and this limited cooling rates to the order of 1° C/day. Typically, crystals could be pulled on the order of 0.5 mm/day during a typical 2-3 week growth interval.

It was found that growth anisotropy in LBO is stronger than it is in BBO, and crystals grown without pulling tended to remain strongly faceted as they grew to significant fractions of the crucible diameter. A photograph of a c-axis crystal grown without pulling is shown in Fig. 5, where its mm orthorhombic symmetry is clearly visible. This crystal developed additional grains during growth. Unpulled crystals were often observed to incorporate secondary grains that nucleated spontaneously and floated on the melt surface. While they tended to line up with, and incorporate on existing facets, they usually produced highly strained boundaries that caused fractures upon cooling. Crystals grown with pulling from the very beginning of growth tended to round out when their diameters became large enough that the volume pulled per unit time equaled the volumetric amount of solute (LBO) rejected from the growth solution per unit time due to the slow cooling imposed on the system. Seed orientation was found to influence the faceting as well. Growth normal to the (101) plane resulted in oval cross-section crystals that could be pulled rather successfully. Growth normal to the (010) plane, in contrast, resulted in a highly faceted habit that was not suitable for pulling.

5. Control of Surface Stability during Growth

During growth in the ambient, it was found that LBO crystal surfaces gradually formed a thin white surface layer. This layer grew in thickness and lateral extent during the entire time, eventually covering the free surface of the crystal (including the seed) with a millimeter thick, optically opaque polycrystalline skin. The layer generally replicated the original surface of the growing crystal, as shown in fig. 6a. Upon cooling, severe cracking occured on the crystal surfaces adjacent to the layer, while less severe cracking occured deeper into the bulk of the boule, as shown in fig. 6b. The cracking had been attributed by others to LBO's large thermal expansion anisotropy. [14] Other researchers simply reported that LBO crystals decomposed at temperatures in excess of ~500° C. [15]

Cross-sectional microscopic examination of LBO seeds that were surrounded by a platinum seed holder during growth, Fig. 7., showed that the surface layer was a reaction product rather than a deposit because there was no deposit on the adjacent platinum

Figure 5. C-axis LBO crystal grown with minimal pulling.

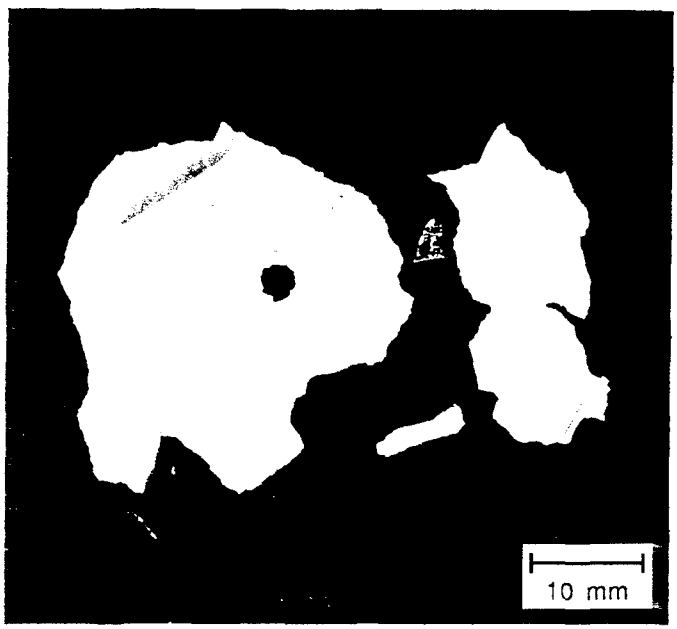

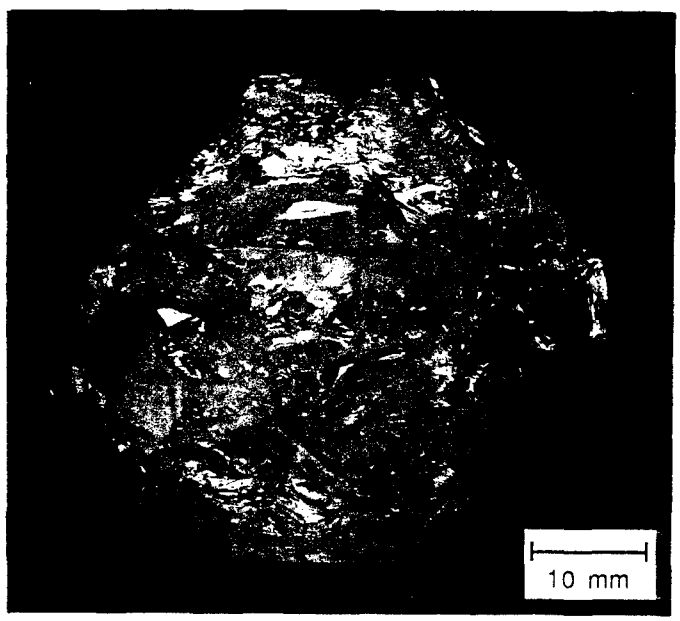

Figure 6. A.) Decomposed polycrystalline surface layer removed from c-axis crystal after growth showing the surface features of the original crystal.
B.) Underlying c-axis crystal showing significant amount of fracturing that correlates with the presence of the surface decomposition layer.

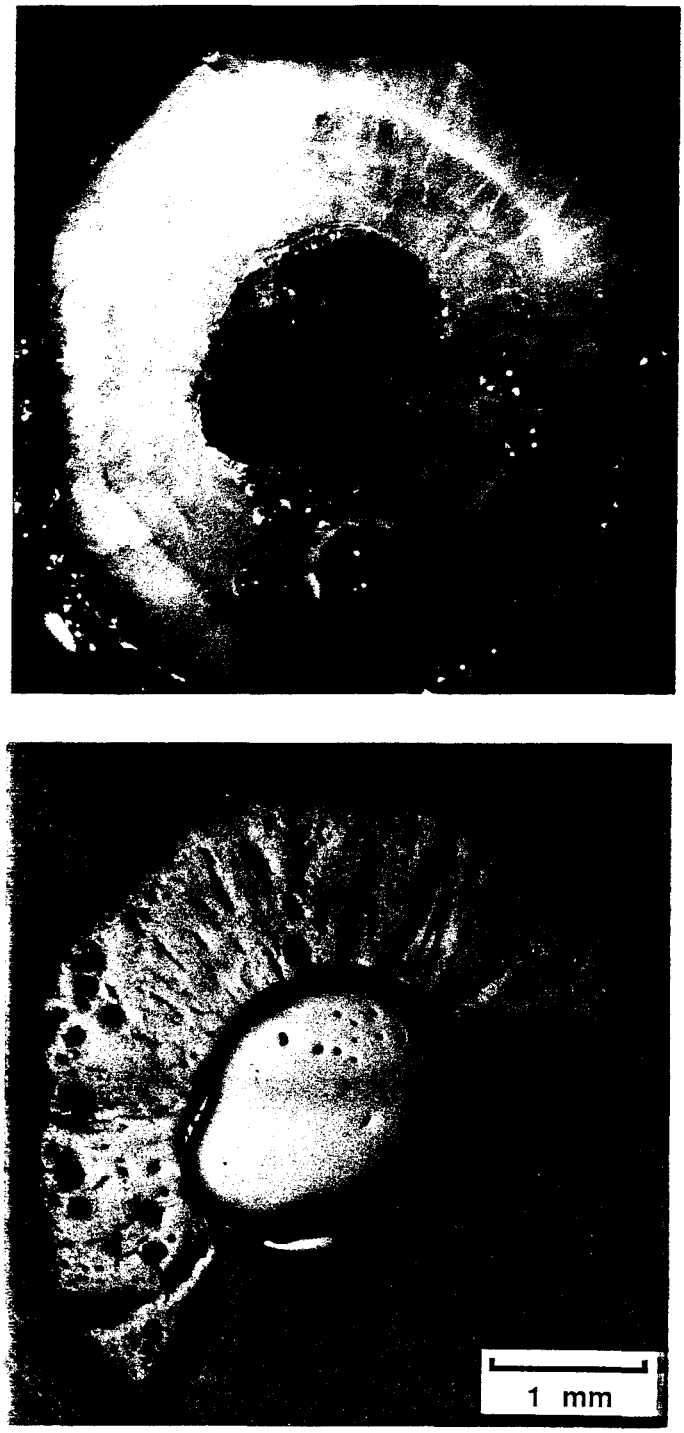

Figure 7. Cross-sectional study of LBO seed after growth showing that a very significant fraction of its original cross-section had decomposed during the growth process. (Once seed decomposition is complete, mechanical attachment to the crystal is lost and it is rarely possible to retrieve the crystals from the growth solutions when that happens.)

surfaces. The layer caused few problems during growth other than to impede visual monitoring of the crystal's optical quality. The surface layer itself was found to be quite fragile, and would not likely lead to large enough tensile or compressive stresses to fracture the underlying crystal during the cooling cycle. Thus, while the cracking process appeared to be closely related to this layer, the mechanism by which cracking occured was not obvious.

Powder x-ray diffraction (XRD) analysis revealed that the surface layer consisted mainly of the compound identified by Sastry and Hummel as $Li_4OB_{10}O_{17}$. [8] This compound is slightly richer in Li_2O than LiB_3O_5, and it was thought initially it that this phase might be formed by a reaction between the crystal surface and Li_2O-rich vapor coming off the melt. However, high temperature surface stability experiments revealed a similar surface reaction even when no melt was present. This finding verified that the surface layer formed by a surface decomposition process.

Tang et al. [15] had reported that the white surface layer on their LBO crystals contained a compound of composition, $Li_3B_7O_{12}$. This compound was not reported by Sastry and Hummel, op cit., but it is close in composition to their compound $Li_4B_{10}O_{17}$. Little was known about the $Li_4B_{10}O_{17}$ compound. Single crystals had not been reported, nor had structural analysis of its unit cell been reported. To elucidate the apparent descrepancy between the two studies, sintering and quenching experiments were carried out at 800° C using 5 g samples compounded at 1.5 mol% intervals throughout the range between the congruent phase, $Li_2B_4O_7$, and LiB_3O_5. The disappearing phase analysis technique was used, together with powder diffractometry, to determine the extent of the various two-phase fields. It was found that the x-ray pattern for $Li_4B_{10}O_{17}$ actually corresponded better with the $Li_3B_7O_{12}$ composition reported by Tang et al., op cit.

The stability and reactivity of LBO crystal surfaces was studied by heat-treating TSSG-grown LBO crystals and finely ground powders under different atmospheres using the growth furnace with a melt present, and an atmosphere-controlled tube furnace with no melt present. Clear evidence of surface decomposition was easily detectable with optical microscopy, as shown in fig. 8. Surface decomposition was found to occur in all cases where moisture was present in the ambient atmosphere. The absence or presence of oxygen did not appear to be related to the decomposition process. X-ray diffraction peaks obtained from the surface reaction layer usually indicated the presence of the lithium-rich compound $Li_3B_7O_{12}$ in addition to LiB_3O_5. XRD analysis indicated that over a 14 day interval, approximately 50% of typical ground LiB_3O_5 samples had converted to $Li_3B_7O_{12}$.

With one exception, all LBO heat-treated samples exposed to moisture lost weight during heat-treatment. The weight losses (on the order of 0.1-1.0 wt %) did not vary

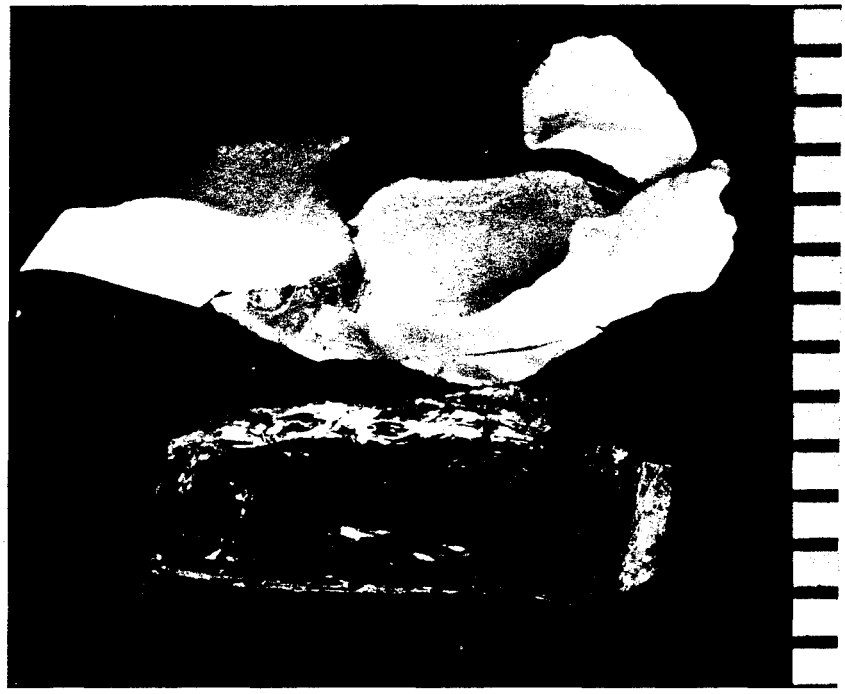

Figure 8. Upper) LBO crystal fragment heat-treated at 750 °C under normal atmospheric conditions for five days. Lower) LBO crystal fragment heat-treated under dry nitrogen for a similar length of time. (millimeter scale)

systematically with temperature, however, and it was not possible to determine the kinetics of the decomposition reaction(s) from these samples. TGA experiments carried out in the 650°- 800° C range were more definitive. Weight losses from 1.9 10^{-5}g/ min to 4.0 x 10^{-5} g/min were found when either wet nitrogen or wet oxygen was present, while under dry nitrogen, sample weights remained constant within experimental error over the same period. A typical thermogravimetric scan of a 50 mg LBO sample alternately under dry and wet nitrogen is shown in Fig. 9. Reaction rates were found to display an Arrhenius behavior over the temperature range studied, with calculated activation energies of 17.8 and 17.9 kcal/mol for wet nitrogen and oxygen atmospheres, respectively.

The formation of $Li_3B_7O_{12}$ in the presence of H_2O was described by two possible chemical reactions

$$2H_2O(g) + 6LiB_3O_5(s) \rightarrow 2Li_3B_7O_{12}(s) + 4HBO_2(l) \rightarrow 2Li_3B_7O_{12}(s) + 2H_2O(g) + 2B_2O_3(l). \quad (1)$$

$$H_2O(g) + 8LiB_3O_5(s) \rightarrow 2\{Li_3B_7O_{12}\}(s) + 5B_2O_3(l) + 2LiOH(l). \quad (2)$$

In the first, water vapor enters the process by forming the intermediate compound HBO_2. At elevated temperature, the HBO_2 formed should decompose into B_2O_3 and H_2O. [16] However, HBO_2 was also shown in [16] to be slightly volatile at elevated temperatures, and this could account for the small weight losses observed during the heat-treatment process. Because of the very complex powder patterns, it was not possible to detect diffraction lines from either HBO_2 or LiOH in the surface reaction layers.

Fourier transform infrared (FTIR) absorption analysis was carried out on finely-ground powders of the surface coating material suspended in pressed KBr pellets. While the transmission spectra obtained did not prove the validity of either proposed reaction, the observed lack of absorbance in the 1250 cm-1 region (which is the assigned frequency for the Li-O-H bending mode) [17] suggested that LiOH was not present in the samples studied. Additionally, very broad absorption bands were found in the 4-13 μm region of the spectra that are not present in pure LBO. This absorption spectra is similar to that reported for B_2O_3 glass. [18]

Small quantities (mg amounts) of an alcohol and water soluble white condensate or subliminate was observed to build up slowly on the quartz muffle in the atmosphere-controlled tube furnace during heat-treatment experiments, as long as water vapor was present. Diffraction peaks could not be obtained from the small amounts collected. (This

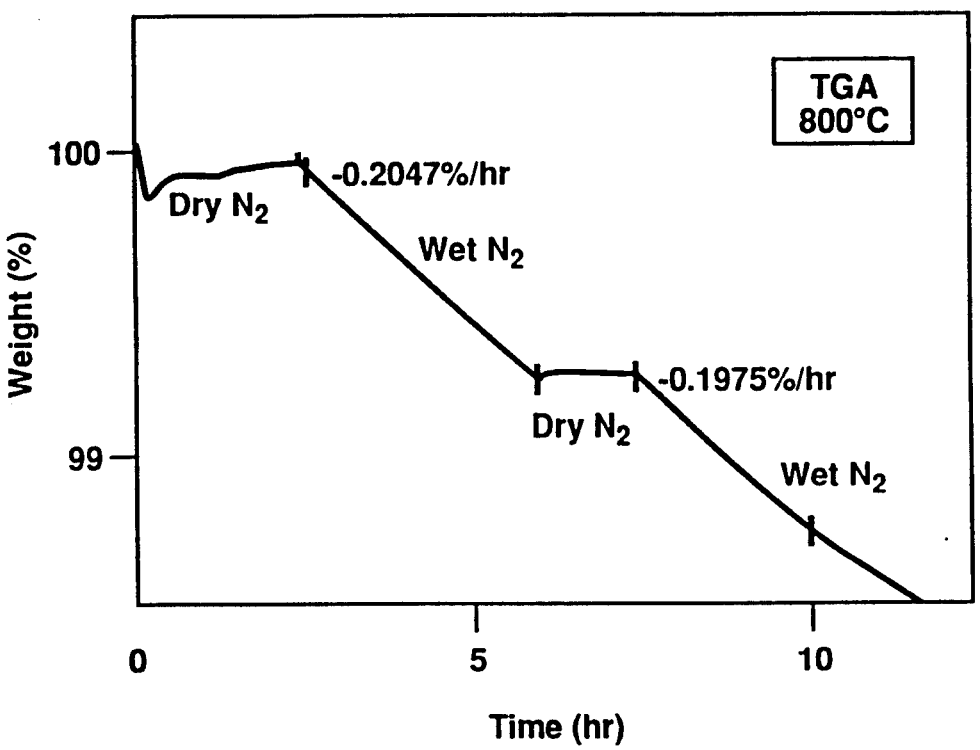

Figure 9. Thermogravimetric analysis showing the effects of water vapor on the stability of LBO under wet and dry nitrogen. Under wet conditions, continuous weight loss by decomposition is seen, while under dry conditions, weights remain stable.

may also have indicated that the unknown material was amorphous.) Flame tests (by the absence of a red color) indicated that lithium was not present in this material. Micro-Raman analysis revealed peaks at 881 nm and 941 nm. Several acid borates also produced Raman lines at 881 nm, but the one at 941 nm was not identified. The solubility of this unknown material in alcohol and water, the Raman result, and the negative flame test for lithium suggested that the white coating on LBO crystals was an acid borate. While this evidence was not conclusive, the strong FTIR absorption at 1250 cm^{-1} pointed to the first reaction as being the more probable.

Both of the proposed chemical reactions involve the formation of B_2O_3 in the surface layer. The formation of excess B_2O_3 on the top surface of a growing crystal could lead to partial dissolution of the LiB_3O_5 in contact with it, and on cooling could easily cause the severe cracking that was seen. (It is well known that molten B_2O_3 in contact with fused silica will cause serious cracking upon cooling. B_2O_3 melts adhere strongly to many oxide materials, and because solidified B_2O_3 glass is reasonably strong, large stresses can be developed due to differential expansion.) This work is described more completely in [19].

6. Growth of Optical Crystals

Once the cause of surface degradation was identified, growth under nitrogen was instituted and crystal surfaces remained pristine. Slow pulling to enhance crystal length was also used. Pulled crystals all exhibited some degree of undercutting if constant cooling and pulling rates were used, for the same reasons described in the previous section. And, in the same manner used for BBO, calculating the yield of solid material per degree of cooling based on analysis of previous growth runs made it possible to adjust the growth parameters and minimize the effect. The most successful seed orientation was the c-axis (001) since it was possible to pull crystals in lengths greater than 20 mm by adjusting growth parameters accordingly. An LBO crystal grown under nitrogen is shown in Fig. 10.

The next most significant challange encountered in the growth of LBO crystals from B_2O_3 solutions was the problem of avoiding interface breakdown, which necessitated the use of the very low growth rates mentioned (less than 1° C/day). Crystals that were cooled significantly faster than this, or that were inadvertently pulled faster than their corresponding linear growth rates allowed, inevitably developed unstable, cellular growth interfaces due to constitutional supercooling. This was assumed to be due mainly to mass transport limitations caused by the extremely high melt viscosities. (Forced convective stirring through seed rotation was found to be relatively ineffective.)

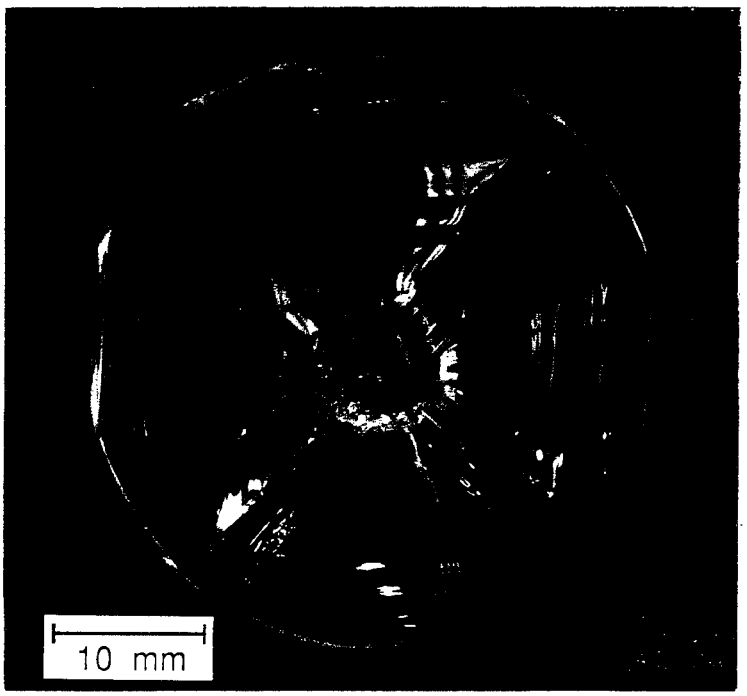

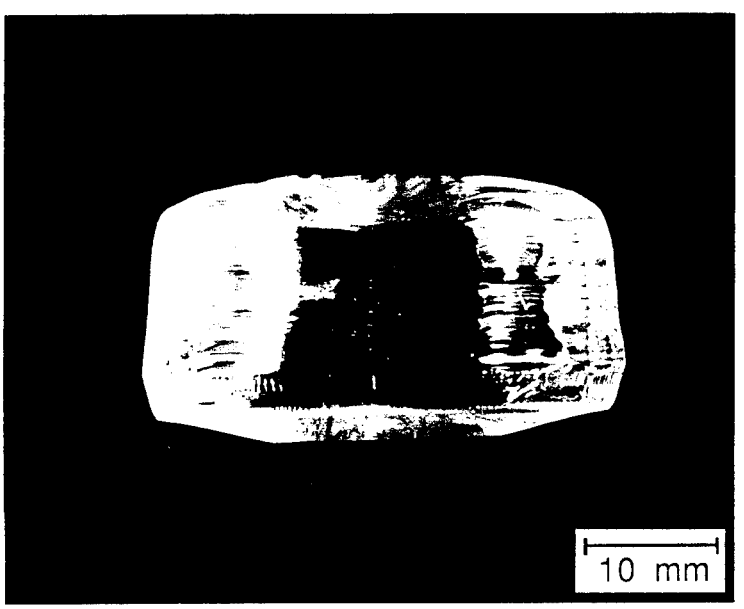

Figure 10. LBO crystal grown along the c-axis under dry nitrogen. A.) Top view along the c-direction showing the orthorhombic symmetry (in dark field illumination), B.) Front view through naturally occurring facet showing a core region of inclusions/voids along the center line of the crystal.

In slowly grown c-axis crystals, a core several millimeters in diameter consisting of solvent inclusions and/or voids often occurred, and was thought to be due to localized fluid stagnation at the center of the growth interface. Farther out from the crystal axis, relatively few macroscopic optical defects were found. Significantly less optical scatter was found in LBO crystals than was typically seen in BBO crystals. This difference was surprising since the viscosities of the LBO melts used were much higher than Na_2O-based BBO melts, and one might anticipate a greater density of solvent inclusions as a consequence. We had earlier postulated that, in the case of BBO, because of the occurrence of widely distributed solvent inclusions far from regions of interface instability which are clearly caused by constitutional supercooling, a second solvent inclusion mechanism may exist, and that this could account for the enhanced optical scatter seen in BBO crystals. None has been identified to date and the exact mechanism(s) of their formation remains unknown.

The yield of high quality optical crystals from slowly pulled boules grown under nitrogen was quite good. High power, high efficiency resonant second harmonic generation of the 1.06 μm line was demonstrated at Stanford using an 11 mm long optical LBO crystal grown here, [3] and a series of crystals was also fabricated in order to determine the temperature dependent Sellmier coefficients. LBO crytals cut for SHG were supplied to NRAD and ARPA for coordinated device testing in other laboratories.

7. Patent Issues

Private communications with industrial collaborators [20] during the program, however, revealed growing uncertainty in the commercial sector because of the restrictive US patent position held by the Chinese Academy of Sciences on virtually all aspects of the preparation and use of LBO for nonlinear optics.[10] For this reason, and because BBO appeared to have theoretically superior performance in high peak power resonant SHG applications and because it phase-matched far deeper into the UV, emphasis on LBO was diminished in 1993 in favor of further development of BBO, upon which restrictive patent positions do not exist.

8. Summary of Results

1. Multi-centimeter diameter LiB_3O_5 crystals up to 15 mm in length have been grown from 10 wt % Li_2O - 90 wt % B_2O_3 solutions using both c-axis (001) and (101) seeds.

2. High thermal gradient TSSG furnaces like those used for the growth of BBO were used successfully for the growth of good quality LBO crystals, but only at cooling rates less than 1° C/day and linear growth rates of less than 1 mm/day. Pulling, as long as it was initiated at the beginning of the growth cycle, was found to result in longer boules with higher yields than unpulled boules.

3. With the exception of a 1-2 mm core region that did have a high density of (solvent) inclusions, relatively few optical defects due to solvent inclusions were found elsewhere in the crystals.

4. Melts with excess B_2O_3 as the solvent were found to have very high viscosities, and mass transport was, therefore, concluded to be the rate limiting mechanism in this system. Limited experiments using flux modifiers did not result in improved crystal quality or an increase in maximum allowable growth rate. Reduced melt viscosities through the identification of a more suitable flux modifier should be pursued, however, as a means to increase the maximum allowable growth rates.

5. The decomposition of lithium triborate (LiB_3O_5) crystal surfaces at high temperatures has been studied. In all cases, crystal surfaces exposed to water vapor in the ambient atmosphere decomposed to form the lithium-rich compound, $Li_3B_7O_{12}$. Surfaces exposed to dry nitrogen or air, on the other hand, were not damaged. A possible chemical reaction to explain the decomposition of LiB_3O_5 in the presence of water vapor has been suggested.

6. LBO crystals grown by the top-seeded solution growth method under normal air ambient conditions exhibit surface decomposition and related cracking, while crystals grown under dry nitrogen atmospheres retain water-clear surfaces during the growth process and show no tendency to crack during cooling.

9. References: Part B:

1. C. Chen, Y. Wu, A. Jiang, B. Wu, G. You, R. Li, and S. Lin, "New nonlinear-optical crystal: LiB_3O_5," J. Opt. Soc. Am. 6 (4), 616-621 (April 1989).

2. J. P. Chernoch, M. J. Kukla, W. T. Lotshaw and J. R. Unternahrer, Soc. for Optics & Quantum Elec., Proc. from Lasers '91, STS Press, McLean, VA (1991).

3. S. T. Yang, Optics Letters 16 (1991) 1493.

4. C. Mazzetti and F. D. Carli, Gazz. Chim. Ital. 56 (1926) 23.

5. A. P. Rollet and R. Bouaziz, Compt. Rend. (Paris) 240 (1955) 2417.

6. H. König and R. Hoppe, Z. Anorg. Allg. Chem. 439 (1978) 71.

7. B. S. R. Sastry and F. A. Hummel, J. Am. Ceram. Soc. 41 (1958) 8.

8. B. S. R. Sastry and F. A. Hummel, J. Am. Ceram. So. 42 (1959) 216.

7. S.-q. Zhao, Thesis, Academia Sinica, Inst. of Physics, Beijing, China (1987).

9. C. Chen, Y. Wu, A. Jiang, B. Wu, G. You, R. Li and S. Lin, J. Opt. Soc. Am. B-6 (1989) 616.

10. US Patent 4,826,283 "LiB_3O_5 Crystal and its Nonlinear Optical Devices," issued to Chen, Chuangtian, et al. and assigned to the Fujian Institute of Research on the Structure of Matter, Fujian, China (1989).

11. Private communication with B. H. T. Chai (1990).

12. S. Zhao, C. Huang and H. Zhang, J. Crystal Growth 99 (1990) 805.

13. L. Shartsis, W. Capps and S. Spinner, "Viscosity and electgrical resistivity of molten alkali borates," J. Amer. Cer. Soc. 36 (10), 319 (Oct. 1, 1953).

14. W. Lin, G. Dai, Q. Huang, A. Zhen and J. Liang, J. Phys. D (Appl. Phys.) 23 (1990) 1073.

15. D. Tang, Q. Lin, W. Zeng, C. He, J. Wang, X. Lin and H. Hong, J. Synthetic Crystals 20 (1991) 303.

16. D. Meschi, W. Chupka and J. Berkowitz, J. Chem. Physics 33 (1960) 530.

17. D. Meschi, W. Chupka and J. Berkowitz, J. Chem. Physics 33 (1960) 533.

18. F. A. Miller and C. H. Wilkins, Anal. Chem. 24 (1952) 1253.

19. E. Brück, R. J. Raymakers, R. K. Route and R. S. Feigelson, J. Crystal Growth 128, 933 (1993).

20. Personal communications with L. Shiozawa of Cleveland Crystals, Inc. and W. Ruderman of INRAD (1992).

C. SILVER GALLIUM SELENIDE

1. Objectives

Program objectives relating to silver gallium selenide were 1.) to develop a better understanding of the optical damage mechanism(s) and 2.) if possible, to increase its damage resistance through modifications in the growth technology or the post-growth processing. We sought to do this through evaluation of laser-damaged crystals and investigation of optical loss mechanisms at low power levels, as well as by seeking an increased understanding of the chemistry, the mass transport and the kinetics of the growth and heat-treatment process.

2. Background on Crystal Growth and Processing

Single crystals of $AgGaSe_2$ with high optical quality have potentially important infrared nonlinear optical applications.[1] However, due to an off-stoichiometric congruency, $AgGaSe_2$ always grows slightly rich in Ga_2Se_3 in accordance with the known phase equilibria in the Ag_2Se-Ga_2Se_3 pseudobunary system. [2,3] This inevitably leads, upon cooling, to the formation of Ga_2Se_3-rich precipitates that cause appreciable optical scattering in the near-infrared wavelength (0.73-2 μm) region. The precipitates can be eliminated either by quenching or heat-treating the crystals in the presence of Ag_2Se.[3] In the quenching technique, as-grown crystals are cooled rapidly to room temperature from an elevated temperature. Although effective in eliminating the precipitates, quenching usually leads to the crystals cracking, and for this reason annealing in the presence of Ag_2Se, which causes less damage to the crystals, is preferred.

Several variations to the annealing techniques have been reported, depending on whether or not there is contact between the crystal and annealing medium, or whether there was an annealing medium present at all.[3-6] In our laboratory, analyses of the chemical reaction products and the condensed volatile species found within the heat treatment ampoule in the temperature range of 500 °C to 800° C revealed no significant differences between the contact and the contactless cases. However, for complete elimination of the precipitate phase, it was empirically determined that direct contact was necessary.

The high temperature heat-treatment process for eliminating second phase precipitates utilizes a binary diffusion couple which places $AgGaSe_2$ crystals in direct contact with a small amount (approximately 1.0 mol%) of an annealing medium, typicallly Ag_2Se, for three weeks at 800° C in an evacuated and sealed quartz ampoule.[6] The process is modeled by the line X-Y on the phase diagram shown in Fig. 1. The $AgGaSe_2$

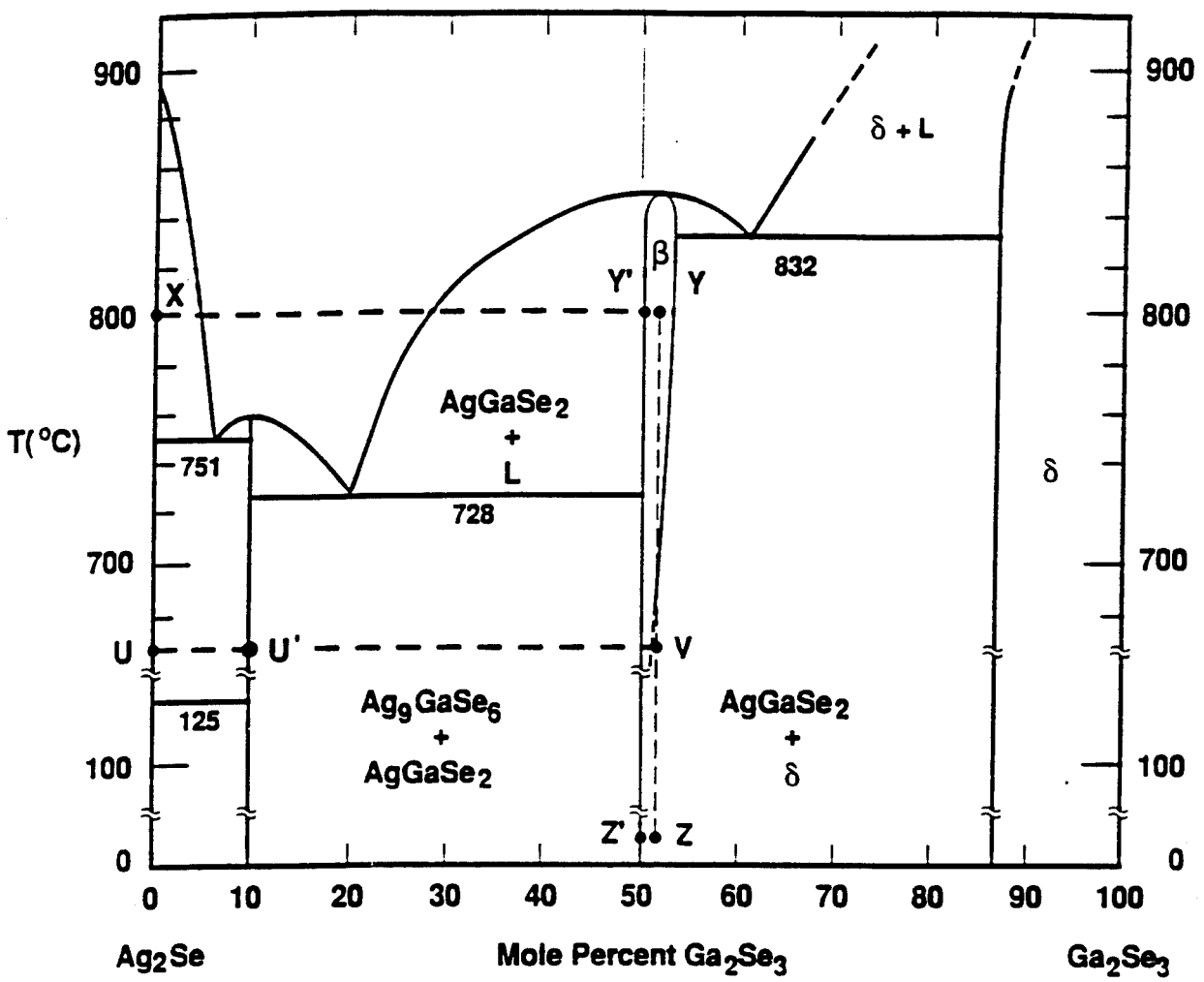

Figure 1. Phase equilibria in the Ag_2Se-Ga_2Se_3 pseudobinary system after Mikkelsen [2] showing the 800° C diffusion couple (X-Y) used during commercial heat-treatment processing and the two isoconcentration cooling paths followed by as-grown cloudy crystals (Y-Z) and heat-treated clear crystals (Y'-Z'). The line (U'-V) represents the low temperature diffusion process that makes use of Ag_9GaSe_6 phase as the annealing medium. Since heat-treatment in this case is carried out below the eutectic temperature, no liquid phases are formed and therefore no damage to the crystal occurs during cooling.

is usually placed on top of the Ag_2Se to ensure good physical contact, and annihilation of the Ga_2Se_3-rich precipitates proceeds uniformly inward from the free surfaces of the crystal due to a Ag_9GaSe_6 surface layer that quickly forms by reactive diffusion and provides a sink for the excess Ga_2Se_3 dissolved in the bulk of the crystal. With Ag_2Se as the annealing medium, a liquid phase forms at the junction where the annealing medium and the crystal meet, and upon cooling, minor cracking of the crystals often occurs.

Research under a previous ARO program, DAAL03-86-K-0129, was devoted to gaining a better understanding of the heat-treatment process, analyzing the chemical reactions that occur, and determining the chemical interdiffusion coefficients for the mobile species. [7] We also developed a chemical mass balance model that made it possible to predict the kinetics of the heat treatment process from fundamental parameters. Our most important finding was that the intermediate phase, Ag_9GaSe_6, when used as the annealing medium, eliminated the formation of a liquid phase and the consequent cracking damage to the $AgGaSe_2$ crystals. Also, the kinetics of the heat-treatment process appeared to be faster with Ag_9GaSe_6 as the annealing medium.[8]

After a single heat-treatment procedure, microscopic scattering remnants were still found, but in significantly reduced concentrations. They did not significantly affect optical transparency or the efficiency of non-resonant second harmonic generation of the CO_2 laser.[9,10] However, in resonant intracavity applications such as tunable optical parametric oscillators, [11] small absorption and scattering losses can have more serious consequences. Careful power balance measurements on many crystals from different singly heat-treated $AgGaSe_2$ boules always yielded losses in the 0.5-2.5 % cm^{-1} range,[12] varying from one crystal to the next. Only weak correlations could be made between power loss measurements and the size and density of the residual defects shown in Fig. 2. In 1990, we began using a scattered light technique to observe scattering defects in heat-treated $AgGaSe_2$ crystals,[6] relying on the near-IR sensitivity of CCD video cameras with either silicon vidicon or CCD array detectors, and the high resolution of current video equipment. With this improved imaging techniques, we discovered that far more microscopic scattering remnants remain in singly heat-treated crystals than had been thought, and in a pattern that suggested an incomplete diffusion process, Fig. 3. A multiple cycle heat-treatment process was developed to further reduce the density of residual scattering centers, and material with near-theoretical transparency was obtained. Quantitative measurements using spectrophotometry and laser calorimetry have revealed absorption coefficients as low as 0.012 cm^{-1} at 2.1 μm in multiply heat-treated crystals. [13]

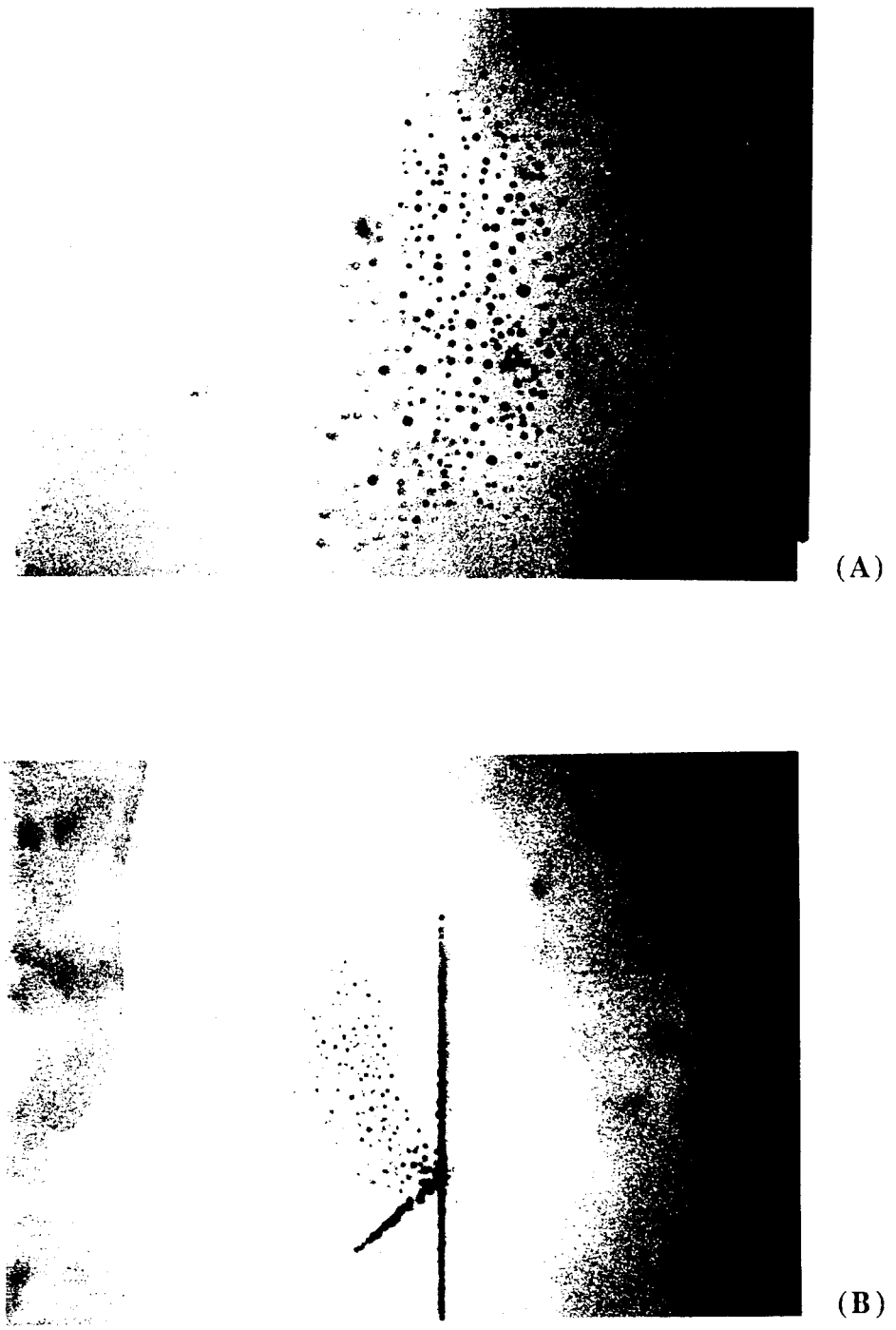

Figure 2. Optical micrographs (transmitted visible light) of remnant scattering defects in heat-treated $AgGaSe_2$ crystals. Three dimensionsl clusters of a) random shape, and b.) shapes reminescent of precipitates in as-grown crystals.

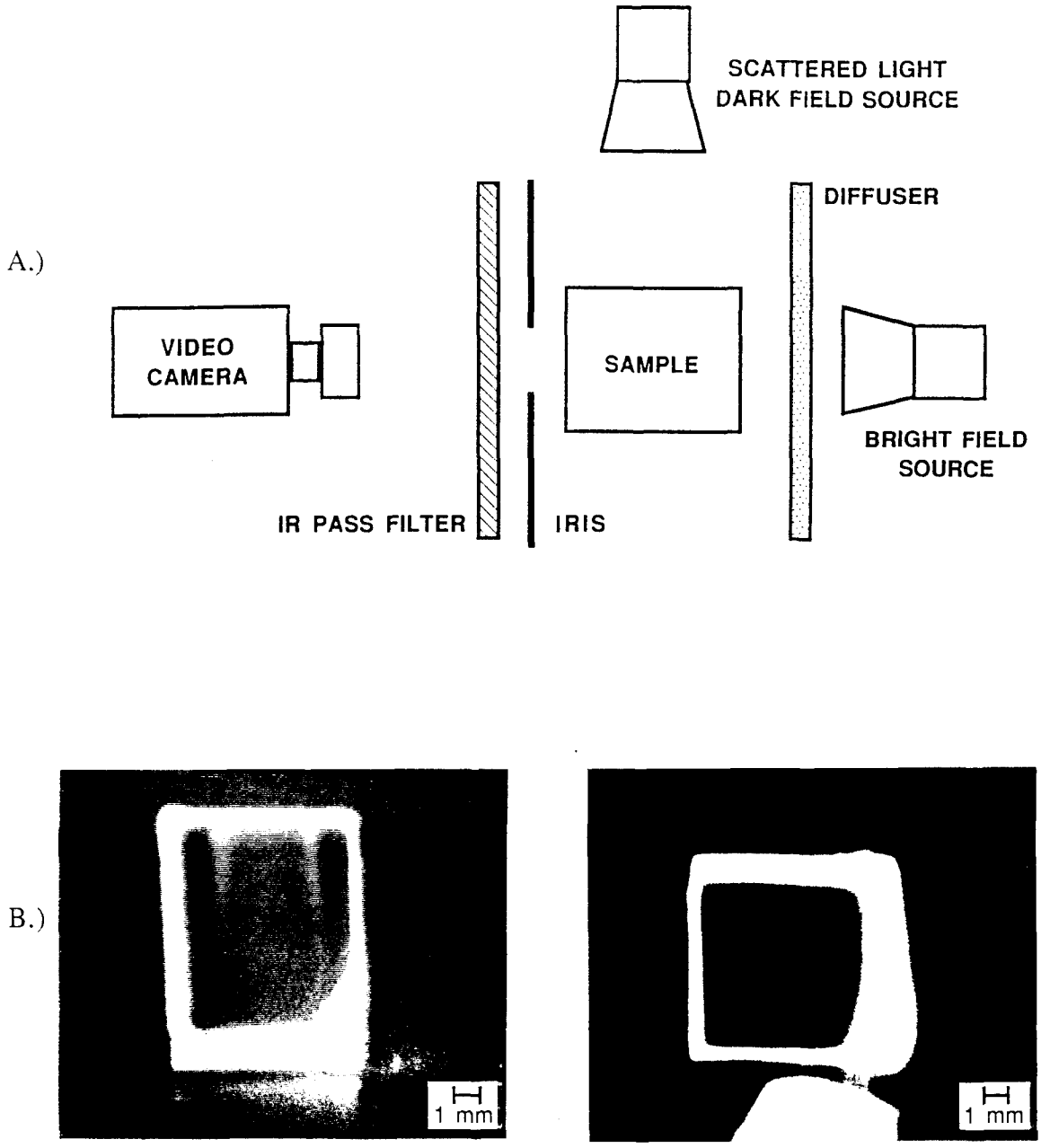

Figure 3. A.) CCD-based infrared video image converter reveals scatter in $AgGaSe_2$ crystals. B.) Left - light scattering from core region in a 30 mm thick, singly heat-treated crystal., Right - Complete absence of light scattering from a doubly heat-treated crystal.

3. Collaborative Studies on Non-Resonant (Surface) Laser Damage

The power handling capability of $AgGaSe_2$ in loose focus applications has always been limited by the occurrence of surface damage which occured in the 13-20 MW/cm^2 range. [14] Narrow band AR coatings commerically available raised this threshold by a factor of 2, but wide band AR coatings seemed to be less effective.[12] Tight focus studies carried out in R. L. Byer's group have determined that the threshold for bulk laser damage is at least ten times as great.[12] Early threshold determinations were made on singly heat-treated crystals. Fewer multiply heat-treated crystals have been studied to date.

In Figs. 4-6, we show microstructural studies on both uncoated and AR-coated $AgGaSe_2$ specimens damaged with lasers having a variety of wavelengths. With one exception, these studies suggest that the damage site has undergone surface melting and resolidification. In Fig. 4, damage from a 1.06 μm source on an uncoated $AgGaSe_2$ surface has created an annular pattern of craters or tear-outs. Backscattered electron (BSE) imaging did not suggest the formation of additional phases. In Fig. 5, a very complex pattern of damage from a free-electron laser operating at 4 μm incident on an AR-coated $AgGaSe_2$ crystal is shown. In Fig. 6, damage from a CO_2 laser operating at 10.6 μm with a Gaussian beam is shown. In this case, absorption in the AR coating was quite strong and this may have localized the damage nearer to the surface than would have otherwise occurred. A glassy surface at the damage site is evident, along with substructural features and a radiating network of cracks. No additional phases were suggested by BSE analysis.

Surface damage studies in 1991 by Ziegler and Scheppler [13] and in 1994 by Marquardt et al. [15] included Stanford-grown crystals that had been singly and multiply heat-treated. The aim of these studies was to elucidate the effects of residual surface polishing damage on optical damage thresholds. Test crystals were polished by a number of vendors and tested using pulsed lasers operating near 2.1 μm. Both uncoated and AR-coated crystals were included in the study. Damage thresholds were found to be dependent on total absorbed energy rather than peak power or electric field intensity, and varied in the range 1.4 to 3.3 $J\ cm^{-2}$. [13] This conclusion supports the model of damage being due to surface heating by optical absorption to a temperature where chemical decomposition occurs. Crystals finished to lower surface RMS roughness values gave higher damage thresholds, as shown in Table 1 and Fig. 7. No correlations were possible regarding limitations due to residual bulk scattering because damage always occurs on the entrance surface. Improvements in surface finishing procedures and reductions in absorption in the various pump wavebands will further increase surface damage thresholds and allow mid-IR tunable OPOs to operate at higher power levels.

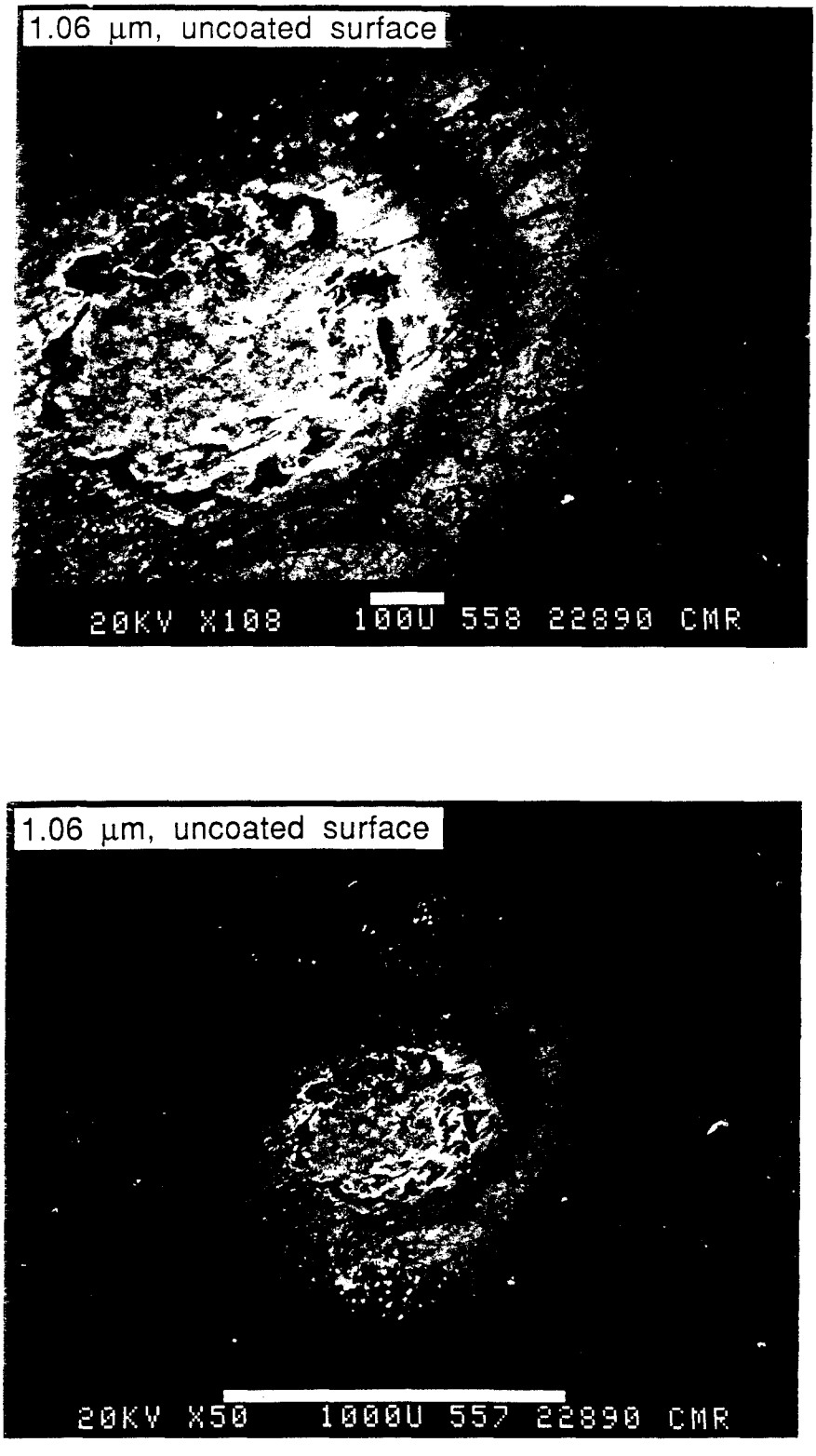

Figure 4. Laser surface damage from a 1.06 μm source incident on an uncoated $AgGaSe_2$ surface.

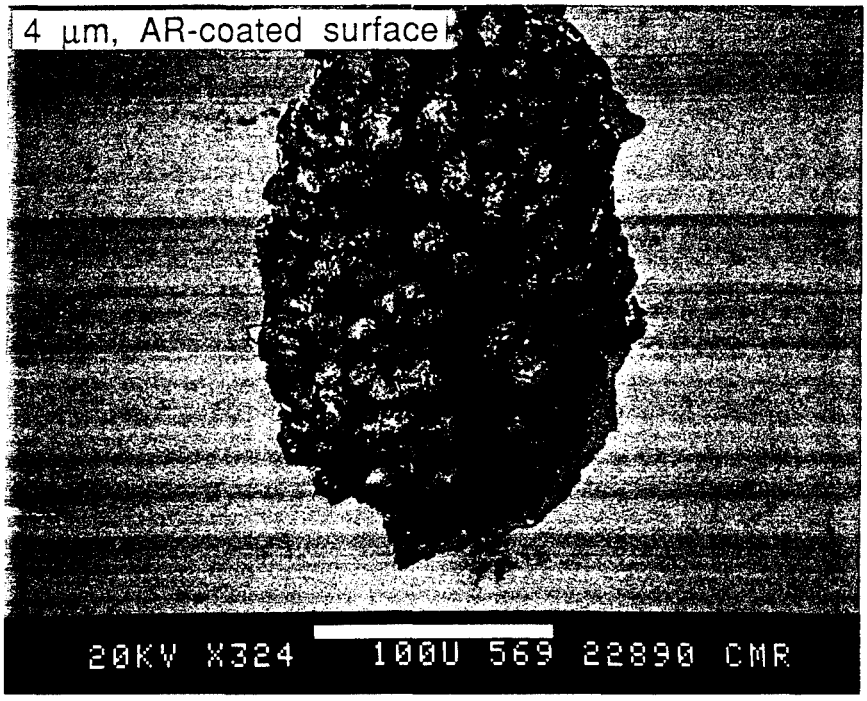

Figure 5. Surface damage on an AR-coated $AgGaSe_2$ crystal caused by a 4 µm free electron laser source.

Figure 6. Optical and SEM study of a 10.6 μm surface damage site. (Enhanced absorption in the AR coating may have influenced the thermal heating profile and contributed tito the rediating crack network.

Table I. Damage threshold measurements at 2.1 μm [13]

	Initial Sample		Repolished Sample		
Sample Identification	Surface Roughness [Å (rms)]	Coated J/cm²	Surface Roughness [Å (rms)]	Not Recoated J/cm²	Recoated J/cm²
A-W	42	–	6	–	–
B-W	40	1.4[a]	10	1.4[b]	2.8[b]
C-W	40	2.5[a]	7	–	–
D-W	27	1.1–2.2[a]	8	2.1[b]	3.3[b]
E-W	26	2.0[a]	14	–	–
W-1	–	1.6[b]	–	–	–
W-2	–	1.8[a]	9	1.6[b]	3.0[b]

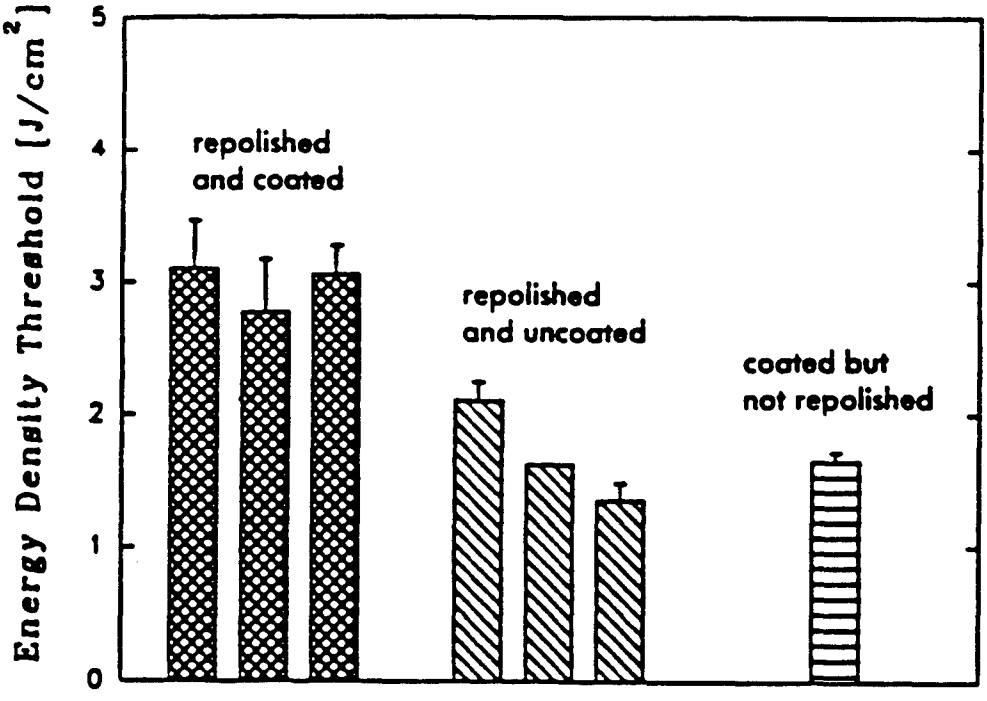

Figure 7. $AgGaSe_2$ damage threshold measurements comparing standard and repolished samples. [13]

4. Collaborative Studies on Resonant (Bulk) Laser Damage

In 1992, it became evident that the major limitation to the use of $AgGaSe_2$ in high power (>10W) tunable OPOs pumped at 2 μm was not surface damage, but wavefront distortion due to thermal lensing. [16,17] Studies of over 25 different crystals, again including Stanford-grown material, characterized the effect. Basically, it was found that all melt-grown $AgGaSe_2$ crystals exhibit a small, but broad absorption band centered at 2.2 μm for e-polarized propagation, Fig. 8, which is the polarization required for the pump laser in a broadly tunable OPO covering the 2.5-12 μm waveband. $AgGaSe_2$ furthermore exhibits rather poor thermal conductivity, 0.01 W/cmK[19], which is roughly fifty times lower than that of GaAs, and for this reason, strong thermal wavefront distortion occurs as the beam path heats, Fig. 9a. [15] OPO output power levels are currently limited to ~ 1W because of this effect, Fig. 9b.

Spectrophotometric and laser calorimetric data [17] along with scattering theory [20] indicate that 1.) the cause of the absorption is due to a bulk effect, and 2.) it is an extrinsic defect with its principal absorption dipole aligned along the c-axis. These works strongly suggested that a stoichiometry-related point defect is the most likely cause.

Prior results on the growth of defect free $AgGaS_2$ crystals - Based on our long term studies on the optical scattering defects found in $AgGaS_2$, we suggested in 1987 that optically clear material, free of precipitates might by grown from Ag_2S-rich solutions in which the liquidus temperature is below the point at which the existence region departs from stoichiometry. [21] A series of solution-Bridgman growth experiments was carried out using Ag_2S-rich solutions to demonstrate this effect. For a solution with 65 mole % Ag_2S, in which the liqiudus temperatures was in the neighborhood of 960 °C, an optically clear crystal was obtained. Results of the study are illustrated in Fig. 10, where it can be seen that the melt-grown crystal had the usual density of precipitates (it was cloudy) whereas the solution grown crystal was clear. The crystal grown from 65 mole % Ag_2S was thought to have grown without precipitates ever having formed, based on our understanding of the phase equilibria in the Ag_2S-Ga_2S_3 pseudobinary system. (This could not easily be verified at the time because of the possibility of auto heat-treatment in the growth ampoule. The growth conditions closely resembled the post-growth heat-treatment process.) At the time, the method was thought to be impractical as a commercial process for growing large high quality crystals due to the obvious difficulties in seeding and the need to reject large amounts of Ag_2S-rich material from the the crystal growth interface which necessitated very slow growth rates on the order of 1-2 mm/day in contrast to 8-12 mm/day used in growth from near-stoichiometric melts.

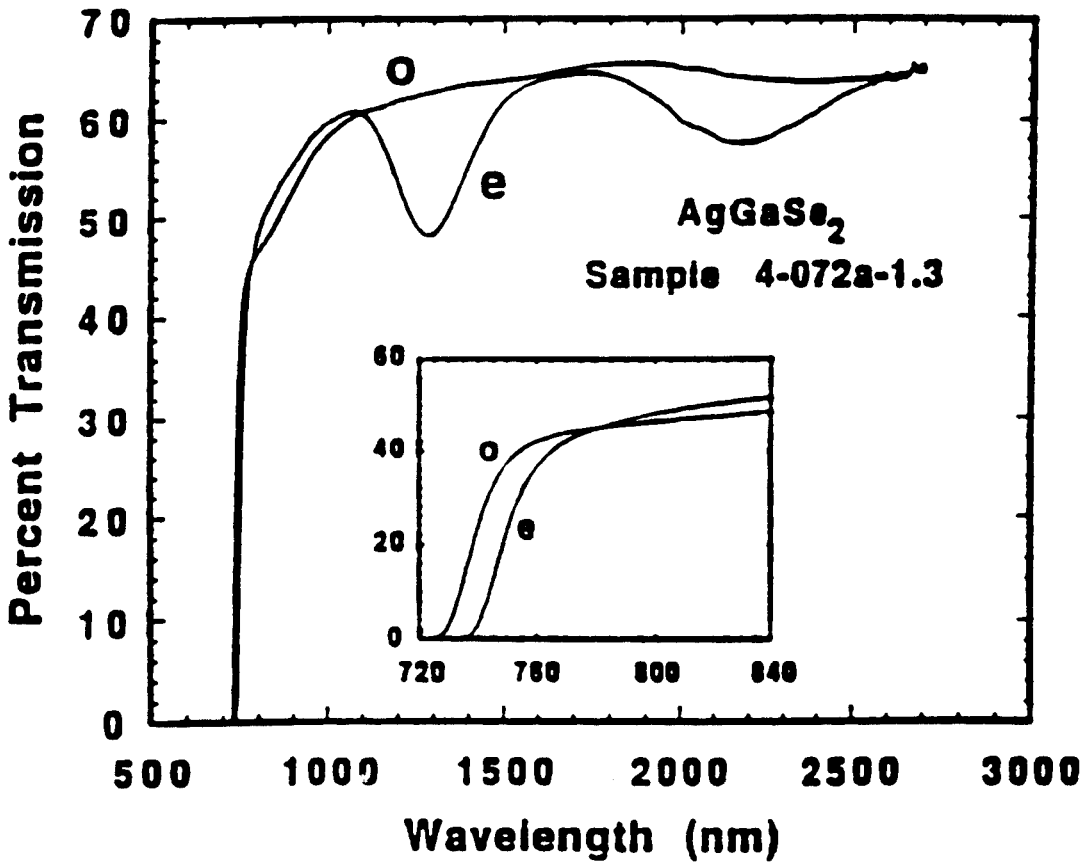

Figure 8. Polarized mid-IR transmission spectra of $AgGaSe_2$ OPO; path length = 24-mm; phase matching angle = 46 °. Details of the region near the band edge are shown in the inset. In most $AgGaSe_2$ crystals, the 1.3 μm band is barely detectable. [17]

A.)

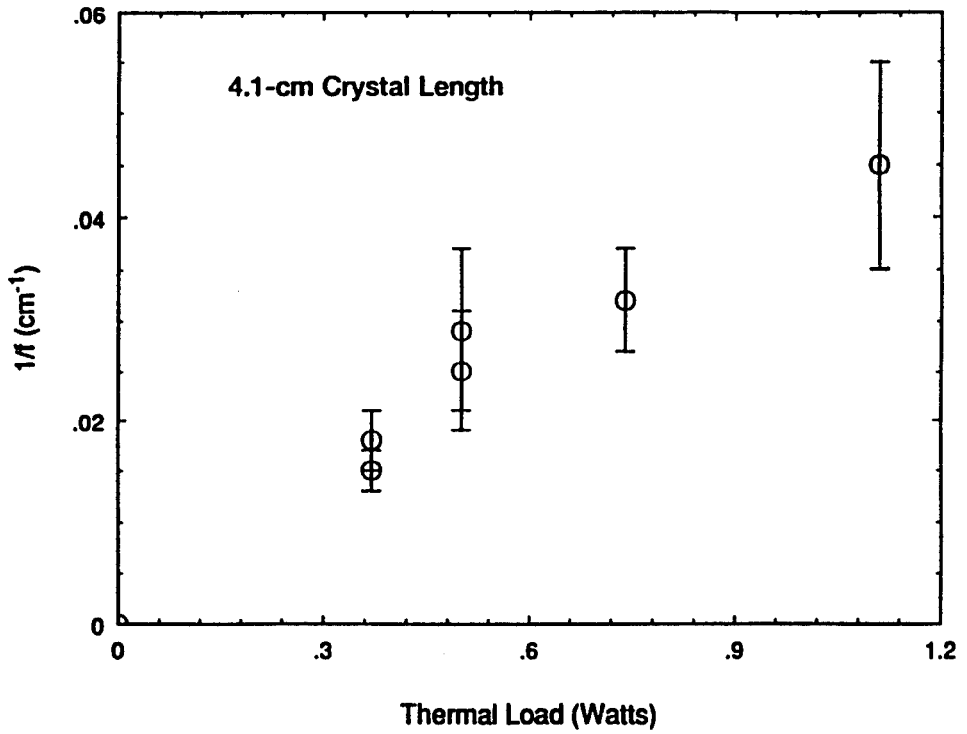

B.)

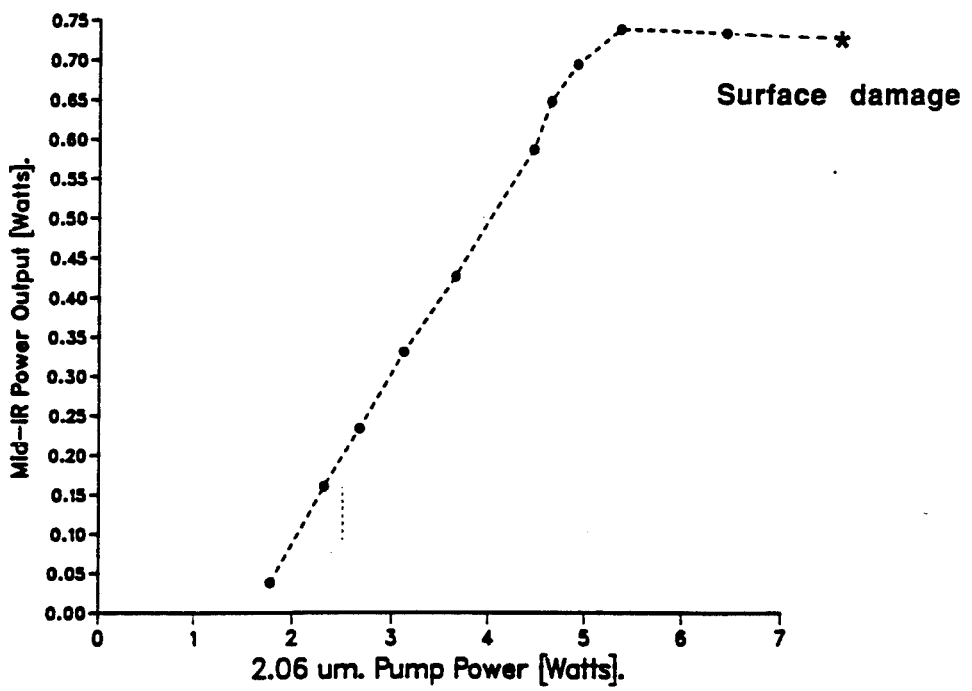

Figure 9. A.) Thermal lensing in 41 mm long $AgGaSe_2$ crystal grown elsewhere. [16] B.) Typical limitation in OPO output power caused primarily by beam distortion. [19] Ultimately, the front surfaces of the crystals damage due to localized heating.

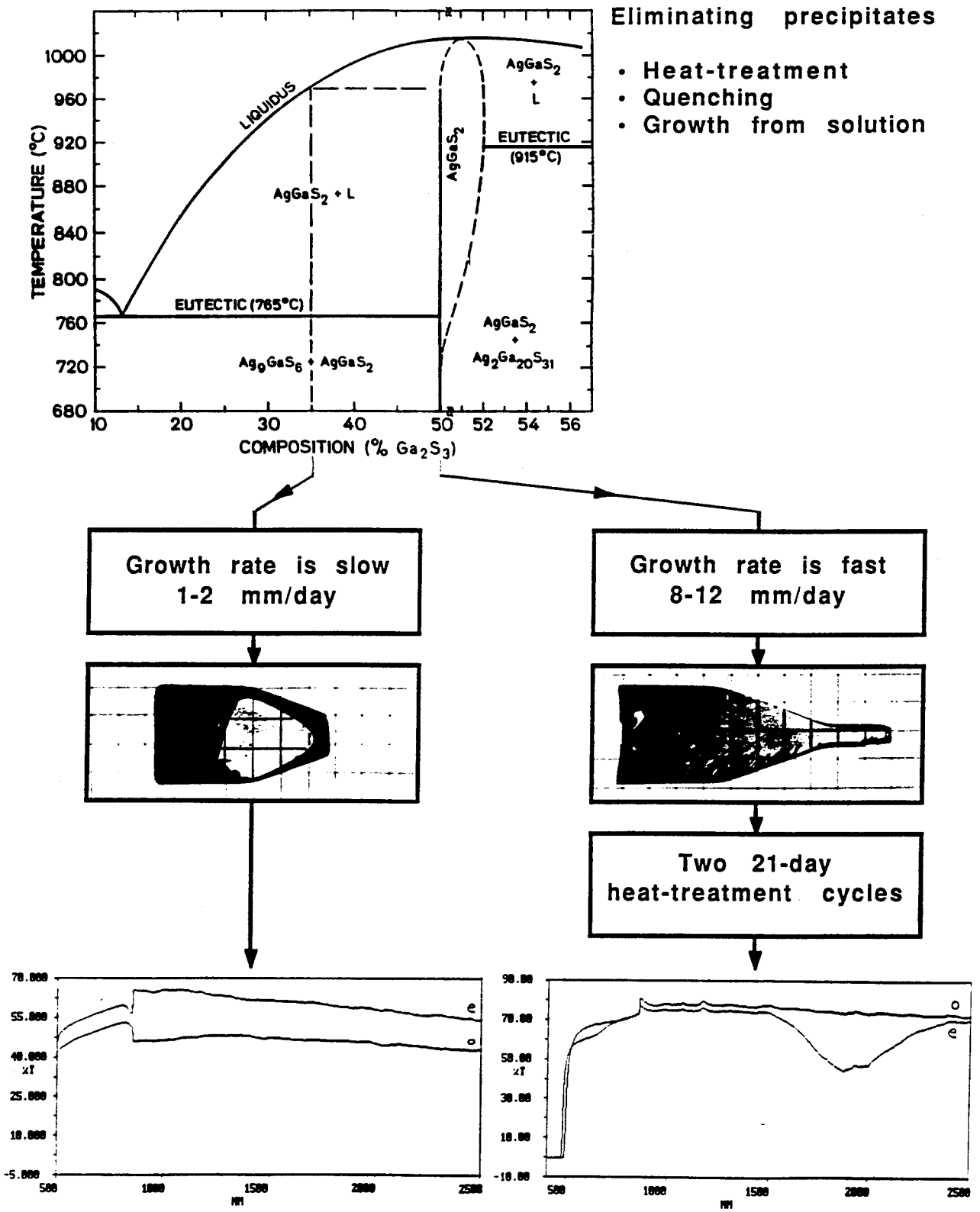

Figure 10. Prior results comparing $AgGaS_2$ crystals grown from Ag_2S-rich melts using solution techniques (left) with crystals grown from stoichiometric melts (right). The crystals from solution grew free of the precipitate phase (clear) while melt-grown crystals contained precipitates (cloudy). The 2 μm absorption band (bottom) was not found in the solution grown crystals.

Crystals from these experiments were randomly oriented because seeding had not been attempted. After it was verified that optical propagation was not coincident with the c-axis, a variety of input beam polarizations were used to measure optical transparency with spectrophotometry. None of the scans revealed absorption features in the 2 μm waveband. In contrast, $AgGaS_2$ crystals that had been grown from near-stoichiometric melts and then heat-treated, displayed the usual 2 μm absorption with absorption coefficients in the 2-3% cm^{-1} range. This finding was consistent with Catella et al's conclusion that the absorption feature is a stoichiometric point defect, and growth experiments were initiated to confirm that this finding would also apply to the $AgGaSe_2$ system.

5. Growth of Defect-Free $AgGaSe_2$ Crystals from Solution

The phase equilibria in the Ag_2Se-Ga_2Se_3 system is shown in Fig. 11 which also illustrates experiments carried out on the growth of $AgGaSe_2$ from solutions with compositions of 60 mole% Ag_2Se - 40 mole% Ga_2Se_3. In contrast to our earlier study on $AgGaS_2$, these growth experiments utilized c-axis seeds since we wanted to minimize cracking and maximize crystal dimensions for optical characterization. Seed pockets exceeding 25 mm were used and temperatures at the initiation of growth where maximum seed meltback occurs were estimated from the phase diagram. In the first growth experiment carried out at a rate of 1-3 mm/day, total melting of the seed column occurred and this resulted in a polycrystal that cracked during cooling. The crystal was also found to contain a cylinderical core of inclusions along its entire length that limited the maximum optical path length. Only short pathlength (<10 mm) specimens could be harvested for optical analysis. Unoriented specimens were examined using multiple input beam polarization orientations. In none of the scans was the 2 μm absorption feature detected. By comparison, typical melt-grown and heat-treated crystals all reveal detectable e-polarized absorption on the order of 0.025 cm^{-1}, as shown in Fig. 12. This figure also shows measurements made on $AgGaSe_2$ grown and heat-treated in the Soviet Union. These crystals were significantly bigger and clearer of residual optical scatter than any we had produced at Stanford, but they still displayed the 2 μm absorption feature, though with slightly lower absorption coefficients in the range 0.015-0.021 cm^{-1}.

In our second experiment carried out with slightly slower growth rates of 1-2 mm/day, seeding was successfull and the crystal remained uncracked. A cylinderical core of inclusions was found in this crystal as well, confirming that the growth rate was still too fast for the given system parameters, and that constitutional supercooling had occured a second time. Optical test specimens with significantly longer pathlengths could not be

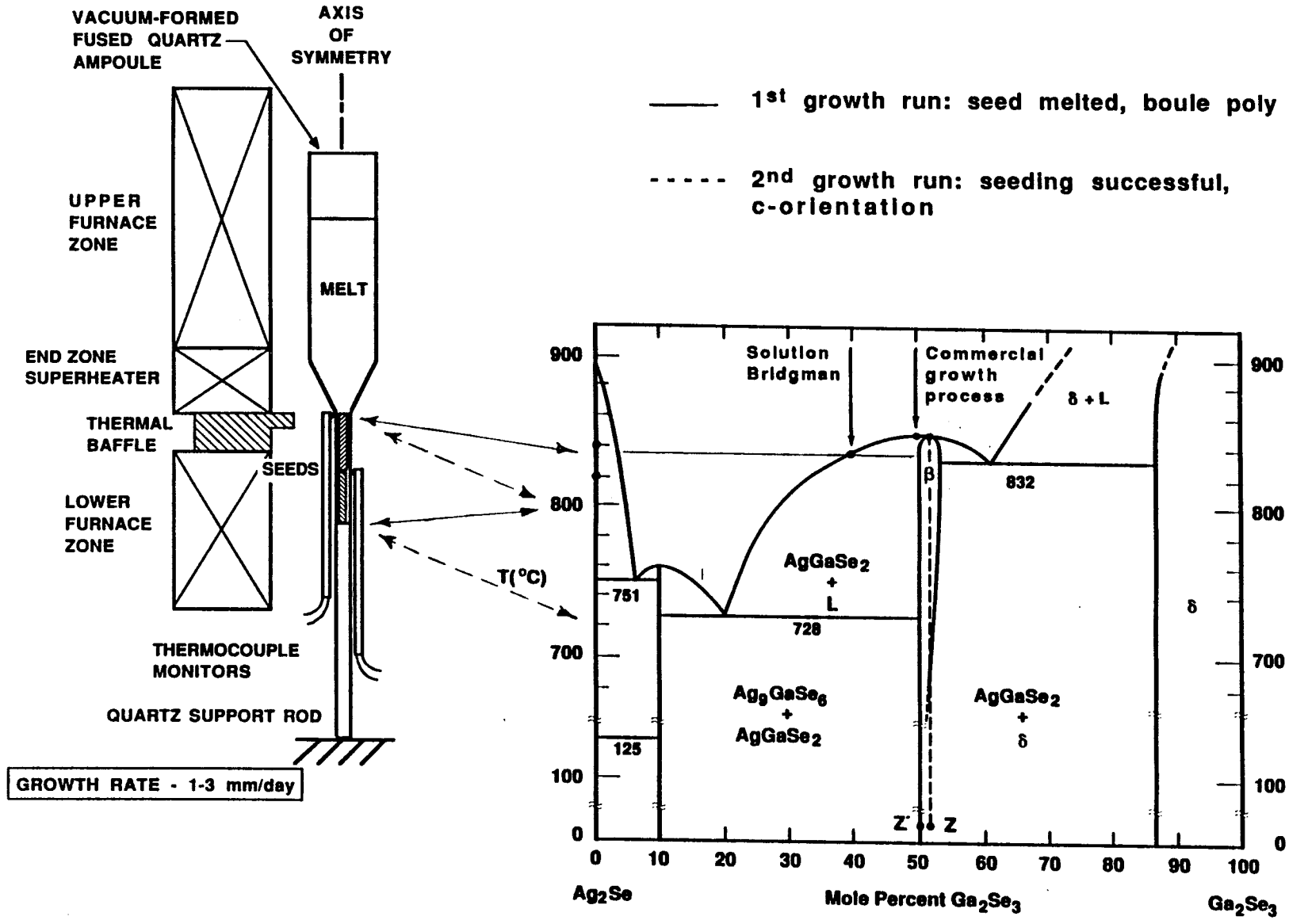

Figure 11 Illustration of solution growth of $AgGaSe_2$ crystals from Ag_2Se-rich melts. In the first experiment (solid lines) seeding was unsuccessful. In the second (dashed lines) the bottom of the seed column was maintained at lower temperatures and seeding was successful.

Stanford
Melt grown
49° OPO crystal
l = 25 mm
α ≅ 2.25% cm^{-1}
@ 2.2 μm

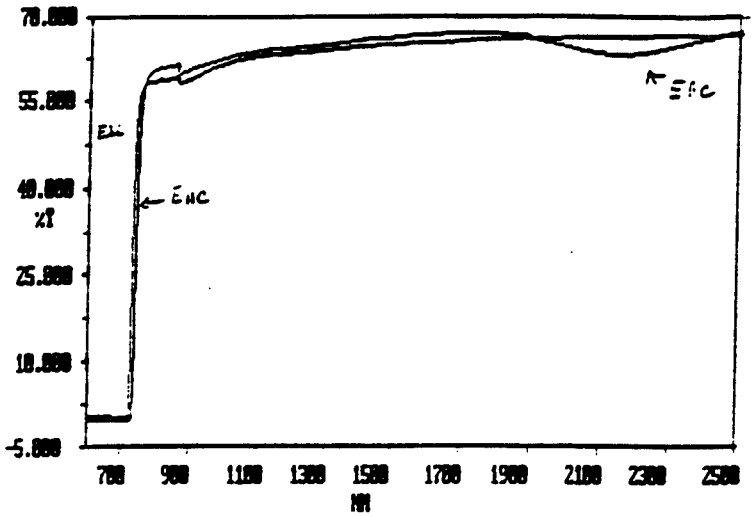

Russian
? grown
52° SHG crystal
l = 29 mm
α ≅ 1.5-2.1% cm^{-1}
@ 2.2 μm

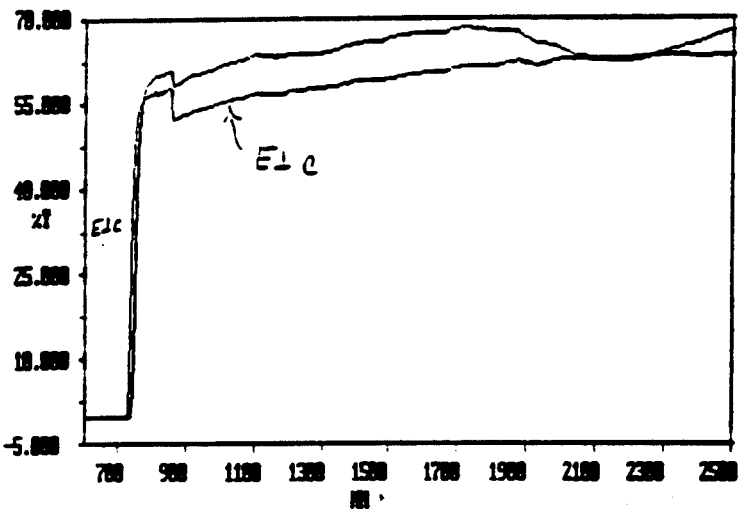

Stanford
Solution Bridgman
θ°, θ+60° and θ+120°
l = 7mm
α = low (?)

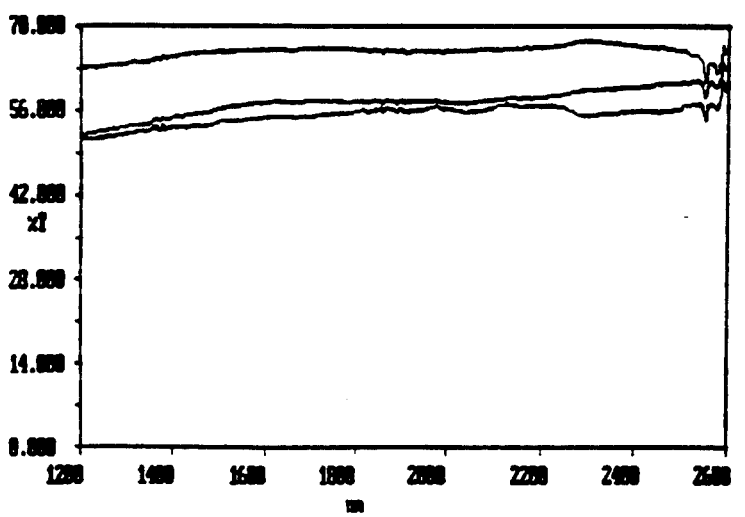

Figure 12 Optical absorption measurements comparing Stanford melt-grown, Russian melt-grown(?) and Stanford solution-grown $AgGaSe_2$ crystals.

fabricated, and no transmission measurements were made. Additional vertical Bridgman growth experiments using accelerated crucible rotaion and coupled vibrational stirring are being carried out under CNOM support with the aim of increasing melt stirring ahead of the growth interface to stabilize it, and obtaining cm+ lengths of inclusion-free material for detailed optical characterization.

6. Summary of Results

1. In collaborative studies, the cause of non-resonant laser damage was identified as localized surface heating, caused by low levels of optical absorption at surface defects. Improved polishing techniques increased threshold energy densities by a factor of two, to > 3 J cm^{-2}.
2. Resonant OPO applications remain limited to output powers < 1 W due to thermal defocusing of the 2 μm pump beam that is caused by a weak absorption of e-polarized radiation in crystals grown from near-stoichiometric melt compositions. The problem is thought to be extrinsic, most likely a stoichiometry-related point defect with its absorption dipole aligned along the c-axis.
3. In collaborative experiments, residual absorptions in the 2 μm waveband have been shown to be dependent on the post-growth heat-treatment process, and continued improvements in that area are hoped to achieve the significant reductions needed in e-polarized absorption to the 0.002 cm^{-1} level.
4. Ag_9GaSe_6 has been shown to be a superior to Ag_2Se which is the annealing medium used commercially. Ag_9GaSe_6 eliminates cracking during cooling and the surface diffusion kinetics appear to be faster, allowing the heat-treatment procedure to be carried out in shorter times.
5. The vertical (flux) Bridgman method has been used to grow $AgGaSe_2$ crystals from Ag-rich solutions for the first time .
6. We have shown that anomolous 2 μm absorption occurring in both melt-grown $AgGaS_2$ and $AgGaSe_2$ is not found in crystals grown from Ag-rich solutions. This finding suggests that these two materials may have applications in high power resonant OPO devices.
7. The occurrence of constitutional supercooling during flux growth of $AgGaSe_2$ points to the need to increase melt homogenization ahead of the growth interface using forced convection. Seeding has been accomplished under unstirred conditions and an extension of the process to include melt stirring seems feasible.

7. References: Part C

1. J. L. Shay and J. H. Wernick, Ternary Chalcopyrite Semiconductors - Growth, Electronic Properties and Applications, Ch. 1, (Pergamon Press, 1975).

2. J. C. Mikkelsen, Jr., Mat. Res. Bull. 12, 497-502 (1977).

3. R. K. Route, R. S. Feigelson, R. J. Raymakers, and M. M. Choy, J. Crystal Growth 33, 239-245 (1976).

4. N. B. Singh, R. H. Hopkins, and J. D. Feichtner, J. Mat. Sci. 21, 837-842 (1986).

5. N. B. Singh, R. H. Hopkins, R. Mazelsky, and H. H. Dorman, Mat. Letters 4 (8-9), 357-359 (1986).

6. R. S. Feigelson and R. K. Route, Mat. Res. Bull. 25, 1503-1511 (1990).

7. N.-H. Kim, R.S. Feigelson and R.K. Route, "Surface migration and volume diffusion in the $AgGaSe_2$-Ag_2Se system," J. Mater. Res. 7, 1215 (1992).

8. N. H. Kim, "Growth and Heat Treatment of Silver Gallium Diselenide Crystals for Nonlinear Optical Applications," Ph. D. dissertation, Stanford University (1992).

9. R. C. Eckardt, Y. X. Fan, R. L. Byer, R. K. Route, R. S. Feigelson, and J. van der Laan, "Efficient Second Harmonic Generation of 10-μm Radiation in $AgGaSe_2$," Appl. Phys. Lett. 47(8), 786-788 (1985).

10. R. C. Eckardt, R. L. Byer, L. A. Newman and J. Kennedy, "High-Average-Intensity Nonlinear Infrared Frequency Conversion in $AgGaSe_2$," paper WM33, Proc. Conference on Lasers and Electro-Optics, Anaheim, CA (April 1988).

11. R. C. Eckardt, Y. X. Fan, R. L. Byer, C. L. Marquardt, M. E. Storm and L. Esterowitz, "Broadly Tunable Infrared Parametric Oscillator Using $AgGaSe_2$," Appl. Phys. Lett. 49(11), 608-613 (1986).

12. R. C. Eckardt, private communication.

13. B. C. Ziegler and K. L. Schepler, "Transmission and damage-threshold measurements in $AgGaSe_2$ at 2.1 μm," Applied Optics 30, 5077 (1991).

14. R. L. Byer, "Nonlinear Optical Phenomena and Materials," Annual Review of Materials Science, Annual Reviews, Inc., Palo Alto, CA, 4, 147 (1974).

15. C. L. Marquardt, et al. "Thermal lensing in silver gallium selenide parametric oscillator crystals, Applied Optics 33, 3192 (1994).

16. Private communication with D. Lowenthal, Aculight, Inc.

17. G. C. Catella et al. "Mid-IR absorption in AgGaSe2 optical parametric oscillator crystals," Applied Optics 32, 3948 (1993).

18. J. D. Beasley, "Thermal conductivbities of some novel nonlinear optical materials," Applied Optics 33, 1000 (1994).

19. Measurements performed at Lockheed/Sanders using 2.1 μm source.

20. F. K. Hopkins "Optical scattering centers in an as-grown $AgGaSe_2$ sample," private manuscript (1988); F. K. Hopkins and G. J. Brown, "Light scattering by inclusions in crystals," Applied Optics 30, 384 (1991).

21. R. S. Feigelson and R. K. Route, "Recent Developments in the Growth of Chalcopyrite Crystals for Nonlinear Infrared Applications," Opt. Eng. 26 (2), 113 (1987).

D. SEARCH FOR NEW NONLINEAR OPTICAL MATERIALS

1. Introduction

The development of β-barium borate (BBO) and lithium tri-borate (LBO) has permitted major research advances in UV generation and high intensity, high beam quality cw green light generation, respectively. As indicated in previous sections, both materials are difficult to prepare with high optical quality and the long term stability required for commercial applications. Therefore, further developments in borate growth technology were sought on a moderate level-of-effort basis. The study was carried out in collaboration with Dr. D. A. Keszler at Oregon State University through his recent Ph.D. graduate, Dr. K. I. Schaffers, who was a post-doctoral student at Stanford from 9-92 through 1-94 and is currently at the Lawerence Livermore National Laboratories. We also collaborated with Dr. B. H. T. Chai at CREOL.

It is now well established that the favorable nonlinear optical (NLO) properties of BBO and LBO are due to the large microscopic nonlinear susceptibilities of the planar $(B_3O_6)^{3-}$ and helical $(B_3O_7)^{5-}$ boroxol rings that make up these two compounds. Compounds containing highly distorted octahedra, such as $(NbO_6)^{7-}$ which is found in $LiNbO_3$, have favorable NLO properties as well. It is assumed that favorable NLO properties would also occur in other compounds containing similar structural elements. The simple niobate and borate systems had already been extensively explored for easily grown, phasematchable NLO materials, and none have been found. We therefore looked to multicomponent borate systems for new NLO materials with improved properties and/or better growth characteristics.

2. Approach

Our first approach to identifying new NLO compounds involved mixed **cation** substitutions into existing crystal structures with known NLO applications. The aim here was full or partial substitution of one or more elements on the cation sublattice in order to alter the structural arrangement and chemical properties, which affect the optical characteristics. Compositions studied were $SrLiB_9O_{15}$ and $BaLiB_9O_{15}$ (derivatives of LiB_3O_5), and $(La,Gd)Sc_3(BO_3)_4$ (an analog of $YAl_3(BO_3)_4$).

The second approach pursued was based on mixed groupings of known **anionic** structural elements. Initially, we focused on systems incorporating both boroxol rings and distorted niobium or tantalum octahedra. Compounds in the Li_2O-B_2O_3-$(Ta,Nb)_2O_5$ system were investigated.

The third approach involved a review of materials documented to contain non-centrosymmetric structural elements. A great number of these **overlooked phases** have not been fully characterized in terms of their optical properties. The sheer size of this base dictates a highly selective approach, and collaborative interactions with LLNL were established to make use of their data on uncharacterized, but promising materials. One material they had identified was $Al_{18}B_4O_{33}$, and this compound was investigated also using sintering and flux growth methods.

3. Results

a.) $SrLiB_9O_{15}$ and $BaLiB_9O_{15}$ - Phase equilibria are not available for these rhombohedral R3c phases, and phase analysis was required to determine their melting behavior and to identify suitable fluxes. DTA analysis indicated that $SrLiB_9O_{15}$ melted incongruently at 883 °C, and compositions along the SrB_4O_7-$Li_2B_8O_{13}$ (pseudobinary?) join were investigated as possible solvents. Centimeter size crystals of $SrLiB_9O_{15}$ were successfully grown from a melt of composition 15 m% $Li_2B_8O_{13}$ - 85 m% $SrLiB_9O_{15}$ by the top-seeded solution growth method at a melt temperature of 870 °C. Optical index measurements indicating sufficient birefringence for phase matching to occur were carried out at the Lawrence Livermore National Laboratory (LLNL). However, bulk crystals of $SrLiB_9O_{15}$ did not yield detectable SHG signals. Powder SHG tests indicated at best, only a weak effect, possibly due to impurities such as LBO which could have been present in the samples as a result of incomplete synthesis reactions. Dielectric studies on $SrLiB_9O_{15}$ plates carried out at Pennsylvania State University indicated possible ferroelectric behavior, further complicating the issue. Better quality crystals will ultimately be needed to resolve the uncertainty. The compound was not pursued due to the negative SHG results on sintered specimens which we believed were the most reliable indicator.

$BaLiB_9O_{15}$ was prepared by standard sintering techniques and evaluated by powder SHG analysis. A powder SHG test was positive. However, when the same ceramic was taken to melting and recrystallized, the test was negative. We again suspected that the sintering route to phase formation was limited by very sluggish reaction kinetics and incomplete reaction components like LBO could have been present. Even small quantities, undetectable by powder XRD, would be sufficient to yield a postiive powder SHG result. Negative results on $BaLiB_9O_{15}$ were also reported by researchers from OSU [1], and for this reason the compound was not pursued.

b.) $(La,Gd)Sc_3(BO_3)_4$ - Rare earth scandoborates have been studied by a number of authors for application as Nd-doped laser hosts. [2,3] Pure $LaSc_3(BO_3)_4$ is known to melt near-congruently at ~ 1500 °C, and Nd-doped crystals multi-cm in dimension have

been grown by the Czochralski method. The structure of pure $LaSc_3(BO_3)_4$ is monoclinic, C2/c, with a center of symmetry, and is therefore not useable for second order NLO interactions. By heavy Nd- doping or partial substitution with smaller RE ions, it can be stabilized in the rhombohedral R3c Huntite structure which lacks a center of symmetry and is useable for second order NLO applications. [4] It is estimated that 35% Gd substitution is sufficient to stabilize the rhombohedral Huntite structure. [5] We investigated the 50% Gd-substituted composition $La_{0.5}Gd_{0.5}Sc_3(BO_3)_4$. Ceramic specimens prepared by sintering above 1350 °C gave the Huntite XRD pattern and a strong powder SHG signal. Efforts to prepare cm -size single crystals from $K_2Mo_3O_{10}$, $LiBO_2$, and $Li_2Sc(BO_3)_2$ fluxes were not successful due to solvent volatility and/or melt immiscibility.

DTA analysis indicated that either the 50-50 composition melts incongruently at 1370 °C, or there is a phase transition at that temperature and it melts near-congruently at 1475 °C with a small peritectic gap. It is not clear which, if either, interpretation of the DTA results is correct. (Annealing and quenching studies will be needed to make this determination.) However, stoichiometric compositions taken to melting at 1550 °C and cooled slowly did give the desired phase, and based on this result we initiated growth experiments directly from stoichiometric melts using the Czochralski technique. As of this report, single crystals have not yet been successfully grown due to difficulties encountered in achieving stable melts due to uneven heating of the crucibles and volatilization of B_2O_3. This work is considered to be very promising and has been continued with CNOM funding.

c.) $(Li, Na)_2O$-B_2O_3-$(Ta,Nb)_2O_5$ - Interest was stimulated in these materials by unpublished work at CREOL [6] and in the PRC [7] on Na-, K- and Rb- analogs. The phase equilibria in all of these ternary systems are unknown or only poorly documented, and phase identification studies had to be carried out. No phases with the desired structural elements or positive SHG results were found.

d.) $Al_{18}B_4O_{33}$ - Preliminary studies at LLNL on orthorhombic, C2v, $Al_{18}B_4O_{33}$ indicated positive results by the SHG powder test. However, XRD analysis of their sample revealed diffraction lines from extra (impurity) phases estimated at ~10 % by volume. $Al_{18}B_4O_{33}$ melts incongruently at 1440 °C, [8] and it cannot easily be grown from excess B_2O_3 because of volatilization from the melt combined with high melt viscosities. Sintering techniques were used to prepare ceramic specimens of the $Al_{18}B_4O_{33}$ phase. No SHG activity was detected from these samples. Individual $Al_{18}B_4O_{33}$ crystallites displaying needle-like morphology were grown from a calcium borate flux by slow cooling, and again, no SHG activity was detected. We tentatively concluded that the

effect seen in the LLNL specimen was due to contamination by an active nonlinear impurity phase of unknown composition.

4. Summary of Results

a. A promising new nonlinear optical material, $La_{0.5}Gd_{0.5}Sc_3(BO_3)_4$, has been identified by the method of isostructural substitution in known materials with favorable NLO properties to produce derivative phases with similar physical properties.

b. A strong powder SHG response has been detected in $La_{0.5}Gd_{0.5}Sc_3(BO_3)_4$ specimens prepared by different methods, suggesting it is an intrinsic property and not that of an impurity phase.

The anticipated payoff of these studies is the development of new materials that possess superior NLO properties and are easily grown in a commercial environment.

5. References: Part D

1. Private communication
2. S. A. Kutovi, V. V. Laptev and S. Yu. Matsnev, "Lanthanum scandoborate as a new highly efficient active medium of solid state lasers," Sov. J. Electron. 21, 131 (1991).
3. B. Beier, et al. "A 180 mW Nd:$LaSc(BO_3)_4$ single-frequency TEM_{00} microchip laser pumped by an injection-locked diode-laser array," Appl. Phys. B 58, 381 (1994).
4. J. P. Meyn, T. Jensen and G. Huber, "Diode laser-pumped Nd:$LaSc(BO_3)_4$ laser with high efficiency," Abstract of paper presented at CLEO, CPD9-1/18 (1993).
5. Private communication with K. I. Schaffers.
6. Private communication with B. H. T. Chai.
7. Private communication with L-f. Mei.
8. M. Ihara et al. "Crystal structure of boroaluminate, 9 $Al_2O_3 \cdot 2B_2O_3$, Yogyo-Kyokai-Shi 88, 28 (1980). (In Japanese).

III. CONCLUSIONS AND RECOMMENDATIONS FOR FURTHER STUDY

This program has been highly successful in reaching our original goals of developing an effective growth technology for BBO and LBO and transfering it to industry. Beginning with little more than the published phase equilibria in these two systems, we were able to develop high temperature solution growth techniques that produced large, high optical quality boules suitable for property determinations and device research. Ours were literally the first BBO and LBO crystals grown in the U. S., and we were able to provide these to Stanford's device researchers under Professor R. L. Byer within a year of initiating crystal growth studies on each. His research group was, in turn, able to demonstrate important device applications and make more accurate property determinations than were possible at the time because of limited access to crystals grown in the P.R.C.

Our program was the first to demonstrate that the optical scattering defects found in all BBO crystals at the time were due to solvent inclusions. A high thermal gradient growth technique allowed us to achieve maximum growth rates while minimizing the solvent inclusion density. Novel stirring experiments using periodic reversals in seed rotation revealed the importance of maintaining effective melt sweeping across the growing crystal interface, and it pointed out an important avenue for further study under ARPA support through the Center for Nonlinear Optical Materials (CNOM) at Stanford aimed at further reducing the residual scattering losses in this material.

Our program was also the first US study to demonstrate the direct melt growth of BBO (DMBBO) and to quantify the range of thermal conditions under which β-phase material could be grown. We clarified the previously murky issue of melt synthesis and showed that easy-to-synthesize carbonate based melts were adequate. Numerous samples were fabricated from spontaneously nucleated DMBBO boules for optical charecterization. Attempts to use of c-axis seeds to control the growth orientation of DMBBO boules were not successful during this study, but the problem has since been solved under CNOM. Through collaborative studies, we have sought to elucidate the factors limiting the use of BBO at high power levels in the UV, including issues of melt purity. Both surface degradation and bulk degradation (two photon ?) processes were studied. The exact damage mechanisms have not yet been identified. More intensive investigations have since been launched under the CNOM program. UV degradation is the most important issue now limiting commercial application of BBO, and a sustained (multi-year) effort involving both crystal growth and characterization is recommended to solve it.

Early in this program, we transferred our BBO solution growth technology to Cleveland Crystals, Inc. and provided them with oriented seeds with which to get started. Throughout the program, we sought to keep them abreast of our research results and continuing developments in growth technology. Later, we carried out a similar BBO technology transfer and an LBO technology transfer to INRAD, Inc. We also sought to assist other researchers in the field when asked, and provided both information and material to Quantum Technology, Inc., as well. Crystals of BBO and LBO were supplied to (D)ARPA and NRAD during the program, as well.

The growth technology for LBO was not as advanced as it was for BBO at the time growth experiments were initiated. Again using high gradient furnaces, we were able to show that reasonable growth rates could be achieved while minimizing crystal defects. Like TSSG-grown BBO crystals, LBO crystals were found to have a core region containing a high density of optical defects. These were presumed to be due to solvent inclusions as well. Experiments on viscosity-modified growth solutions called into question literature reports that growth rates and crystal quality could be improved by using LiF as a flux additive. We found that solvent aging when more than a trace amount of LiF was present far outweighed any possible gains due to the measured reductions in melt viscosity that were achieved. Our most significant contribution was identification of the surface degradation mechanism that leads to boule cracking. We were able to completely eliminate surface degradation by growing under a dry nitrogen ambient, and other researchers growing LBO now report widespread use of this method. The problem of a restrictive US patent issued to the Chinese Academy of Science covering all aspects of the growth and application of LBO caused us to suspend the study of LBO and look for newer NLO materials with improved properties.

Micro-chemical analytical studies on silver gallium selenide added substantially to our understanding of the heat-treatment process that is used to remove optical scattering defects (precipitates) from as-grown crystals of this material. Low temperature diffusion experiments indicated that Ag_9GaSe_6 may offer advantages over Ag_2Se which is currently used in the commercial process because it minimizes surface damage to the silver gallium selenide crystals. Further research on this low temperature alternate heat-treatment process is recommended. Most significantly, studies of existing $AgGaS_2$ crystals grown from solutions containing excess Ag_2S showed them to be free of the 2 μm absorption that is found in all crystals grown from near-stoichiometric melt compositions. Solution Bridgman growth experiments verified similar behavior in $AgGaSe_2$ and promise a ten-fold reduction in 2 μm absorption. (Absorption in the 2 μm pump waveband currently limits the maximum power of 3-5 μm tunable OPOs to ~ 1W because of thermal defocusing.) A

significant reduction in 2 μm absorption should allow a substantial increase in output power.

Solution growth experiments on $AgGaSe_2$ are being continued, also with CNOM resources. Growth studies on $AgGaSe_2$ are known from past experience to be time consuming and costly, however, and for this reason and because of the important need for high power tunable 3-5 μm sources, it is recommended that the project receive independent funding at a level sufficient to make rapid progress.

A promising new nonlinear optical material, $La_{0.5}Gd_{0.5}Sc_3(BO_3)_4$, has been identified by the method of isostructural substitution, and growth experiments using the Czochralski technique are being carried out under CNOM. Investigations of new materials for possible NLO applications are time consuming, but not overly costly. Sustained support at modest funding levels would permit a systematic survey program to be carried out efficiently.

IV. PUBLICATIONNS

1. S.T. Yang, C.C. Pohalski, E.K. Gustafson, R.L. Byer, R.S. Feigelson, R.J. Raymakers, and R.K. Route, " 6.5 watt cw 532 nm radiation by resonant external cavity SHG of an 18 watt Nd:YAG laser in LBO," Optics Letters 16 (19) 1493-1495 (1991).

2. G.C. Bhar, U. Chatterjee, P.K. Datta, S. Das, R.S. Feigelson and R.K. Route, "Noncritical detection of tunable CO_2 laser radiation into green by upconversion in silver thio-gallate," Applied Physics B 53, 19 (1991).

3. N.-H. Kim, R.S. Feigelson and R.K. Route, "Surface migration and volume diffusion in the $AgGaSe_2$-Ag_2Se system," J. Mater. Res. 7, 1215 (1992).

4. Nam-Hun Kim, "Growth and Heat Treatment of Silver Gallium Diselenide Crystals for Nonlinear Optical Applications," Ph.D. dissertation, Department of Materials Science and Engineering, Stanford University (1993).

5. E. Brück, R. J. Raymakers, R. K. Route and R. S. Feigelson, "Surface stability of lithium triborate crystals grown from excess B_2O_3 solution," J. Crystal Growth 128, 933 (1993).

6. Y. K. Voronko, A. V. Gorbachev, V. V. Osiko, A. A. Sobol, R. S. Feigelson and R. K. Route, " Correlation of the structure of melts and crystals of alkali and alkali earth borates: the crystallization behavior of barium metaborate," J. Physics and Chemistry of Solids 54, 1579 (1993).

7. G. C. Catella, L. R. Shiozawa, J. R. Hietanen, R. C. Eckardt, R. K. Route, R. S. Feigelson, D. G. Cooper and C. L. Marquardt, "Mid-IR absorption in $AgGaSe_2$ optical parametric oscillator crystals," Applied Optics 32, 3948 (1993).

8. G. C. Bhar, S. Das, U. Chatterjee, A. M. Rudra, R. K.Route and R. S. Feigelson "Temperature effects in second harmonic generation in $AgGaSe_2$ cystal," J. Appl. Phys. 74, 1 (1993).

9. L. Gordon, G. L. Woods, R. C. Eckardt, R. K. Route, R. S. Feigelson, M. M. Fejer and R. L. Byer, "Diffusion bonded stacked GaAs for quasi-phase-matched second harmonic generation of a carbon dioxide laser," Electronics Lett. 29, 1942 (1993).

10. G. C. Bhar, S. Das, U. Chatterjee, A. M. Rudra, R. S. Feigelson and R. K.Route, "Evaluation of $AgGaSe_2$ temperature-dependent nonlinear devices," J. Phys. D: Applied Physics 27, 231 (1994).

V. PARTICIPATING PERSONNEL

A. FACULTY AND STAFF	Position
R. S. Feigelson	Director, Advanced Materials Processing Lab Center for Materials Research Professor (Research), Materials Science & Engineering Department
R. K. Route	Senior Research Associate
R. J. Raymakers	Research Technician
M. Wolf	Scientific & Engineering Associate

B. POST-DOCTORAL STUDENTS	Current affilation
Dr. E. H. Brück	Univ. Amsterdam
Dr. K. I. Schaffers	Lawerence Livermore Nat. Labs.

C. GRADUATE STUDENTS	Department / Degrees Earned
N.-H. Kim	MS&E / Ph.D. (1992)
H. Lee	Appl. Phys.
Z. Lu	MS&E / Ph.D. (expected 1994)

D. VISITING RESEARCHERS	Institution
Dr. H. Kimura	Nat. Research Inst. for Metals Tsukuba, Japan
Dr. G-t. Joo	Korea Inst. of Science and Technology Seoul, Korea

REPORT OF INVENTIONS AND SUBCONTRACTS

(Pursuant to "Patent Rights" Contract Clause) (See Instructions on Reverse Side.)

Form Approved
OMB No. 0704-0297
Expires Jun 30, 1992

1a. NAME OF CONTRACTOR / SUBCONTRACTOR	c. CONTRACT NUMBER	2a. NAME OF GOVERNMENT PRIME CONTRACTOR	c. CONTRACT NUMBER	3. TYPE OF REPORT (X one)
Stanford University	N00014-90-J-4092	Dept. of Navy / ONR	Same	a. INTERIM [ ] b. FINAL [X]
b. ADDRESS (Include ZIP Code)	**d. AWARD DATE (YYMMDD)**	**b. ADDRESS (Include ZIP Code)**	**d. AWARD DATE (YYMMDD)**	**4. REPORTING PERIOD (YYMMDD)**
Jordan Quad./Birch Stanford, CA 94305-4125	08/01/90	800 N. Quincy St. Code 1511 Arlington, VA 22217-5000	Same	a. FROM 08/01/90 b. TO 06/30/94

SECTION I – SUBJECT INVENTIONS

5. "SUBJECT INVENTIONS" REQUIRED TO BE REPORTED BY CONTRACTOR / SUBCONTRACTOR (If "None," so state)

a. NAME(S) OF INVENTOR(S) (Last, First, MI)	b. TITLE OF INVENTION(S)	c. DISCLOSURE NO., PATENT APPLICATION SERIAL NO. OR PATENT NO.	d. ELECTION TO FILE PATENT APPLICATIONS				e. CONFIRMATORY INSTRUMENT OR ASSIGNMENT FORWARDED TO CONTRACTING OFFICER	
			(1) United States		(2) Foreign			
			(a) Yes	(b) No	(a) Yes	(b) No	(1) Yes	(2) No
-------	None							

f. EMPLOYER OF INVENTOR(S) NOT EMPLOYED BY CONTRACTOR / SUBCONTRACTOR		g. ELECTED FOREIGN COUNTRIES IN WHICH A PATENT APPLICATION WILL BE FILED	
(1) (a) Name of Inventor (Last, First, MI)	(2) (a) Name of Inventor (Last, First, MI)	(1) Title of Invention	(2) Foreign Countries of Patent Application
(b) Name of Employer	(b) Name of Employer		
(c) Address of Employer (Include ZIP Code)	(c) Address of Employer (Include ZIP Code)		

SECTION II – SUBCONTRACTS (Containing a "Patent Rights" clause)

6. SUBCONTRACTS AWARDED BY CONTRACTOR / SUBCONTRACTOR (If "None," so state)

a. NAME OF SUBCONTRACTOR(S)	b. ADDRESS (Include ZIP Code)	c. SUBCONTRACT NO.(S)	d. DFAR "PATENT RIGHTS"		e. DESCRIPTION OF WORK TO BE PERFORMED UNDER SUBCONTRACT(S)	f. SUBCONTRACT DATES (YYMMDD)	
			(1) Clause Number	(2) Date (YYMM)		(1) Award	(2) Estimated Completion
None							

SECTION III – CERTIFICATION

7. CERTIFICATION OF REPORT BY CONTRACTOR / SUBCONTRACTOR (Not required if [ ] Small Business or [XX] Non-Profit organization.) (X appropriate box)

a. NAME OF AUTHORIZED CONTRACTOR / SUBCONTRACTOR OFFICIAL (Last, First, MI)	c. I certify that the reporting party has procedures for prompt identification and timely disclosure of "Subject Inventions," that such procedures have been followed and that all "Subject Inventions" have been reported.	
Robert S. Feigelson		
b. TITLE	**d. SIGNATURE**	**e. DATE SIGNED**
Principal Investigator	R Feigelson	8/30/94

DD Form 882, OCT 89

Previous editions are obsolete.

971/284